1966

Heat transfer in the shock-induced unsteady boundary layer on a flat plate

Elmer John Felderman
Iowa State University

HEAT TRANSFER IN THE SHOCK-INDUCED UNSTEADY BOUNDARY LAYER ON A FLAT PLATE

by

Elmer John Felderman

A Dissertation Submitted to the
Graduate Faculty in Partial Fulfillment of
The Requirements for the Degree of
DOCTOR OF PHILOSOPHY

Major Subjects: Mechanical Engineering
Aerospace Engineering

Approved:

Signature was redacted for privacy.

In Charge of Major Work

Signature was redacted for privacy.

Heads of Major Departments

Signature was redacted for privacy.

Dean of Graduate College

Iowa State University
Of Science and Technology
Ames, Iowa

1966

TABLE OF CONTENTS

LIST OF SYMBOLS

Symbol	Units	Description
A		Shock strength parameter, U_s/u_o
B	volts	Voltage amplitude when gage is pulsed in air
B^*	volts	Voltage amplitude when gage is pulsed in calibration fluid
C		Dimensionless product of density times viscosity, $\rho\mu/\rho_o\mu_o$
C_p	Btu/lbm ^0R	Specific heat at constant pressure
C_v	Btu/lbm ^0R	Specific heat at constant volume
E	volts	Voltage change across thin film
E_f	volts	Initial voltage drop across thin film
f'		Velocity ratio, u/u_e
H		Dimensionless enthalpy defined in Equation 12
$\bar{H}$		Piecewise linear function for H defined in Equation 38
$H_s(\beta;A)$		Enthalpy in the S region
h	Btu/lbm	Enthalpy
I		Index of points on β axis
IMAX		Total number of division points on β axis

Symbol	Units	Description
I_β		Value of I corresponding to a specific point β
J		Summation index
K		Index of points on α axis
k	Btu/hr ft ^{0}R	Thermal conductivity
KMAX		Total number of division points on α axis
KE		Kinetic energy term, u_o^2/h_o
M		Mach number
M_s		Initial shock Mach number
m		Weighting factor defined in Equation 49
p		Dummy variable of integration
P_1	mm Hg	Initial channel pressure in shock tube
Pr		Prandtl number, $\frac{c_p \mu}{k}$
$\bar{Q}$		Dimensionless heat transfer rate parameter defined in Equation 46
q	Btu/ft^2 sec	Heat transfer rate
r		Weighting factor
S(β;A)		Shear stress in the S region
T	^{0}R	Temperature
t	sec	Time
U_s	ft/sec	Velocity of initial shock wave

Symbol	Units	Description
u	ft/sec	Velocity in x direction
u_o	ft/sec	Free stream velocity behind initial shock wave
v	ft/sec	Velocity in y direction
W		Uncertainty interval
x	ft	Distance from leading edge of flat plate
y	ft	Distance perpendicular to surface of flat plate
α		Independent variable, $x/u_o t$
β		Independent variable, u/u_o
Γ	$Btu/ft^2\ {}^0R\ \sqrt{sec}$	Calibration constant, $\sqrt{k\rho C_p}$
γ		Independent variable, $u_o^2\ t./\nu_o$
Δ		Increment
δ	$1/{}^0R$	Temperature coefficient of resistance
η	sec	Time variable
λ		Dummy variable of integration
μ	lbm/ft sec	Viscosity
ν	ft^2/sec	Kinematic viscosity
ξ	ft	Distance variable
ρ	lbm/ft^3	Density
τ		Shear stress variable defined in Equations 12

Symbol	Units	Description
τ	lbm/ft sec^2	Shear stress, $\mu\frac{\partial u}{\partial y}$
ϕ		Shear stress variable defined in Equation 19
$\bar{\phi}$		Piecewise linear function for ϕ defined in Equation 29

Subscripts	Description
b	Relating to pyrex backing
e	Free stream in coordinate system fixed to the initial shock wave
f	Relating to thin platinum film
i	Summation index
l	Relating to calibration fluid
n	Number of divisions of time axis
o	Free stream in laboratory coordinates
s	Relating to initial shock wave
w	Wall conditions

Superscript	Description
n	iterant index

INTRODUCTION

In recent years it has been necessary to utilize aerodynamic testing devices of limited flow duration in order to attain the desired flow conditions. When using devices of this type it is of considerable interest to know how the flow develops over the test model and how long it takes to establish steady flow conditions. As a rule of thumb the inviscid flow field is considered to be fully developed in the time it takes a particle in the flow to travel from the leading edge of the model to the last downstream point of interest on the model. While this is true of the inviscid flow field about the model it is not true of the boundary layers on the model. It may require three or four times as long for the boundary layers to become fully developed. In certain cases where testing time is severely limited it may not be possible to reach steady state conditions. It is then desirable to be able to predict the values of the significant parameters, notably shear stress and heat transfer rate, in the unsteady region in order to evaluate the experimental data.

Consider the case of a semi-infinite flat plate mounted parallel to the flow direction in a shock tube. The initial shock wave, which is perpendicular to the plate surface, passes over the sharp leading edge of the plate and continues across the plate, setting up the flow field behind it. The boundary layer will be very thin at the leading edge of the plate and also

very thin at the base of the shock. In between, the boundary layer thickness will reach some maximum value. This behavior can be seen qualitatively from the typical schlieren picture of Figure 1. It would be expected that the shear stress and heat transfer rates would be higher in the regions where the boundary layer is thin and somewhat lower elsewhere.

In shock tube flow the initial shock wave travels at a velocity, U_s, while the gas behind it flows at a lower velocity, u_o. In the limiting case when U_s and u_o are equal another interesting application is found. If a coordinate system is fixed to the shock wave both the shock wave and the gas will be at rest but the plate will be moving with some velocity, U_s. The problem is now equivalent to that of a projectile penetrating a barrier and entering a region of gas which is at rest. One application which immediately comes to mind is that of a missile launched from under water.

The purpose of the present investigation was to study the unsteady boundary layer development both on a semi-infinite flat plate mounted in a shock tube and on a semi-infinite flat plate penetrating a barrier. The momentum and energy equations of the boundary layer are developed and numerical solutions are obtained for both cases. Results are presented for the shear stress and enthalpy fields and for the heat transfer rate at the wall. Experimental verification is ob-

Figure 1. Typical schlieren photograph of a developing boundary layer

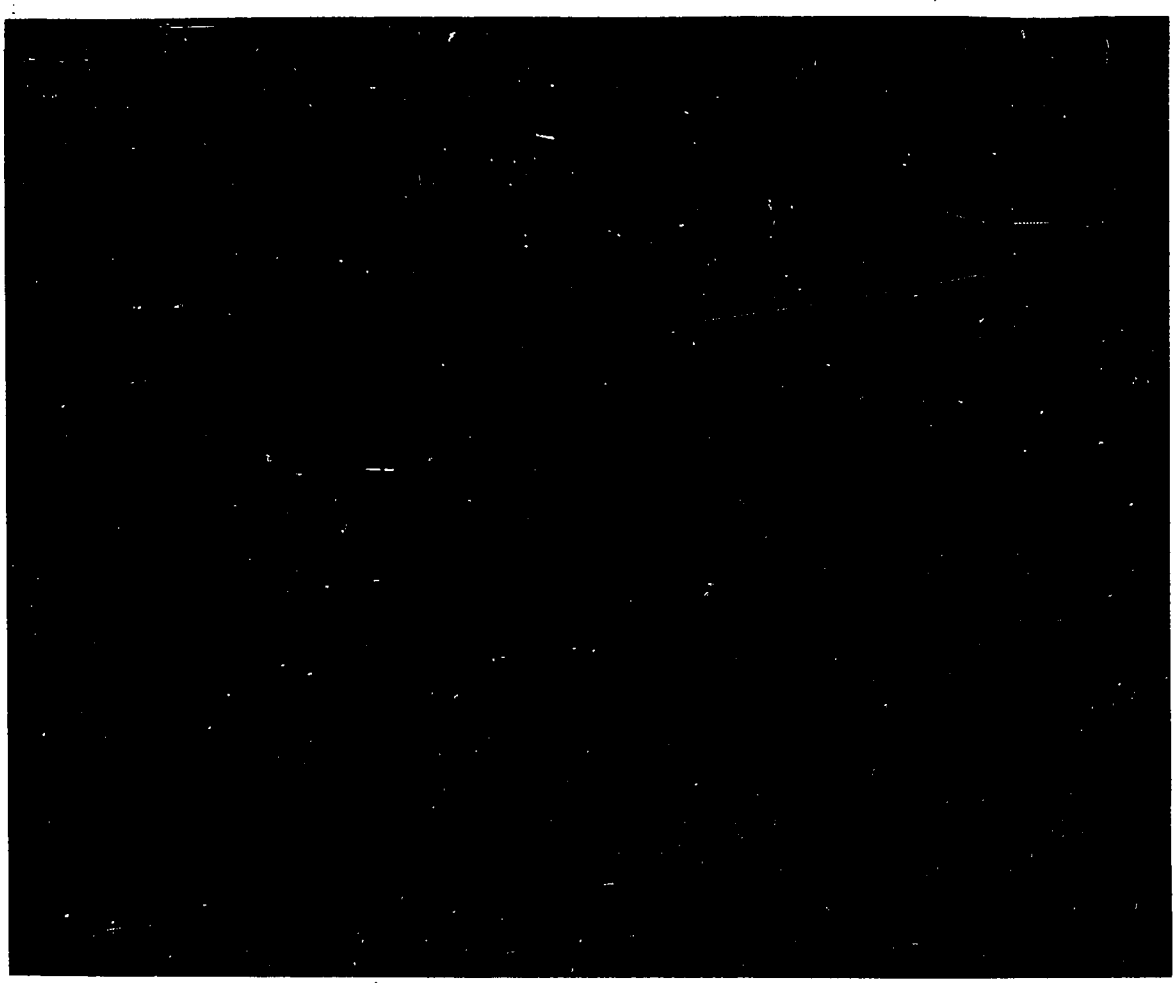

tained over a range of the significant parameters by measuring heat transfer rates on a flat plate mounted in a shock tube.

REVIEW OF LITERATURE

Unsteady Boundary Layers

A review of the general topic of unsteady boundary layers may be found in Stewartson (32,33). Unsteady boundary layers may be divided into three groups. First one might consider the topic of boundary layer instability which has been treated by Schlichting (29) as well as by many other authors. A second class occurs when the boundary layer is basically steady but subject to small pertubations in the free stream properties. A typical problem of this type is treated by Sarma (28) where the boundary layer equations are linearized.

The third class, to which the present problem belongs, is that of developing boundary layers in which the external flow undergoes large changes. Pertinent examples of this class of boundary layers will be considered in more detail in the following sections.

The Rayleigh Problem

The Rayleigh problem, which involves the impulsive setting into motion of a flat plate which is initially at rest in a quiet gas, is of interest because of a limiting case of the present problem. The problem considered here involves a flow field set up by a shock wave moving over a semi-infinite flat plate. Initially the plate and the gas are at rest with respect to each other. Consider the limiting case of a very

weak shock, essentially an acoustic wave, in which property changes across the wave are very small. The fluid velocity behind the wave will be very small, hence a particle near the leading edge of the plate will move a negligible distance in the time required for the shock wave to move across the plate. Therefore, in this limiting case the problem is the same as setting a semi-infinite flat plate into motion impulsively, a form of the Rayleigh problem.

The classical Rayleigh problem involves an infinite flat plate set impulsively into motion. This problem has been treated by Illingworth (16) from a boundary layer point of view which is restricted to large time periods. The case where initial gradients of velocity and enthalpy are allowed in the external flow is treated by Traugott (34) again using a boundary layer approach. The results are then matched with the inviscid outer region by an iterative technique. Howarth (15) uses the equations of motion in a linearized form assuming a small Mach number. The above three treatments all assume compressible flow with viscosity proportional to temperature and Prandtl number equal to unity.

The modified form of the Rayleigh problem which is of the most interest here is that of a semi-infinite flat plate set impulsively into motion. Stewartson (31) treats this problem from a boundary layer point of view. His treatment allows for compressible flow, however, viscosity is assumed propor-

tional to temperature. His results show that for $u_o t < x$ the velocity field is independent of x but for larger values of time the velocity field is a function of both x and t. A numerical solution using the full equations of motion is reported by Harlow and Meixner (13). The results are found to be in basic agreement with the results of Stewartson although some discrepancies are noted.

The Boundary Layer on the Side Wall of a Shock Tube

As a shock wave passes over a semi-infinite flat plate there exists an initial period when the flow is unaware of the leading edge of the plate. During this initial period of time the flow behaves as if the semi-infinite flat plate were an infinite flat plate, such as the shock tube wall.

During the past ten years much work has been done on the boundary layer that builds up on the side wall of a shock tube behind the initial shock wave. One of the earliest investigations of this problem was by Mirels (24). By attaching a coordinate system to the shock wave the boundary layer flow is found to be steady and similar solutions are valid. By defining the appropriate transformations and assuming that viscosity is proportional to temperature ($\rho\mu$ constant across the boundary layer) Mirels showed that the momentum equation for the laminar compressible boundary layer could be written as:

$$f''' + ff'' = 0 \qquad (1)$$

Where: $f' = u/u_e$

This is the familiar Blasius equation which appears in steady flat plate boundary layer flow. However, different boundary conditions are found to apply. Two boundary conditions are common to both cases:

$$f(0) = 0$$

$$f'(\infty) = 1$$

In the case of steady flat plate flow the third boundary condition is:

$$f'(0) = 0$$

since the plate is at rest in this coordinate system and no slip is assumed at the wall.

In the case of a shock tube wall boundary layer the third boundary condition is:

$$f'(0) = \frac{u_w}{u_e}$$

since in the coordinate system attached to the shock wave the wall is moving with velocity u_w and again no slip is assumed at the wall.

The energy equation and its appropriate boundary conditions are the same in both cases. The energy equation is:

$$T'' + PrfT' + Pr(\frac{C_p}{C_v}-1)M_e^2(f'')^2 = 0 \qquad (2)$$

(where Pr is assumed constant)

The boundary conditions on T are fixed by the constant free

stream temperature and, in the case of an isothermal wall, by the constant wall temperature.

In Reference 24 Mirels carries out numerical solutions to these equations. In Reference 22 he presents additional solutions and extends the work to boundary layers behind expansion waves. Solutions for both the momentum and energy equations are presented for values of the parameter u_w/u_e of: 0 (steady flat plate solution), 2, 4, and 6. These last three values correspond to shock Mach numbers of 1.6, 3.15, and 5.75 respectively when real gas effects are considered. Additional results extending up to a shock Mach number of fourteen are presented by Mirels in References 25 and 23. In Reference 25 solutions are carried out allowing the product of density times viscosity, $\rho\mu$, to vary across the boundary layer but assuming the Prandtl number constant and equal to one. In Reference 23 the work is extended to a Prandtl number of 0.72, again assumed constant. In addition References 25 and 23 treat turbulent boundary layers behind advancing shock waves as well as the laminar case.

Other theoretical work on this problem has been presented by Bromberg (3) who solved the momentum and energy equations for the case of $\rho\mu$ constant across the boundary layer and Prandtl number equal to one. Bershader and Allport (2) present a treatment under the same assumptions. A treatment utilizing an integral approach to the boundary layers and

oriented more toward solving the complete flow situation in a shock tube is presented by Trimpi and Cohen (35). A survey paper by Becker (1) reviews the theoretical and experimental work that had been done on shock tube wall boundary layers prior to 1959. An extension to the case of a laminar boundary layer behind a shock wave moving with nonuniform velocity such as an attenuating shock wave or a blast wave was presented by Mirels and Hamman (26). The shock wave was assumed to have a power law variation with time. Both two-dimensional and axisymmetric boundary layers were treated under the assumptions of constant Prandtl number, viscosity proportional to temperature, constant specific heat, and a small wall to free stream temperature ratio.

The validity of the above theories has been checked by experiment at least up to a shock Mach number of 7.5. Hartunian et al. (14) obtained experimental heat transfer data on the side wall of a shock tube in both the laminar and turbulent regime. The data in the laminar regime agreed quite well with Mirels' solutions which assume variable $\rho\mu$ and a Prandtl number of 0.72. The turbulent data also agreed well with Mirels' predictions. Data were taken up to a shock Mach number of 7.5.

Several measurements of velocity profiles in the shock tube boundary layer are available (21,2,9,4). Martin (21) measured density profiles across the boundary layer with an

interferometer and derived velocity profiles from these measurements. Bershader and Allport (2) also measured density profiles with an interferometer. In addition they obtained some wall temperature and heat transfer measurements with thin film resistance thermometers. Gion (9) and Chen and Emrich (4) used a particle tracer technique to measure velocity profiles directly. These investigations show a reasonable amount of agreement with the results of Mirels' theory.

The Shock-Induced Unsteady Laminar Boundary Layer

The boundary layer developing on a flat plate with a sharp leading edge behind an advancing shock wave is treated by Lam and Crocco (19). They developed the unsteady boundary layer equations under the following assumptions:

1. The boundary layer approximations are valid throughout the region of interest.
2. The boundary layer is laminar.
3. The initial shock wave remains plane.
4. Viscosity is proportional to temperature.
5. The Prandtl number is constant.

The momentum equation was put into a form suitable for solution by numerical means and a solution was obtained only for the case of an infinitely weak shock wave. Suggestions were made concerning the numerical solution of the energy

equation although no solutions were attempted. A somewhat more detailed account of this work may be found in Lam (20). The extent of the work of Lam and Crocco (19) will be noted in the development of the problem in the following sections.

DEFINITION OF THE PROBLEM

Consider a flat plate with sharp leading edge mounted in a shock tube as shown in Figure 2(a). Affix the origin of a coordinate system at the leading edge of the plate with positive x measured along the plate and y measured perpendicular to the plate. At time zero the initial shock wave will be located at the leading edge of the plate. As time increases the shock wave will move across the plate with velocity U_s. The shock strength will be characterized by the quantity A defined as the ratio of shock velocity, U_s, to gas velocity behind the shock, u_o.

The unsteady boundary layer which develops behind the initial shock wave will be examined after imposing the following assumptions:

1. The flow is compressible.
2. The boundary layer is laminar.
3. The boundary layer approximations are valid throughout the region of interest.
4. The initial shock wave remains plane as it passes over the plate.
5. The speed of the initial shock wave remains constant and conditions remain uniform in the inviscid region behind the shock wave.
6. The Prandtl number is constant across the boundary layer.

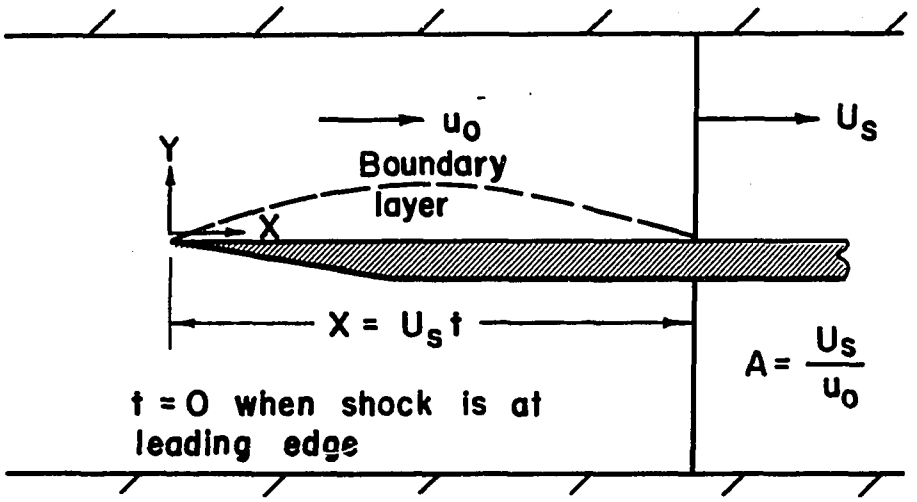

Figure 2(a). Flat plate showing the coordinate system used

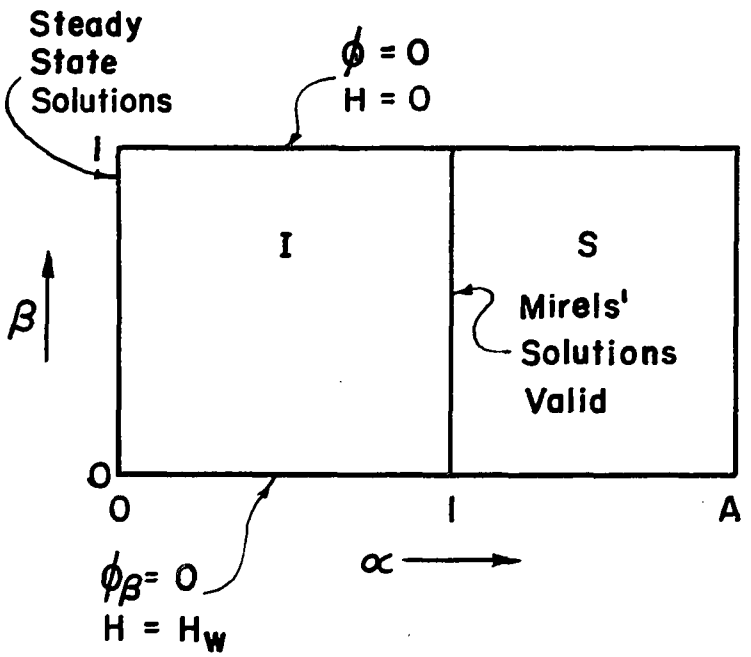

Figure 2(b). Regions of the α-β domain

7. The product $\rho\mu$ is allowed to vary across the boundary layer. However, comparisons are made with solutions assuming $\rho\mu$ constant across the boundary layer.

THEORETICAL TREATMENT

Development of Equations

The unsteady, two-dimensional, compressible, laminar boundary layer equations with zero pressure gradient can be written as follows (32):

Continuity equation:

$$\frac{\partial \rho}{\partial t} + \frac{\partial (\rho u)}{\partial x} + \frac{\partial (\rho v)}{\partial y} = 0 \tag{3}$$

Momentum equation:

$$\rho \frac{\partial u}{\partial t} + \rho u \frac{\partial u}{\partial x} + \rho v \frac{\partial u}{\partial y} = \frac{\partial}{\partial y}(\mu \frac{\partial u}{\partial y}) \tag{4}$$

Energy equation:

$$\rho \frac{\partial h}{\partial t} + \rho u \frac{\partial h}{\partial x} + \rho v \frac{\partial h}{\partial y} = \frac{\partial}{\partial y}(k \frac{\partial T}{\partial y}) + \mu (\frac{\partial u}{\partial y})^2 \tag{5}$$

The boundary conditions for flat plate flow at the wall and in the free stream are:

$$\begin{aligned} u(x, 0, t) &= 0 \\ v(x, 0, t) &= 0 \\ h(x, 0, t) &= h_w \\ u(x, \infty, t) &= u_o \\ h(x, \infty, t) &= h_o \end{aligned} \tag{6}$$

Substituting into the momentum equation, the second boundary condition ($v(x, 0, t) = 0$) may be replaced by:

$$\frac{\partial}{\partial y} (\mu \frac{\partial u}{\partial y}) = 0, \qquad \text{at the wall.}$$

The Crocco transformation will be used in this analysis. The following variables are defined.

$$\underline{\tau} = \mu\frac{\partial u}{\partial y} = \underline{\tau}(\xi, u, \eta)$$

$$h = h(\xi, u, \eta)$$

$$\xi = x \tag{7}$$

$$u = u(x, y, t)$$

$$\eta = t$$

The transformation equations may then be written as:

$$\frac{\partial}{\partial x} = \frac{\partial}{\partial \xi} - \frac{\frac{\partial y}{\partial \xi}}{\frac{\partial y}{\partial u}}\frac{\partial}{\partial u}$$

$$\frac{\partial}{\partial y} = (1/\frac{\partial y}{\partial u})\frac{\partial}{\partial u} \tag{8}$$

$$\frac{\partial}{\partial t} = \frac{\partial}{\partial \eta} - \frac{\frac{\partial y}{\partial \eta}}{\frac{\partial y}{\partial u}}\frac{\partial}{\partial u}$$

With this transformation the continuity and momentum equations can be combined to yield:

$$\underline{\tau}_{uu} + (\frac{\rho\mu}{\underline{\tau}})_{\eta} + u(\frac{\rho\mu}{\underline{\tau}})_{\xi} = 0 \tag{9}$$

The energy equation becomes:

$$\rho\mu[h_{\eta} + uh_{\xi}] + \frac{1}{2}(1-\frac{1}{Pr})(\underline{\tau}^2)_u h_u$$

$$= \underline{\tau}^2[1 + \frac{\partial}{\partial u}(\frac{1}{Pr} h_u)] \tag{10}$$

The boundary conditions can now be written as:

At $u = 0$:

$$\frac{\partial \tau}{\partial u} = 0, \quad h = h_w \tag{11}$$

At $u = u_o$:

$$\underline{\tau} = 0, \quad h = h_o, \quad \underline{\tau}\,\underline{\tau}_u = 0$$

A set of dimensionless variables are defined.

$$\tau = \frac{1}{\rho_o u_o^2} \left[\mu \frac{\partial u}{\partial y}\right]$$

$$H = \frac{h - h_o}{h_o}$$

$$\alpha = \frac{x}{u_o t} \tag{12}$$

$$\beta = u/u_o$$

$$\gamma = \frac{u_o^2 t}{\nu_o}$$

$$C = \frac{\rho \mu}{\rho_o \mu_o}$$

Where the dependent variables are τ and H and the independent variables are α, β, and γ. C will be assumed to be a known function of H only. The transformation equations are:

$$\frac{\partial}{\partial \xi} = \frac{u_o}{\nu_o \gamma} \frac{\partial}{\partial \alpha}$$

$$\frac{\partial}{\partial u} = \frac{1}{u_o} \frac{\partial}{\partial \beta} \tag{13}$$

$$\frac{\partial}{\partial \eta} = \frac{u_o^2}{\nu_o} \left[\frac{\partial}{\partial \gamma} - \frac{\alpha}{\gamma} \frac{\partial}{\partial \alpha}\right]$$

Under this transformation the momentum equation becomes:

$$\tau^2 \tau_{\beta\beta} = C\tau_\gamma - \tau C_\gamma + C\left(\frac{\beta-\alpha}{\gamma}\right)\tau_\alpha + \tau\left(\frac{\alpha-\beta}{\gamma}\right)C_\alpha \tag{14}$$

The energy equation is:

$$\tau^2\left[\frac{u_o^2}{h_o} + (1/Pr)H_{\beta\beta}\right] = CH_\gamma + C\left(\frac{\beta-\alpha}{\gamma}\right)H_\alpha + (1-1/Pr)\tau\tau_\beta H_\beta \tag{15}$$

The boundary conditions become:

$$\begin{aligned} &\beta = 0; \quad \tau_\beta = 0, \quad H = H_w \\ &\beta = 1; \quad \tau = 0, \quad H = 0 \end{aligned} \tag{16}$$

In order to simplify the momentum equation, Equation 14, somewhat, it may be assumed that changes in the fluid properties are significant only across the boundary layer in the direction perpendicular to the main flow. Hence derivatives of C with respect to α and γ may be neglected but derivatives with respect to β must be retained. The momentum equation can then be reduced to:

$$\tau^2 \tau_{\beta\beta} = C\tau_\gamma + C\left(\frac{\beta-\alpha}{\gamma}\right)\tau_\alpha \qquad (17)$$

In order to further simplify both the momentum and energy equations the following procedure is followed. The steady flat plate boundary layer equations are found to be satisfied by a separation of variables solution of the form:

$$\tau = X(x)\cdot U(u) \qquad (18)$$

The solution for the X equation has the form: $X = 1/\sqrt{x}$. This allows the shear stress to become infinite at the leading edge where the boundary layer thickness approaches zero. In the present case a similar dependence on x might be expected although the boundary layer is no longer steady. With this in mind the following dependent variable is defined.

$$\phi(\alpha,\beta,\gamma) = \tau(\alpha,\beta,\gamma)\ \sqrt{\alpha\gamma} \qquad (19)$$

In terms of this variable the momentum and energy equations become respectively:

$$\phi^2\phi_{\beta\beta} + \left(\tfrac{1}{2}\right)\beta C\phi = \alpha(\beta-\alpha)C\phi_\alpha + \alpha\gamma\phi_\gamma \qquad (20)$$

$$\phi^2\left[\frac{u_o^2}{h_o} + \frac{1}{Pr}H_{\beta\beta}\right] = C\alpha(\beta-\alpha)H_\alpha + (1-1/Pr)\phi\phi_\beta H_\beta$$

$$+ C\alpha\gamma H_\gamma \qquad (21)$$

Since this definition of ϕ superimposes an x dependence upon the solution, α might be allowed to be the primary time variable with all derivatives with respect to γ neglected; that is, assuming γ derivatives to be small compared with derivatives with respect to α and β. The validity of this

assumption will be considered further later.

The momentum and energy equations then become partial differential equations in two independent variables, α and β.

$$\phi^2 \phi_{\beta\beta} + \frac{1}{2} \beta C \phi = \alpha(\beta-\alpha) C \phi_\alpha \tag{22}$$

$$\phi^2 \left[\frac{u_o^2}{h_o} + 1/Pr\ H_{\beta\beta}\right] = C\alpha(\beta-\alpha) H_\alpha + (1-1/Pr)\phi\phi_\beta H_\beta \tag{23}$$

The boundary conditions on β are:

$$\begin{aligned} &\beta = 0;\ \phi_\beta(\alpha,0) = 0,\ H(\alpha,0) = H_w \\ &\beta = 1;\ \phi(\alpha,1) = 0,\ H(\alpha,1) = 0 \end{aligned} \tag{24}$$

Consider the domain of the independent variables α and β which is of interest here. It has been noted that $\beta = 0$ corresponds to the wall while $\beta = 1$ corresponds to the free stream. The appropriate boundary conditions on β have already been determined.

The variable α was defined as $\frac{x}{u_o t}$. Since α is primarily a time variable $\alpha = 0$ will correspond to infinite time. At $\alpha = A$ it is noted that $t = \frac{x}{U_s}$. This is the time at which the initial shock wave passes any given x station. Hence it is the earliest time of interest. Thus the domain $0 \leq \beta \leq 1,\ 0 \leq \alpha \leq A$ is of concern.

Consider now the point $\alpha=1$. This gives $t = \frac{x}{u_o}$ or the time required for a particle in the free stream which was just over the leading edge initially to travel to some x station.

At smaller times this x station would not have been aware of the leading edge but at larger times the effects of the leading edge will be felt. Hence in the portion of the domain $1 \leq \alpha \leq A$ the plate will appear to be infinite and the similar solutions of Mirels (23) will be valid. This region is labeled the S region in Figure 2(b). The rest of the region, $0 \leq \alpha \leq 1$, will be denoted as the I region or interaction region in which effects of the leading edge are felt. Since the solutions of Mirels are valid in the S region it is the I region which will be of concern here.

It is necessary to determine the boundary condition on ϕ and H at $\alpha = 0$ and $\alpha = 1$ in order to solve the momentum and energy equations. The similar solutions of Mirels for the shear stress and enthalpy will be denoted by $S(\beta;A)$ and $H_s(\beta;A)$ respectively. When the shock strength parameter A goes to zero these solutions reduce to the steady flat plate solutions. By transforming to the present coordinate system the shear stress and enthalpy in the S region are found to be:

$$\phi(\alpha,\beta) = \frac{\sqrt{\alpha(A-1)}}{A-\alpha} S(\beta;A)$$

$$H(\alpha,\beta) = H_s(\beta;A) \qquad (25)$$

At infinite time, $\alpha = 0$, the well known steady state solutions must be valid. Hence the boundary conditions at $\alpha = 1$ and $\alpha = 0$ may be written as:

$$\phi(1,\beta) = S(\beta;A)$$
$$H(1,\beta) = H_s(\beta;A) \qquad (26)$$
$$\phi(0,\beta) = S(\beta;0)$$
$$H(0,\beta) = H_s(\beta;0)$$

It is noted at this point that the only parameter involved in the momentum and energy equations, Equations 22 and 23, and their boundary conditions, listed above in Equation 24 and 26, is the shock strength A. This is true since for shock tube flow with a fixed initial gas temperature, room temperature in this case, the quantities $\frac{u_o^2}{h_o}$ and H_w are a function only of A.

The problem is now reduced to solving Equation 22 and 23 over the interaction region defined by:

$$0 \leq \alpha \leq 1,\ 0 \leq \beta \leq 1$$

Consider the momentum equation, Equation 22 first. The boundary conditions for $\phi(\alpha,\beta)$ in the above defined region are:

$$\phi(0,\beta) = S(\beta;0)$$
$$\phi(1,\beta) = S(\beta;A)$$
$$\phi_\beta(\alpha,0) = 0$$
$$\phi(\alpha,1) = 0$$

A finite difference procedure was first tried to solve the momentum equation. Since this procedure seemed to be very unstable it was abandoned in favor of the method next described.

Equation 22 is first integrated across the boundary layer, that is, with respect to β. Equation 22 may be rewritten in the form:

$$\phi_{\beta\beta} = \frac{C}{\phi}\left[\alpha(\beta-\alpha)\frac{\phi_\alpha}{\phi} - \beta/2\right] \tag{27}$$

Integrating from the wall to some arbitrary point p in the boundary layer:

$$\int_o^p \phi_{\beta\beta}(\alpha,\lambda)\,d\lambda = \int_o^p \frac{C(\lambda)}{\phi(\alpha,\lambda)}\left[\alpha(\lambda-\alpha)\frac{\phi_\alpha}{\phi}(\alpha,\lambda) - \lambda/2\right]d\lambda$$

Carrying out the integration of the left hand side and applying the boundary condition at the wall yields:

$$\int_o^p \phi_{\beta\beta}(\alpha,\lambda)\,d\lambda = \phi_\beta(\alpha,\lambda)\Big|_o^p$$

$$= \phi_\beta(\alpha,p) - \phi_\beta(\alpha,0) = \phi_\beta(\alpha,p)$$

A second integration is carried out from a point of interest, β, to the free stream. It is noted that:

$$\int_\beta^1 2\phi(\alpha,p)\phi_\beta(\alpha,p)\,dp = \int_\beta^1 [\phi^2(\alpha,p)]_\beta\,dp$$

$$= \phi^2(\alpha,p)\Big|_\beta^1 = \phi^2(\alpha,1) - \phi^2(\alpha,\beta)$$

$$= -\phi^2(\alpha,\beta)$$

where the boundary condition at the free stream, $\beta = 1$, has been applied. The momentum equation now becomes:

$$\phi(\alpha,\beta) = \left[\int_{\beta}^{1} \phi(\alpha,p)\,dp \int_{o}^{p} \frac{C(\lambda)}{\phi(\alpha,\lambda)} (\lambda - 2\alpha(\lambda-\alpha)\frac{\phi_\alpha}{\phi}(\alpha,\lambda))\,d\lambda\right]^{1/2} \tag{28}$$

Equation 28 is an expression for $\phi(\alpha,\beta)$ at any point (α,β) which involves the solution for ϕ over the α-β field. This expression might be used in an iteration technique.

Equation 28 with $C(\lambda) = 1$ was developed by Lam and Crocco (19) and used in an integral iteration procedure. One solution was carried out for the case of an infinitely weak shock, $A = \infty$. Simpson's rule was used in the numerical integration and a central difference approximation was used for derivatives with respect to α. Some convergence problems were noted, probably due to a lack of significant figures, but a seemingly realistic solution was obtained.

The right hand side of Equation 28 could be evaluated numerically with a conventional integration rule. Instead ϕ was approximated by a piecewise linear function since it is somewhat more well behaved than the integrand.

The β axis was divided into IMAX-1 equal increments and the α axis into KMAX-1 equal increments. A piecewise linear function $\bar{\phi}$ is defined as follows:

$$\bar{\phi}(\lambda) = \phi(I-1) + \frac{\phi(I) - \phi(I-1)}{\beta(I) - \beta(I-1)} (\lambda - \beta(I-1)) \tag{29}$$

Where:

$$\beta(I-1) \leq \lambda \leq \beta(I)$$

$$I = 2,3,\text{---} \text{ IMAX}$$

It will be understood that ϕ is to be evaluated at some point K on the α axis unless otherwise noted. Evaluating λ from the above one obtains:

$$\lambda = C1(I)\bar{\phi}(\lambda) + C2(I) \tag{30}$$

Where:

$$C1(I) = \frac{\beta(I) - \beta(I-1)}{\phi(I) - \phi(I-1)} \tag{31}$$

$$C2(I) = \beta(I-1) - C1(I)\phi(I-1) \tag{32}$$

The following central difference approximation was used for partial derivatives with respect to α.

$$\phi_\alpha(\alpha,\lambda) = \frac{\phi(\alpha+\Delta\alpha,\lambda) - \phi(\alpha-\Delta\alpha,\lambda)}{2\Delta\alpha} \tag{33}$$

These relations are substituted into Equation 28 and the indicated integration is performed. After considerable, though straightforward, algebraic manipulation the following expression for the momentum equation is obtained.

$$\phi(\alpha,\beta) = \left\{ \sum_{J=I_\beta+1}^{IMAX} C1(J) \left[C5(J)C9(J) + C6(J)(\phi^3(J) - \phi^3(J-1)) \right.\right.$$

$$\left.\left. + C7(J)(\phi(J) - \phi(J-1)) + \frac{C8(J)}{2}(\phi^2(J) - \phi^2(J-1)) \right] \right\}^{1/2} \tag{34}$$

Where:

$$C9(J) = \frac{\phi^2(J)}{2} \ln \phi(J) - \frac{\phi^2(J-1)}{2} \ln \phi(J-1) - \frac{\phi^2(J)}{4} + \frac{\phi^2(J-1)}{4}$$

$$C8(J) = \sum_{I=2}^{J-1}\left[C5(I)\ \ln\frac{\phi(I)}{\phi(I-1)} + C6(I)(\phi(I) - \phi(I-1)) + C7(I)\left(\frac{1}{\phi(I)} - \frac{1}{\phi(I-1)}\right)\right]$$

$$- \left[C5(J)\ \ln\phi(J-1) + C6(J)\phi(J-1) + \frac{C7(J)}{\phi(J-1)}\right]$$

$$C7(J) = \frac{\alpha}{\Delta\alpha}\left[C1(J)C2(J)C4(J) - \alpha C1(J)C4(J)\right]\left[\frac{C(J) + C(J-1)}{2}\right]$$

$$C6(J) = \left[\frac{C(J) + C(J-1)}{2}\right]\left[C1(J)\right]^2\left[1 - \frac{\alpha C3(J)}{\Delta\alpha}\right]$$

$$C5(J) = C1(J)\left[\frac{C(J) + C(J-1)}{2}\right]\left[C2(J) - \frac{\alpha}{\Delta\alpha}^2 C3(J) - \frac{\alpha}{\Delta\alpha}(C2(J)C3(J) + C1(J)C4(J))\right]$$

$$C4(J) = \frac{(C1(K-1,J) - C1(K+1,J))C2(K,J)}{C1(K+1,J)C1(K-1,J)} + \frac{C1(K+1,J)C2(K-1,J) - C1(K-1,J)C2(K+1,J)}{C1(K+1,J)C1(K-1,J)}$$

$$C3(J) = \frac{(C1(K-1,J) - C(K+1,J))C1(K,J)}{C1(K+1,J)C1(K-1,J)}$$

Equation 34 is the form of the momentum equation which was used in the numerical solutions.

The energy equation, Equation 23, will now be considered. The boundary conditions for $H(\alpha,\beta)$ over the region, $0 \leq \alpha \leq 1$, $0 \leq \beta \leq 1$, are:

$$H(0,\beta) = H_s(\beta;0)$$

$$H(1,\beta) = H_s(\beta;A)$$

$$H(\alpha,0) = H_w$$

$$H(\alpha,1) = 0$$

Equation 23 may be rewritten as:

$$H_{\beta\beta} = Pr\left\{-\frac{u_o^2}{h_o} + \frac{1}{\phi^2}\left[\alpha(\beta-\alpha)CH_\alpha + (1-1/Pr)\phi\phi_\beta H_\beta\right]\right\} \qquad (35)$$

Rearranging and multiplying thru by ϕ^{1-Pr} yields:

$$H_{\beta\beta}\phi^{1-Pr} + (1-Pr)\phi^{-Pr}\phi_\beta H_\beta = \frac{Pr\ u_o^2}{h_o}\phi^{1-Pr} + \frac{CPr\alpha(\beta-\alpha)H_\alpha}{\phi^{1+Pr}} \qquad (36)$$

It is noted that:

$$\frac{\partial}{\partial\beta}\left(\phi^{1-Pr}H_\beta\right) = H_{\beta\beta}\phi^{1-Pr} + (1-Pr)\phi^{-Pr}\phi_\beta H_\beta$$

By integrating Equation 36 from the wall to some arbitrary point p in the boundary layer in a like manner as with the momentum equation one obtains:

$$\int_o^p \frac{\partial}{\partial\beta}\left(\phi^{1-Pr}(\alpha,\lambda)H_\beta(\alpha,\lambda)\right)d\lambda = -\frac{Pr\ u_o^2}{h_o}\int_o^p \phi^{1-Pr}(\alpha,\lambda)\,d\lambda$$

$$+ \alpha Pr \int_o^p \frac{C(\lambda)(\lambda-\alpha)H_\alpha(\alpha,\lambda)}{\phi^{1+Pr}(\alpha,\lambda)} d\lambda$$

Evaluating the left side and rearranging one obtains:

$$H_\beta(\alpha,p) = H_\beta(\alpha,0)\left[\frac{\phi(\alpha,0)}{\phi(\alpha,p)}\right]^{1-Pr} - \frac{Pr\ u_o^2}{h_o}\int_o^p \left[\frac{\phi(\alpha,\lambda)}{\phi(\alpha,p)}\right]^{1-Pr} d\lambda$$

$$+ \alpha Pr \int_o^p \frac{C(\lambda)\ (\lambda-\alpha)H_\alpha(\alpha,\lambda)}{\phi^{1-Pr}(\alpha,p)\phi^{1+Pr}(\alpha,\lambda)} d\lambda$$

Again it is necessary to integrate a second time from a point, β, to the free stream. Applying the boundary condition in the free stream to the left hand side yields:

$$\int_\beta^1 H_\beta(\alpha,p)dp = H(\alpha,1) - H(\alpha,\beta)$$

$$= -H(\alpha,\beta)$$

Hence the energy equation becomes:

$$H(\alpha,\beta) = -H_\beta(\alpha,0)\int_\beta^1 \left[\frac{\phi(\alpha,0)}{\phi(\alpha,p)}\right]^{1-Pr} dp$$

$$+ \frac{Pr\ u_o^2}{h_o}\int_\beta^1 dp \int_o^p \left[\frac{\phi(\alpha,\lambda)}{\phi(\alpha,p)}\right]^{1-Pr} d\lambda$$

$$- \alpha Pr \int_\beta^1 dp \int_o^p \frac{C(\lambda)(\lambda-\alpha)H_\alpha(\alpha,\lambda)}{\phi^{1-Pr}(\alpha,p)\phi^{1+Pr}(\alpha,\lambda)} d\lambda \qquad (37)$$

The piecewise linear expression for ϕ defined by Equation 29 will be used again. In a like manner a piecewise linear function $\bar{H}$ is defined.

$$\bar{H}(\lambda) = H(I-1) + \frac{H(I) - H(I-1)}{\beta(I) - \beta(I-1)} (\lambda - \beta\ (I-1)) \qquad (38)$$

where

$$\beta(I-1) \leq \lambda \leq \beta\ (I)$$

$$I = 2,3,\ldots\ IMAX$$

Partial derivatives with respect to α will be approximated with the central difference approximation as used before in Equation 33.

$$H_\alpha(\alpha,\lambda) = \frac{H(\alpha+\Delta\alpha,\lambda) - H(\alpha-\Delta\alpha,\lambda)}{2\Delta\alpha} \qquad (39)$$

These substitutions are made in Equation 37 and the indicated integrations are carried out. The first term becomes after some manipulation:

$$\int_\beta^1 \left[\frac{\phi(\alpha,0)}{\phi(\alpha,p)}\right]^{1-Pr} dp = [\phi(\alpha,0)]^{1-Pr} \sum_{I_\beta+1}^{IMAX} \frac{C1(I)}{Pr} \left[\phi^{Pr}(I) - \phi^{Pr}(I-1)\right] \qquad (40)$$

Where C1(I) and C2(I) are defined as in Equation 31 and 32.

The second term becomes:

$$\int_\beta^1 dp \int_0^p \left[\frac{\phi(\alpha,\lambda)}{\phi(\alpha,p)}\right]^{1-Pr} d\lambda \qquad (41)$$

$$= \sum_{I_\beta+1}^{IMAX} \left[\frac{C1(J)C11(J)}{Pr} (\phi^{Pr}(J) - \phi^{Pr}(J-1)) + \frac{C1^2(J)}{2(2-Pr)} (\phi^2(J) - \phi^2(J-1)\right]$$

where

$$C11(J) = \sum_{I=2}^{J-1}\left[\frac{C1(I)}{2-Pr}\left(\phi^{2-Pr}(I)-\phi^{2-Pr}(I-1)\right)\right]$$

$$- \left(\frac{C1(J)}{2-Pr}\right)\phi^{2-Pr}(J-1)$$

The last term becomes:

$$\int_{\beta}^{1} dp \int_{o}^{p} \frac{C(\lambda)(\lambda-\alpha)H_{\alpha}(\alpha,\lambda)}{\phi^{1-Pr}(\alpha,p)\phi^{1+Pr}(\alpha,\lambda)}\, d\lambda$$

$$= \sum_{I_{\beta}+1}^{IMAX} C1(J)\left[\frac{C16(J)}{Pr}\left(\phi^{Pr}(J) - \phi^{Pr}(J-1)\right) + C18(J)\left(\phi(J)-\phi(J-1)\right)\right.$$

$$\left. + \frac{C19(J)}{2}\left(\phi^{2}(J)-\phi^{2}(J-1)\right)\right] + \sum_{I_{\beta}+1}^{IMAX-1}\left[C1(J)C17(J)\ln\frac{\phi(J)}{\phi(J-1)}\right] \quad (42)$$

where

$$C19(J) = \frac{C1(J)C15(J)C10(J)}{2-Pr}$$

$$C18(J) = \left[\frac{C1(J)C14(J)-C15(J)(\alpha-C2(J))}{1-Pr}\right]C10(J)$$

$$C17(J) = \left[\frac{C14(J)(\alpha-C2(J))}{Pr}\right]C10(J)$$

$$C16(J) = \sum_{I=2}^{J-1}\left[C17(J)\left\{\phi^{-Pr}(I) - \phi^{-Pr}(I-1)\right\}\right.$$

$$+C18(I)\ \{\phi^{1-Pr}(I) - \phi^{1-Pr}(I-1)\} + C19(I)\{\phi^{2-Pr}(I) - \phi^{2-Pr}(I-1)\}\Big]$$

$$= C17(J)\phi^{-Pr}(J-1) - C18(J)\phi^{1-Pr}(J-1) - C19(J)\phi^{2-Pr}(J-1)$$

$$C15(J) = C1(J)\ [C3(K+1,J) - C13(K-1,J)]$$

$$C14(J) = C12(K+1,J) - C12(K-1,J)$$

$$+ C2(J)\ [C13(K+1,J) - C13(K-1,J)]$$

$$C13(J) = \frac{H(J) - H(J-1)}{\beta(J) - \beta(J-1)}$$

$$C12(J) = H(J-1) - C13(J)\beta(J-1)$$

It is assumed that terms are evaluated at the point K on the α axis unless noted otherwise.

The following second order expression was used for the partial derivative of H with respect to β at the wall.

$$H_\beta(\alpha,0) = (3H_w + 4H(\alpha,\Delta\beta) - H(\alpha,2\Delta\beta))/2\Delta\beta \qquad (43)$$

The final expression for the energy equation then can be written:

$$H(\alpha,\beta) =$$

$$-[3H_w+4H(\alpha,\Delta\beta)-H(\alpha,2\Delta\beta)]\frac{[\phi(\alpha,0)]^{1-Pr}}{2\Delta\beta}\sum_{I_\beta+1}^{IMAX}\frac{C1(I)}{Pr}[\phi^{Pr}(I)-\phi^{Pr}(I-1)]$$

$$+ \frac{Pr\ u_o^2}{h_o} \sum_{I_\beta+1}^{IMAX} \left[\frac{C1(J)C11(J)}{Pr} \{\phi^{Pr}(J) - \phi^{Pr}(J-1)\} \right.$$

$$\left. + \frac{C1^2(J)}{2(2-Pr)} \{\phi^2(J) - \phi^2(J-1)\} \right]$$

$$- \alpha Pr \sum_{I_\beta+1}^{IMAX} C1(J) \left[\frac{C16(J)}{Pr} \{\phi^{Pr}(J) - \phi^{Pr}(J-1)\} \right.$$

$$\left. + C18(J)\{\phi(J) - \phi(J-1)\} + \frac{C19(J)}{2} \{\phi^2(J) - \phi^2(J-1)\} \right]$$

$$- \alpha Pr \sum_{I_\beta+1}^{IMAX-1} \left[C1(J)C17(J) \ln \frac{\phi(J)}{\phi(J-1)} \right] \qquad (44)$$

This is the final form of the energy equation as it was used in the numerical solutions.

The heat transfer rate at the wall may be written as:

$$q_w = - k_w \left(\frac{\partial T}{\partial y}\right)_w$$

By transforming into the dimensionless variables used here one obtains:

$$q_w = - \frac{\sqrt{\rho_o \mu_o u_o}\ h_o}{Pr\ \sqrt{x}}\ \phi(\alpha,0)\ H_\beta(\alpha,0) \qquad (45)$$

Finally a dimensionless heat transfer parameter is defined which will be used to present the results of this investigation.

$$\bar{Q} = \frac{-q_w Pr\ \sqrt{x}}{\sqrt{\rho_o \mu_o u_o}\ h_o} = \phi(\alpha,0) H_\beta(\alpha,0) \qquad (46)$$

Numerical Solutions

The momentum equation and the energy equation were used in the numerical solutions in the form given in Equations 34 and 44.

Procedure

The numerical procedure will first be described for the case of $C(\lambda) = 1$, viscosity proportional to temperature, and then extended to the case of $C(\lambda) \neq 1$. For the case of $C(\lambda)=1$ the momentum equation, Equation 34, does not depend on the H field and may be solved independently of the energy equation. Equation 34 will be used in an iteration procedure where it has effectively the form:

$$\phi'(\alpha,\beta) = F(\phi(\alpha',\beta')) \tag{47}$$

where α' and β' may vary over the whole domain. A sequence of iterants is now defined:

$$\phi^{(n+1)} = [m(\alpha)\phi^{(n)}+\phi']/[1+m(\alpha)] \tag{48}$$

where $m(\alpha)$ is a weighting factor used to stabilize the iterants. It was found that the following expression for $m(\alpha)$ was satisfactory.

$$m(\alpha) = 1 + 7\alpha \tag{49}$$

The initial iterant is defined as:

$$\phi^{(0)}(\alpha,\beta) = \text{maximum of } [S(\beta;0);\ \frac{\sqrt{\alpha(A-1)}}{A-\alpha} S(\beta;A)]$$

In other words, both the steady state flat plate solution and Mirels' solution valid in the S region are extended beyond their limits of applicability and the one giving the larger result is used. Starting from this initial iterant an iteration procedure is carried out over the interior values of α. The values at $\alpha = 0$ and $\alpha = 1$ are maintained at their originally correct values. In practice it was found desirable to specify that $\phi_\alpha = 0$ at $\alpha = 0$ rather than to specify the value of ϕ at $\alpha = 0$. This allows solving for the steady state solution in the same iteration used for the interaction regime. It was necessary, however, to have the correct values for ϕ at $\alpha = 1$ before beginning the iteration.

A similar procedure was used for the energy equation. Again the case of $C(\lambda) = 1$ is considered first. Equation 44 has the following effective form for iteration:

$$H'(\alpha,\beta) = G[\phi(\alpha',\beta'), H(\alpha',\beta')] \qquad (50)$$

Since the momentum equation has been solved the ϕ field is available for use in this calculation. A series of iterants is defined as with the momentum equation:

$$H^{(n+1)} = [rH^{(n)} + H']/[1+r] \qquad (51)$$

Here r is a weighting factor found necessary to be at least 12 in order to stabilize the iteration. The initial iterant is defined as:

$$H^{(0)}(\alpha,\beta) = H_s(\beta;0) + \alpha[H_s(\beta;A) - H_s(\beta;0)]$$

Again an iteration procedure can be carried out on the internal values of α and β since for an isothermal wall the values of H are fixed all around the boundaries. From initial calculations with values of H specified along $\alpha = 0$ and $\alpha = 1$ it was noted that $H_\alpha = 0$ was valid at these boundaries. This behavior can be seen in Figure 3 which is a plot of H_β at the wall as a function of α for a typical shock strength. This behavior is reasonable since the similar solutions valid at the steady state and in the S region require uniform H profiles. It was found desirable to specify $H_\alpha = 0$ at $\alpha = 0$ and at $\alpha = 1$ rather than to fix the values of H there. In this way it is possible to solve for the steady state values and also determine the solution in the S region for cases where these values might not be available. It is then only necessary to have approximate values of H at $\alpha = 0$ and $\alpha = 1$ to serve as initial iterants.

The additional steps necessary when $C(\lambda) \neq 1$ but instead depends on H will now be considered. The momentum and energy equations are now coupled. It is necessary to assume a solution for H in order to solve the momentum equation. The resulting solution for ϕ is then used to solve the energy equation. This solution for H can then be used to go back and resolve the momentum equation. This procedure can be continued until the desired degree of convergence is obtained.

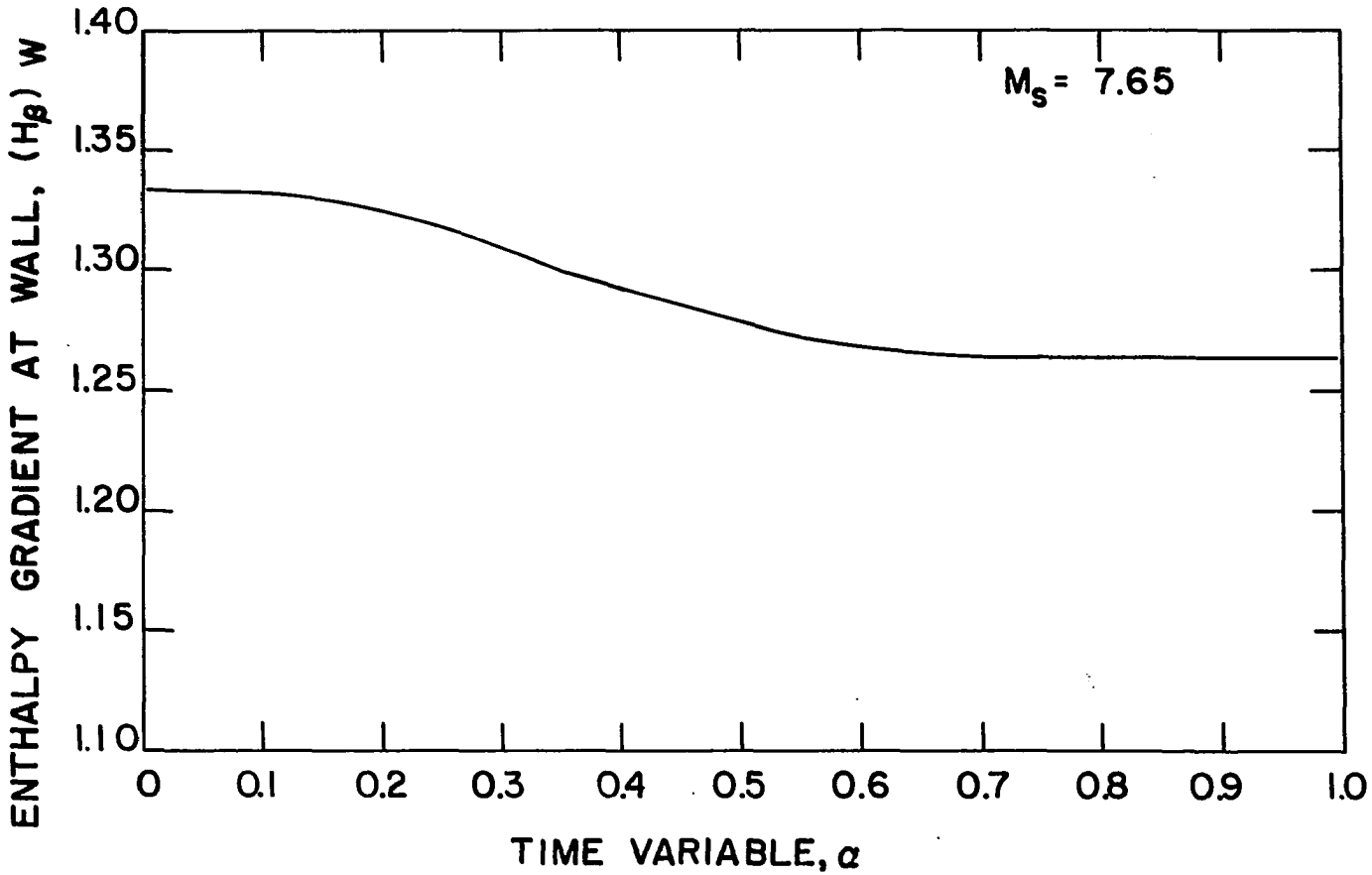

Figure 3. Enthalpy gradient at the wall as a function of α for a shock Mach number of 7.65

Observations on accuracy

For the case of $C(\lambda) \neq 1$ Mirels' (23) presents values for shear stress and heat transfer only at the wall. It was noted above that one must have values for ϕ at all values of β for $\alpha = 1$ before iteration can be carried out. Hence, it was necessary to duplicate some of Mirels' work in order to obtain these values. An integral iteration procedure of the same type as used in the interaction region was used to duplicate this work. Since the result for ϕ at the wall was given by Mirels (23) this was used as a check on the accuracy of the present numerical method. Calculations were carried out with ten and twenty divisions of the domain of β, $0 \leq \beta \leq 1$. The result at the wall agreed with that of Mirels within 0.5 per cent for ten divisions and within 0.25 per cent for twenty divisions. On the basis of this it was decided to use ten divisions of β and twenty divisions of α for the numerical solutions in the interaction region. It was found necessary to use double precision, sixteen significant figures, in order to obtain convergence.

At least eight iterations were carried out for solutions to the momentum equation. At this point successive iterations varied by less than 0.05 per cent. Fifteen iterations were carried out for a solution to the energy equation. Successive iterations then varied by less than 0.02 per cent. The larger number of iterations for the energy equation was necessary

because the initial values for H at $\alpha = 0$ and $\alpha = 1$ were simply taken as the values for $C = 1$ even in the case when $C \neq 1$.

For the case of $C \neq 1$ an initial linear relation for H between the wall and free stream values was assumed. The second set of iterations was found to give satisfactory results. This was decided because the third iteration solution to the momentum equation varied from the second by less than 0.02 per cent. Also, the heat transfer results from the second iteration solution at the wall for $\alpha = 1$ matched with that given by Mirels (23) within 1.0 per cent.

Results from numerical solutions

The properties of air used in the numerical calculation were taken from Feldman (8) for the higher values of shock Mach number and from Keenan and Kaye (17) for the lower values. The parameter A/A-1 is plotted as a function of M_s in Figure 4. The parameters $\frac{u_o^2}{h_o}$ and H_w are plotted as a function of M_s in Figure 5. An initial shock tube channel pressure, P_1, of 0.01 atmosphere is assumed in order to obtain these values.

Numerical calculations were carried out for values of the parameter A/A-1 of 2,4,6,7.5,9,10, and 10.65. These values correspond respectively to shock Mach numbers of 1.6, 3.15, 5.75, 7.65, 9.35, 11.3, and 14. The final iteration for the shear stress, ϕ, fields are reproduced in Tables 1 thru 7. The enthalpy, H, fields appear in Tables 8 thru 14. A summary of the heat transfer results is given in Table 15. The above

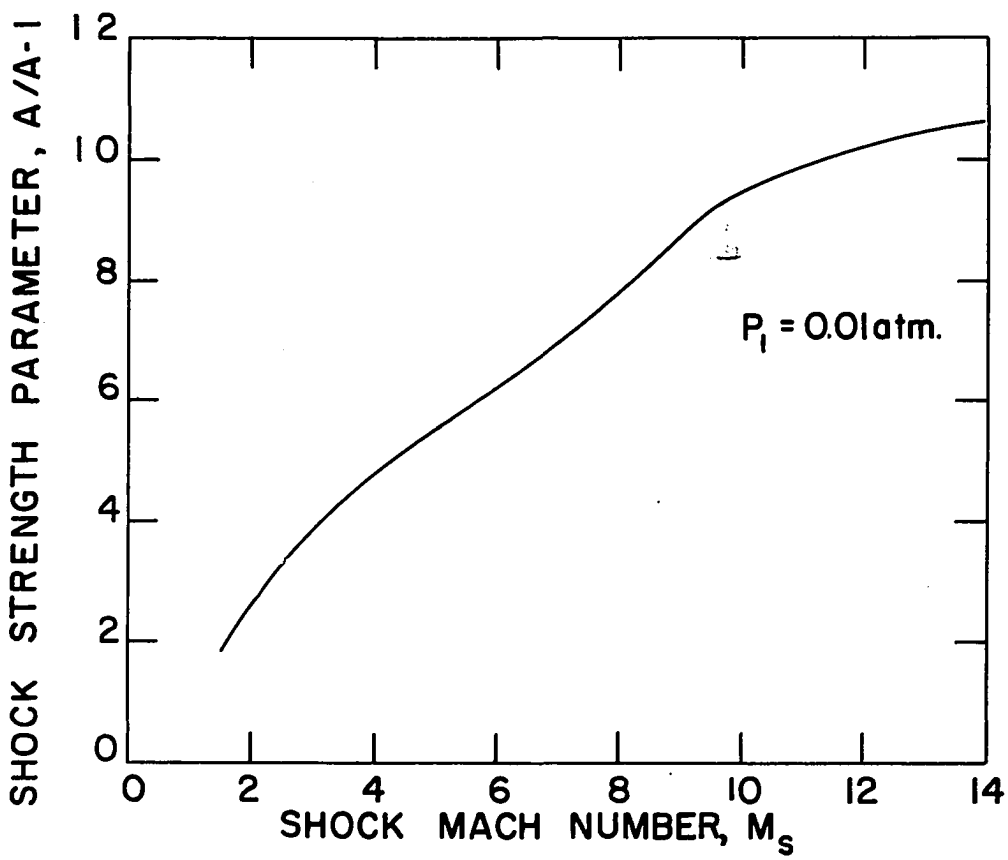

Figure 4. Shock strength parameter, A/A-1, as a function of shock Mach number

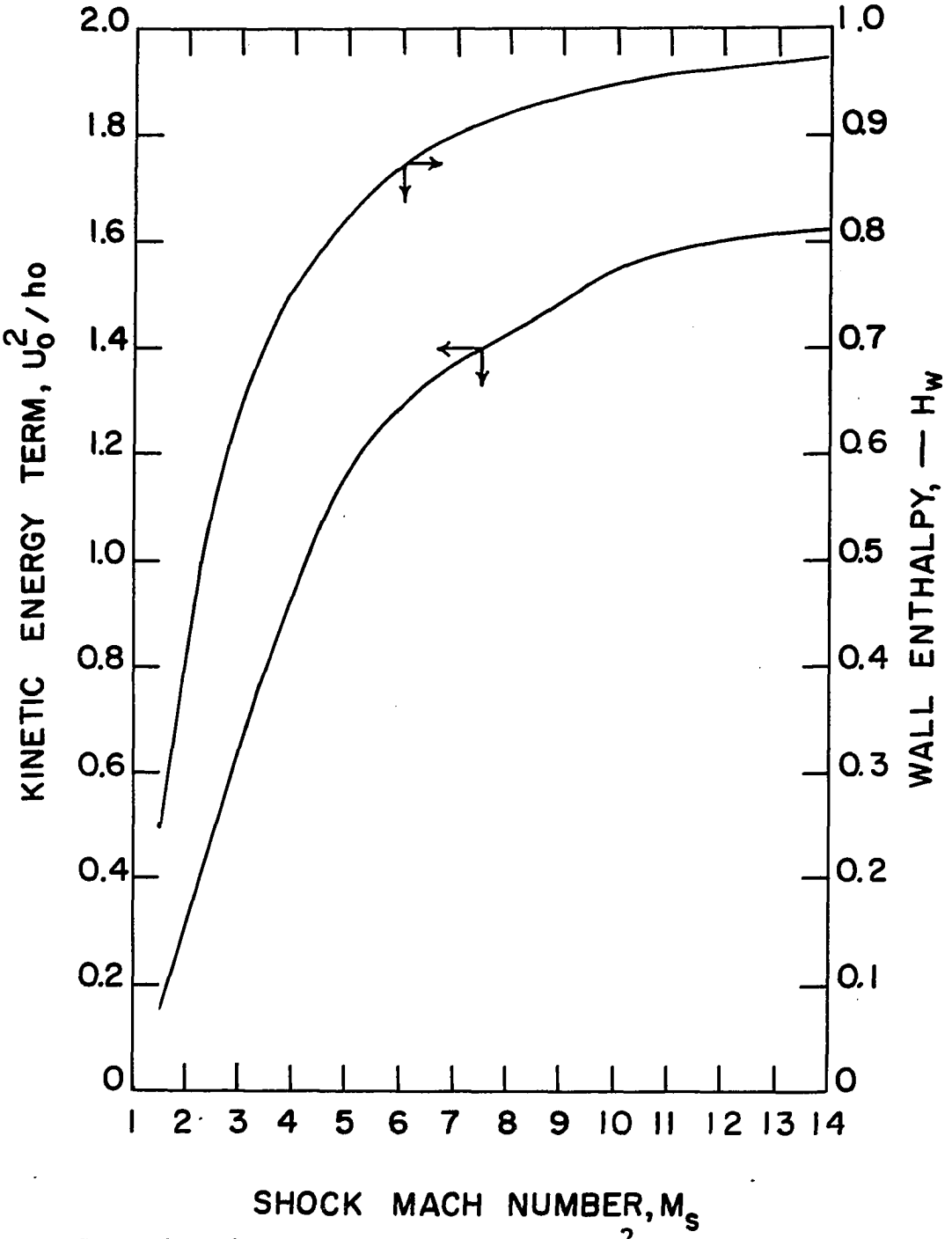

Figure 5. Kinetic energy parameter, $\frac{u_o^2}{h_o}$, and wall enthalpy, H_w, as a function of shock Mach number

Table 1. Shear stress, ϕ, as a function of α and β for $M_s = 1.6$

▼ I S U COMPUTATION CENTER; AMES, IOWA

A/(A-1)	PR	-HW	KE	DVR	IMAX	KMAX	I1	I3	KI	KF
2.0000	0.7200	0.2850	0.1850	1.0890	11	21	1	8	2	20

BETA= 0.0	0.1000	0.2000	0.3000	0.4000	0.5000	0.6000	0.7000	0.8000	0.9000	1.0
ALPHA PHI FIELD										
1.0000 0.7369	0.7296	0.7083	0.6734	0.6251	0.5633	0.4876	0.3970	0.2895	0.1609	0.0
0.9500 0.7009	0.6940	0.6738	0.6405	0.5946	0.5358	0.4638	0.3776	0.2754	0.1530	0.0
0.9000 0.6666	0.6600	0.6408	0.6092	0.5655	0.5095	0.4410	0.3591	0.2619	0.1455	0.0
0.8500 0.6335	0.6273	0.6090	0.5789	0.5374	0.4843	0.4192	0.3413	0.2489	0.1383	0.0
0.8000 0.6017	0.5958	0.5784	0.5499	0.5104	0.4599	0.3981	0.3241	0.2364	0.1314	0.0
0.7500 0.5710	0.5653	0.5488	0.5218	0.4843	0.4365	0.3779	0.3078	0.2248	0.1254	0.0
0.7000 0.5407	0.5354	0.5199	0.4944	0.4591	0.4141	0.3590	0.2932	0.2152	0.1223	0.0
0.6500 0.5117	0.5067	0.4922	0.4683	0.4353	0.3932	0.3417	0.2803	0.2075	0.1217	0.0
0.6000 0.4836	0.4790	0.4655	0.4434	0.4128	0.3738	0.3261	0.2692	0.2020	0.1211	0.0
0.5500 0.4566	0.4524	0.4401	0.4200	0.3921	0.3565	0.3130	0.2608	0.2006	0.1204	0.0
0.5000 0.4318	0.4281	0.4170	0.3988	0.3737	0.3415	0.3018	0.2561	0.1981	0.1188	0.0
0.4500 0.4055	0.4023	0.3928	0.3771	0.3551	0.3266	0.2935	0.2510	0.1943	0.1165	0.0
0.4000 0.3853	0.3825	0.3740	0.3599	0.3409	0.3179	0.2869	0.2455	0.1902	0.1141	0.0
0.3500 0.3665	0.3641	0.3575	0.3472	0.3319	0.3105	0.2811	0.2415	0.1880	0.1135	0.0
0.3000 0.3462	0.3452	0.3415	0.3342	0.3222	0.3039	0.2774	0.2401	0.1882	0.1142	0.0
0.2500 0.3365	0.3361	0.3339	0.3284	0.3182	0.3015	0.2762	0.2396	0.1879	0.1138	0.0
0.2000 0.3343	0.3341	0.3322	0.3271	0.3171	0.3006	0.2754	0.2388	0.1871	0.1132	0.0
0.1500 0.3345	0.3342	0.3324	0.3273	0.3173	0.3008	0.2755	0.2390	0.1872	0.1131	0.0
0.1000 0.3345	0.3342	0.3323	0.3272	0.3173	0.3007	0.2754	0.2388	0.1870	0.1129	0.0
0.0500 0.3345	0.3342	0.3323	0.3272	0.3173	0.3007	0.2754	0.2388	0.1869	0.1128	0.0
0.0000 0.3345	0.3342	0.3323	0.3272	0.3173	0.3007	0.2754	0.2388	0.1869	0.1128	0.0

Table 2. Shear stress, ϕ, as a function of α and β for $M_s = 3.15$

▼ I S U COMPUTATION CENTER; AMES, IOWA

A/(A-1)	PR	-HW	KE	CVR	IMAX	KMAX	I1	I3	KI	KF
4.0000	0.7200	0.6640	0.7000	1.3918	11	21	1	8	2	20

BETA=	0.0	0.1000	0.2000	0.3000	0.4000	0.5000	0.6000	0.7000	0.8000	0.9000	1.0
ALPHA	PHI FIELD										
1.0000	1.0577	1.0452	1.0091	0.9517	0.8744	0.7783	0.6638	0.5310	0.3789	0.2046	0.0
0.9500	0.9621	0.9507	0.9178	0.8656	0.7953	0.7078	0.6037	0.4829	0.3446	0.1860	0.0
0.9000	0.8811	0.8707	0.8406	0.7928	0.7283	0.6482	0.5529	0.4422	0.3155	0.1704	0.0
0.8500	0.8109	0.8013	0.7736	0.7296	0.6703	0.5965	0.5088	0.4069	0.2903	0.1567	0.0
0.8000	0.7488	0.7399	0.7143	0.6737	0.6189	0.5508	0.4698	0.3757	0.2681	0.1447	0.0
0.7500	0.6932	0.6849	0.6613	0.6236	0.5729	0.5099	0.4349	0.3479	0.2483	0.1342	0.0
0.7000	0.6424	0.6348	0.6129	0.5780	0.5312	0.4730	0.4037	0.3235	0.2317	0.1265	0.0
0.6500	0.5961	0.5891	0.5690	0.5370	0.4939	0.4405	0.3770	0.3035	0.2197	0.1242	0.0
0.6000	0.5538	0.5474	0.5290	0.4997	0.4604	0.4117	0.3538	0.2870	0.2106	0.1238	0.0
0.5500	0.5149	0.5092	0.4926	0.4662	0.4308	0.3869	0.3348	0.2745	0.2066	0.1233	0.0
0.5000	0.4797	0.4746	0.4599	0.4365	0.4051	0.3661	0.3197	0.2661	0.2050	0.1224	0.0
0.4500	0.4471	0.4427	0.4301	0.4098	0.3825	0.3483	0.3077	0.2619	0.2018	0.1203	0.0
0.4000	0.4167	0.4131	0.4025	0.3853	0.3619	0.3333	0.2997	0.2555	0.1969	0.1174	0.0
0.3500	0.3941	0.3910	0.3818	0.3670	0.3489	0.3249	0.2927	0.2500	0.1933	0.1156	0.0
0.3000	0.3709	0.3692	0.3636	0.3538	0.3389	0.3176	0.2880	0.2477	0.1928	0.1161	0.0
0.2500	0.3547	0.3540	0.3510	0.3443	0.3325	0.3140	0.2866	0.2478	0.1937	0.1169	0.0
0.2000	0.3504	0.3501	0.3479	0.3421	0.3311	0.3131	0.2860	0.2472	0.1929	0.1160	0.0
0.1500	0.3500	0.3497	0.3475	0.3418	0.3308	0.3127	0.2855	0.2466	0.1923	0.1155	0.0
0.1000	0.3505	0.3501	0.3480	0.3422	0.3311	0.3129	0.2857	0.2467	0.1923	0.1155	0.0
0.0500	0.3505	0.3501	0.3479	0.3421	0.3310	0.3128	0.2855	0.2466	0.1921	0.1153	0.0
0.0000	0.3505	0.3501	0.3479	0.3421	0.3310	0.3128	0.2855	0.2466	0.1921	0.1153	0.0

Table 3. Shear stress, ϕ, as a function of α and β for $M_s = 5.75$

▼ I S U COMPUTATION CENTER; AMES, IOWA

A/(A-1)	PR	-HW	KE	DVR	IMAX	KMAX	I1	I3	KI	KF
6.0000	0.7200	0.8650	1.2720	1.9593	11	21	1	8	2	20

BETA= 0.0	0.1000	0.2000	0.3000	0.4000	0.5000	0.6000	0.7000	0.8000	0.9000	1.0
ALPHA PHI FIELD										
1.0000 1.3727	1.3535	1.2998	1.2175	1.1101	0.9797	0.8280	0.6555	0.4620	0.2456	0.0
0.9500 1.2000	1.1831	1.1362	1.0642	0.9702	0.8562	0.7236	0.5728	0.4037	0.2145	0.0
0.9000 1.0672	1.0522	1.0104	0.9463	0.8627	0.7613	0.6433	0.5092	0.3589	0.1907	0.0
0.8500 0.9599	0.9465	0.9089	0.8512	0.7760	0.6848	0.5786	0.4580	0.3227	0.1715	0.0
0.8000 0.8704	0.8582	0.8241	0.7718	0.7036	0.6209	0.5247	0.4153	0.2926	0.1555	0.0
0.7500 0.7940	0.7828	0.7517	0.7040	0.6418	0.5664	0.4786	0.3788	0.2670	0.1419	0.0
0.7000 0.7273	0.7171	0.6886	0.6449	0.5880	0.5190	0.4387	0.3475	0.2453	0.1310	0.0
0.6500 0.6678	0.6585	0.6325	0.5926	0.5407	0.4778	0.4047	0.3219	0.2292	0.1253	0.0
0.6000 0.6152	0.6068	0.5831	0.5470	0.4999	0.4429	0.3768	0.3020	0.2183	0.1256	0.0
0.5500 0.5675	0.5598	0.5386	0.5060	0.4636	0.4124	0.3531	0.2859	0.2105	0.1251	0.0
0.5000 0.5246	0.5178	0.4990	0.4703	0.4328	0.3876	0.3351	0.2753	0.2095	0.1247	0.0
0.4500 0.4864	0.4806	0.4642	0.4391	0.4064	0.3668	0.3204	0.2690	0.2066	0.1228	0.0
0.4000 0.4503	0.4455	0.4318	0.4107	0.3830	0.3489	0.3105	0.2638	0.2028	0.1204	0.0
0.3500 0.4203	0.4163	0.4050	0.3873	0.3637	0.3369	0.3024	0.2572	0.1978	0.1176	0.0
0.3000 0.3962	0.3930	0.3838	0.3707	0.3530	0.3288	0.2962	0.2530	0.1956	0.1169	0.0
0.2500 0.3738	0.3724	0.3677	0.3588	0.3445	0.3235	0.2937	0.2526	0.1965	0.1181	0.0
0.2000 0.3644	0.3639	0.3610	0.3542	0.3419	0.3223	0.2935	0.2529	0.1967	0.1180	0.0
0.1500 0.3629	0.3625	0.3600	0.3534	0.3411	0.3215	0.2925	0.2518	0.1956	0.1170	0.0
0.1000 0.3633	0.3629	0.3603	0.3536	0.3412	0.3215	0.2925	0.2517	0.1954	0.1169	0.0
0.0500 0.3635	0.3631	0.3605	0.3538	0.3413	0.3216	0.2925	0.2516	0.1953	0.1168	0.0
0.0000 0.3635	0.3631	0.3605	0.3538	0.3413	0.3216	0.2925	0.2516	0.1953	0.1168	0.0

Table 4. Shear stress, ϕ, as a function of α and β for $M_s = 7.65$

▼ I S U COMPUTATION CENTER; AMES, IOWA

A/(A-1)	PR	-HW	KE	CVR	IMAX	KMAX	I1	I3	KI	KF
7.5000	0.7200	0.9190	1.4120	2.3777	11	21	1	8	2	20

BETA= 0.0	0.1000	0.2000	0.3000	0.4000	0.5000	0.6000	0.7000	0.8000	0.9000	1.0
ALPHA PHI FIELD										
1.0000 1.5778	1.5536	1.4875	1.3884	1.2613	1.1091	0.9336	0.7359	0.5160	0.2724	0.0
0.9500 1.3428	1.3222	1.2658	1.1815	1.0732	0.9436	0.7942	0.6260	0.4388	0.2316	0.0
0.9000 1.1725	1.1544	1.1052	1.0315	0.9370	0.8238	0.6933	0.5464	0.3830	0.2021	0.0
0.8500 1.0407	1.0247	0.9810	0.9156	0.8316	0.7311	0.6153	0.4849	0.3399	0.1793	0.0
0.8000 0.9343	0.9199	0.8807	0.8219	0.7466	0.6564	0.5524	0.4353	0.3051	0.1610	0.0
0.7500 0.8457	0.8327	0.7972	0.7440	0.6758	0.5942	0.5001	0.3941	0.2762	0.1458	0.0
0.7000 0.7701	0.7582	0.7259	0.6775	0.6154	0.5411	0.4555	0.3592	0.2520	0.1334	0.0
0.6500 0.7037	0.6929	0.6635	0.6195	0.5631	0.4956	0.4180	0.3307	0.2338	0.1263	0.0
0.6000 0.6456	0.6359	0.6092	0.5694	0.5184	0.4574	0.3874	0.3089	0.2219	0.1263	0.0
0.5500 0.5934	0.5846	0.5606	0.5248	0.4790	0.4243	0.3616	0.2912	0.2128	0.1257	0.0
0.5000 0.5469	0.5391	0.5179	0.4862	0.4457	0.3975	0.3420	0.2795	0.2112	0.1255	0.0
0.4500 0.5053	0.4985	0.4801	0.4525	0.4172	0.3749	0.3261	0.2720	0.2086	0.1238	0.0
0.4000 0.4673	0.4617	0.4461	0.4228	0.3927	0.3564	0.3152	0.2673	0.2052	0.1216	0.0
0.3500 0.4331	0.4285	0.4158	0.3965	0.3713	0.3420	0.3065	0.2603	0.1999	0.1185	0.0
0.3000 0.4073	0.4036	0.3932	0.3775	0.3587	0.3333	0.2996	0.2552	0.1967	0.1172	0.0
0.2500 0.3830	0.3812	0.3754	0.3651	0.3495	0.3272	0.2962	0.2541	0.1972	0.1183	0.0
0.2000 0.3702	0.3695	0.3662	0.3587	0.3457	0.3255	0.2960	0.2548	0.1981	0.1187	0.0
0.1500 0.3680	0.3675	0.3647	0.3577	0.3449	0.3247	0.2951	0.2537	0.1969	0.1177	0.0
0.1000 0.3680	0.3675	0.3647	0.3576	0.3447	0.3243	0.2947	0.2532	0.1964	0.1173	0.0
0.0500 0.3685	0.3680	0.3651	0.3580	0.3450	0.3246	0.2949	0.2534	0.1964	0.1173	0.0
0.0000 0.3685	0.3680	0.3651	0.3580	0.3450	0.3246	0.2949	0.2534	0.1964	0.1173	0.0

Table 5. Shear stress, ϕ, as a function of α and β for $M_s = 9.35$

ISU COMPUTATION CENTER; AMES, IOWA

A/(A-1)	PR	-HW	KE	CVR	IMAX	KMAX	I1	I3	KI	KF
9.0000	0.7200	0.9450	1.5090	2.7466	11	21	1	8	2	20

BETA=	0.0	0.1000	0.2000	0.3000	0.4000	0.5000	0.6000	0.7000	0.8000	0.9000	1.0
ALPHA	PHI FIELD										
1.0000	1.7573	1.7284	1.6510	1.5374	1.3933	1.2221	1.0261	0.8065	0.5636	0.2962	0.0
0.9500	1.4590	1.4349	1.3706	1.2762	1.1564	1.0143	0.8515	0.6691	0.4675	0.2456	0.0
0.9000	1.2536	1.2329	1.1776	1.0964	0.9935	0.8713	0.7314	0.5747	0.4015	0.2109	0.0
0.8500	1.1003	1.0821	1.0336	0.9623	0.8719	0.7647	0.6419	0.5044	0.3523	0.1850	0.0
0.8000	0.9799	0.9637	0.9205	0.8570	0.7765	0.6810	0.5717	0.4492	0.3138	0.1648	0.0
0.7500	0.8818	0.8672	0.8283	0.7712	0.6988	0.6128	0.5144	0.4042	0.2824	0.1484	0.0
0.7000	0.7993	0.7861	0.7509	0.6991	0.6335	0.5556	0.4665	0.3667	0.2564	0.1351	0.0
0.6500	0.7278	0.7159	0.6839	0.6369	0.5775	0.5070	0.4264	0.3363	0.2368	0.1272	0.0
0.6000	0.6658	0.6550	0.6261	0.5837	0.5300	0.4665	0.3940	0.3131	0.2240	0.1266	0.0
0.5500	0.6104	0.6007	0.5747	0.5367	0.4886	0.4317	0.3668	0.2945	0.2144	0.1261	0.0
0.5000	0.5614	0.5528	0.5298	0.4961	0.4536	0.4034	0.3461	0.2819	0.2120	0.1259	0.0
0.4500	0.5173	0.5099	0.4899	0.4606	0.4236	0.3797	0.3294	0.2737	0.2097	0.1244	0.0
0.4000	0.4782	0.4719	0.4550	0.4301	0.3985	0.3607	0.3177	0.2692	0.2064	0.1222	0.0
0.3500	0.4412	0.4361	0.4224	0.4020	0.3756	0.3448	0.3087	0.2619	0.2009	0.1190	0.0
0.3000	0.4140	0.4099	0.3986	0.3816	0.3616	0.3355	0.3012	0.2562	0.1971	0.1173	0.0
0.2500	0.3886	0.3864	0.3797	0.3686	0.3520	0.3288	0.2971	0.2545	0.1972	0.1182	0.0
0.2000	0.3730	0.3722	0.3685	0.3607	0.3472	0.3266	0.2968	0.2554	0.1985	0.1189	0.0
0.1500	0.3702	0.3697	0.3667	0.3594	0.3464	0.3259	0.2961	0.2544	0.1973	0.1179	0.0
0.1000	0.3699	0.3694	0.3664	0.3590	0.3459	0.3253	0.2953	0.2537	0.1966	0.1174	0.0
0.0500	0.3706	0.3700	0.3669	0.3595	0.3463	0.3256	0.2956	0.2539	0.1967	0.1174	0.0
0.0000	0.3706	0.3700	0.3669	0.3595	0.3463	0.3256	0.2956	0.2539	0.1967	0.1174	0.0

Table 6. Shear stress, ϕ, as a function of α and β for M_s = 11.3

▼ I S U COMPUTATION CENTER; AMES, IOWA

A/(A-1)	PR	-HW	KE	CVR	IMAX	KMAX	I1	I3	KI	KF
10.0000	0.7200	0.9620	1.5980	3.1741	11	21	1	8	2	20

BETA= 0.0	0.1000	0.2000	0.3000	0.4000	0.5000	0.6000	0.7000	0.8000	0.9000	1.0
ALPHA PHI FIELD										
1.0000 1.8898	1.8567	1.7699	1.6449	1.4880	1.3030	1.0921	0.8568	0.5974	0.3131	0.0
0.9500 1.5448	1.5177	1.4467	1.3444	1.2160	1.0647	0.8922	0.6998	0.4879	0.2556	0.0
0.9000 1.3145	1.2915	1.2309	1.1438	1.0346	0.9058	0.7590	0.5953	0.4149	0.2173	0.0
0.8500 1.1463	1.1261	1.0734	0.9974	0.9021	0.7898	0.6618	0.5190	0.3617	0.1894	0.0
0.8000 1.0162	0.9984	0.9516	0.8842	0.7998	0.7002	0.5867	0.4601	0.3207	0.1680	0.0
0.7500 0.9115	0.8955	0.8535	0.7931	0.7173	0.6280	0.5263	0.4127	0.2877	0.1507	0.0
0.7000 0.8242	0.8098	0.7718	0.7172	0.6487	0.5680	0.4760	0.3735	0.2606	0.1368	0.0
0.6500 0.7491	0.7360	0.7017	0.6522	0.5902	0.5172	0.4341	0.3416	0.2398	0.1281	0.0
0.6000 0.6841	0.6722	0.6412	0.5966	0.5407	0.4750	0.4003	0.3172	0.2261	0.1268	0.0
0.5500 0.6264	0.6157	0.5879	0.5478	0.4977	0.4388	0.3720	0.2979	0.2161	0.1265	0.0
0.5000 0.5753	0.5658	0.5411	0.5057	0.4613	0.4093	0.3503	0.2845	0.2129	0.1263	0.0
0.4500 0.5293	0.5211	0.4996	0.4688	0.4302	0.3849	0.3331	0.2756	0.2111	0.1252	0.0
0.4000 0.4890	0.4821	0.4638	0.4375	0.4045	0.3654	0.3206	0.2714	0.2079	0.1230	0.0
0.3500 0.4500	0.4444	0.4297	0.4081	0.3806	0.3482	0.3115	0.2641	0.2024	0.1197	0.0
0.3000 0.4210	0.4164	0.4043	0.3864	0.3650	0.3384	0.3034	0.2578	0.1981	0.1176	0.0
0.2500 0.3952	0.3920	0.3844	0.3725	0.3552	0.3312	0.2988	0.2556	0.1978	0.1183	0.0
0.2000 0.3770	0.3759	0.3718	0.3634	0.3494	0.3284	0.2982	0.2564	0.1991	0.1193	0.0
0.1500 0.3730	0.3724	0.3693	0.3618	0.3485	0.3277	0.2976	0.2556	0.1982	0.1183	0.0
0.1000 0.3726	0.3720	0.3688	0.3612	0.3478	0.3269	0.2967	0.2547	0.1973	0.1177	0.0
0.0500 0.3732	0.3727	0.3694	0.3618	0.3483	0.3273	0.2970	0.2550	0.1975	0.1178	0.0
0.0000 0.3732	0.3727	0.3694	0.3618	0.3483	0.3273	0.2970	0.2550	0.1975	0.1178	0.0

Table 7. Shear stress, ϕ, as a function of α and β for $M_s = 14$

▼ I S U COMPUTATION CENTER; AMES, IOWA

A/(A-1)	PR	-HW	KE	DVR	IMAX	KMAX	I1	I3	KI	KF
10.6500	0.7200	0.9750	1.6200	3.9531	11	21	1	8	2	20

BETA=	0.0	0.1000	0.2000	0.3000	0.4000	0.5000	0.6000	0.7000	0.8000	0.9000	1.0
ALPHA	PHI	FIELD									
1.0000	2.0550	2.0166	1.9178	1.7785	1.6057	1.4032	1.1736	0.9185	0.6388	0.3337	0.0
0.9500	1.6637	1.6326	1.5525	1.4396	1.2995	1.1355	0.9495	0.7430	0.5166	0.2697	0.0
0.9000	1.4074	1.3810	1.3132	1.2177	1.0991	0.9603	0.8030	0.6283	0.4367	0.2280	0.0
0.8500	1.2225	1.1995	1.1406	1.0576	0.9547	0.8341	0.6974	0.5456	0.3793	0.1980	0.0
0.8000	1.0809	1.0606	1.0086	0.9352	0.8441	0.7375	0.6167	0.4825	0.3354	0.1751	0.0
0.7500	0.9676	0.9495	0.9029	0.8372	0.7557	0.6603	0.5521	0.4320	0.3003	0.1568	0.0
0.7000	0.8738	0.8574	0.8153	0.7560	0.6824	0.5963	0.4986	0.3902	0.2714	0.1418	0.0
0.6500	0.7934	0.7786	0.7404	0.6867	0.6200	0.5420	0.4536	0.3556	0.2483	0.1311	0.0
0.6000	0.7234	0.7099	0.6754	0.6269	0.5667	0.4964	0.4168	0.3298	0.2325	0.1274	0.0
0.5500	0.6618	0.6498	0.6187	0.5751	0.5210	0.4580	0.3868	0.3080	0.2218	0.1279	0.0
0.5000	0.6069	0.5961	0.5685	0.5297	0.4817	0.4257	0.3626	0.2926	0.2159	0.1279	0.0
0.4500	0.5576	0.5483	0.5242	0.4904	0.4487	0.3999	0.3447	0.2828	0.2155	0.1277	0.0
0.4000	0.5143	0.5063	0.4858	0.4568	0.4210	0.3789	0.3306	0.2778	0.2127	0.1257	0.0
0.3500	0.4734	0.4669	0.4502	0.4264	0.3966	0.3608	0.3211	0.2722	0.2084	0.1231	0.0
0.3000	0.4397	0.4346	0.4213	0.4019	0.3770	0.3493	0.3129	0.2655	0.2036	0.1204	0.0
0.2500	0.4132	0.4094	0.3992	0.3856	0.3671	0.3416	0.3074	0.2621	0.2020	0.1202	0.0
0.2000	0.3920	0.3905	0.3854	0.3759	0.3606	0.3381	0.3063	0.2627	0.2034	0.1214	0.0
0.1500	0.3857	0.3851	0.3815	0.3735	0.3594	0.3377	0.3063	0.2627	0.2032	0.1210	0.0
0.1000	0.3851	0.3844	0.3809	0.3728	0.3586	0.3367	0.3052	0.2615	0.2020	0.1201	0.0
0.0500	0.3855	0.3849	0.3813	0.3731	0.3589	0.3369	0.3053	0.2615	0.2020	0.1200	0.0
0.0000	0.3855	0.3849	0.3813	0.3731	0.3589	0.3369	0.3053	0.2615	0.2020	0.1200	0.0

Table 7. Shear stress, ϕ, as a function of α and β for $M_s = 14$

▼ I S U COMPUTATION CENTER; AMES, IOWA

A/(A-1)	PR	-HW	KE	DVR	IMAX	KMAX	I1	I3	KI	KF
10.6500	0.7200	0.9750	1.6200	3.9531	11	21	1	8	2	20

BETA=	0.0	0.1000	0.2000	0.3000	0.4000	0.5000	0.6000	0.7000	0.8000	0.9000	1.0
ALPHA	PHI FIELD										
1.0000	2.0550	2.0166	1.9178	1.7785	1.6057	1.4032	1.1736	0.9185	0.6388	0.3337	0.0
0.9500	1.6637	1.6326	1.5525	1.4396	1.2995	1.1355	0.9495	0.7430	0.5166	0.2697	0.0
0.9000	1.4074	1.3810	1.3132	1.2177	1.0991	0.9603	0.8030	0.6283	0.4367	0.2280	0.0
0.8500	1.2225	1.1995	1.1406	1.0576	0.9547	0.8341	0.6974	0.5456	0.3793	0.1980	0.0
0.8000	1.0809	1.0606	1.0086	0.9352	0.8441	0.7375	0.6167	0.4825	0.3354	0.1751	0.0
0.7500	0.9676	0.9495	0.9029	0.8372	0.7557	0.6603	0.5521	0.4320	0.3003	0.1568	0.0
0.7000	0.8738	0.8574	0.8153	0.7560	0.6824	0.5963	0.4986	0.3902	0.2714	0.1418	0.0
0.6500	0.7934	0.7786	0.7404	0.6867	0.6200	0.5420	0.4536	0.3556	0.2483	0.1311	0.0
0.6000	0.7234	0.7099	0.6754	0.6269	0.5667	0.4964	0.4168	0.3288	0.2325	0.1274	0.0
0.5500	0.6618	0.6498	0.6187	0.5751	0.5210	0.4580	0.3868	0.3080	0.2218	0.1279	0.0
0.5000	0.6069	0.5961	0.5685	0.5297	0.4817	0.4257	0.3626	0.2926	0.2159	0.1279	0.0
0.4500	0.5576	0.5483	0.5242	0.4904	0.4487	0.3999	0.3447	0.2828	0.2155	0.1277	0.0
0.4000	0.5143	0.5063	0.4858	0.4568	0.4210	0.3789	0.3306	0.2778	0.2127	0.1257	0.0
0.3500	0.4734	0.4669	0.4502	0.4264	0.3966	0.3608	0.3211	0.2722	0.2084	0.1231	0.0
0.3000	0.4397	0.4346	0.4213	0.4019	0.3770	0.3493	0.3129	0.2655	0.2036	0.1204	0.0
0.2500	0.4132	0.4094	0.3992	0.3856	0.3671	0.3416	0.3074	0.2621	0.2020	0.1202	0.0
0.2000	0.3920	0.3905	0.3854	0.3759	0.3606	0.3381	0.3063	0.2627	0.2034	0.1214	0.0
0.1500	0.3857	0.3851	0.3815	0.3735	0.3594	0.3377	0.3063	0.2627	0.2032	0.1210	0.0
0.1000	0.3851	0.3844	0.3809	0.3728	0.3586	0.3367	0.3052	0.2615	0.2020	0.1201	0.0
0.0500	0.3855	0.3849	0.3813	0.3731	0.3589	0.3369	0.3053	0.2615	0.2020	0.1200	0.0
0.0000	0.3855	0.3849	0.3813	0.3731	0.3589	0.3369	0.3053	0.2615	0.2020	0.1200	0.0

Table 8. Enthalpy, H, as a function of α and β for M_s = 1.6

ISU COMPUTATION CENTER; AMES, IOWA

A/(A-1)	PR	-HW	KE	DVR	IMAX	KMAX	I1	I3	KI	KF
2.0000	0.7200	0.2850	0.1850	1.0890	11	21	1	15	2	20

BETA=	0.0	0.1000	0.2000	0.3000	0.4000	0.5000	C.6000	0.7000	0.8000	0.9000	1.0
ALPHA	H FIELD (NEGATIVE VALUES)										
1.0000	0.2850	0.2551	0.2262	0.1984	0.1715	0.1453	C.1196	0.0939	0.C680	C.0394	0.0
0.9500	0.2850	0.2551	0.2262	0.1984	0.1715	0.1453	C.1196	0.0939	0.C680	0.0394	0.0
0.9000	0.2850	0.2550	0.2262	0.1984	0.1714	0.1452	C.1194	0.0938	0.C679	0.0394	0.0
0.8500	0.2850	0.2551	0.2262	0.1983	0.1714	0.1452	C.1194	0.0938	0.C678	0.0394	0.0
0.8000	0.2850	0.2550	0.2261	0.1983	0.1713	0.1451	0.1193	0.0937	0.C678	0.0394	0.0
0.7500	0.2850	0.2550	0.2261	0.1982	0.1712	0.1450	0.1192	0.0936	0.C677	0.0394	0.0
0.7000	0.2850	0.2550	0.2260	0.1981	0.1711	0.1448	C.1190	0.0935	0.C675	0.0393	0.0
0.6500	0.2850	0.2549	0.2259	0.1979	0.1708	0.1445	C.1188	0.0932	0.C673	0.0392	0.0
0.6000	0.2850	0.2548	0.2257	0.1977	0.1706	0.1442	C.1184	0.0928	0.C670	C.0390	0.0
0.5500	0.2850	0.2547	0.2255	0.1974	0.1702	0.1438	C.1180	0.0924	0.C666	0.0388	0.0
0.5000	0.2850	0.2546	0.2253	0.1971	0.1698	0.1434	C.1175	0.0919	0.C662	0.0386	0.0
0.4500	0.2850	0.2545	0.2250	0.1967	0.1694	0.1429	C.1171	0.0916	0.C659	C.0385	0.0
0.4000	0.2850	0.2543	0.2248	0.1964	0.1690	0.1425	C.1167	0.0912	0.C656	0.0383	0.0
0.3500	0.2850	0.2542	0.2245	0.1961	0.1687	0.1421	C.1163	0.0909	0.C654	C.0382	0.0
0.3000	0.2850	0.2540	0.2242	0.1956	0.1682	0.1416	C.1159	0.0905	0.C651	0.0380	0.0
0.2500	0.2850	0.2539	0.2240	0.1953	0.1678	0.1412	C.1154	0.0901	C.C648	C.0378	0.0
0.2000	0.2850	0.2538	0.2238	0.1951	0.1675	0.1409	C.1151	0.0898	0.C645	0.0377	0.0
0.1500	0.2850	0.2537	0.2237	0.1950	0.1673	0.1407	C.1149	0.0895	0.C642	0.0375	0.0
0.1000	0.2850	0.2537	0.2237	0.1949	0.1672	0.1406	C.1147	0.0894	0.C640	C.0374	0.0
0.0500	0.2850	0.2537	0.2236	0.1947	0.1670	0.1403	0.1145	0.0891	0.C638	0.0372	0.0
0.0000	0.2850	0.2537	0.2236	0.1947	0.1670	0.1403	0.1145	0.0891	0.C638	C.0372	0.0

Table 9. Enthalpy, H, as a function of α and β for $M_s = 3.15$

▼ I S U COMPUTATION CENTER; AMES, IOWA

A/(A-1)	PR	-HW	KE	DVR	IMAX	KMAX	I1	I3	KI	KF
4.0000	0.7200	0.6640	0.7000	1.3918	11	21	1	15	2	20

BETA=	0.0	0.1000	0.2000	0.3000	0.4000	0.5000	0.6000	0.7000	0.8000	0.9000	1.0
ALPHA	H FIELD (NEGATIVE VALUES)										
1.0000	0.6640	0.5859	0.5123	0.4428	0.3771	0.3147	0.2550	0.1975	0.1407	0.0821	0.0
0.9500	0.6640	0.5859	0.5123	0.4428	0.3771	0.3147	0.2550	0.1975	0.1407	0.0821	0.0
0.9000	0.6640	0.5859	0.5122	0.4426	0.3768	0.3143	0.2547	0.1972	0.1404	0.0819	0.0
0.8500	0.6640	0.5859	0.5121	0.4425	0.3767	0.3142	0.2546	0.1971	0.1404	0.0819	0.0
0.8000	0.6640	0.5859	0.5120	0.4424	0.3765	0.3141	0.2544	0.1969	0.1403	0.0818	0.0
0.7500	0.6640	0.5858	0.5119	0.4422	0.3763	0.3138	0.2542	0.1967	0.1401	0.0817	0.0
0.7000	0.6640	0.5857	0.5117	0.4420	0.3760	0.3135	0.2539	0.1964	0.1399	0.0816	0.0
0.6500	0.6640	0.5856	0.5114	0.4415	0.3754	0.3128	0.2532	0.1958	0.1394	0.0813	0.0
0.6000	0.6640	0.5854	0.5110	0.4409	0.3747	0.3120	0.2523	0.1949	0.1386	0.0808	0.0
0.5500	0.6640	0.5851	0.5104	0.4401	0.3737	0.3109	0.2512	0.1937	0.1376	0.0802	0.0
0.5000	0.6640	0.5847	0.5098	0.4392	0.3726	0.3096	0.2498	0.1924	0.1365	0.0796	0.0
0.4500	0.6640	0.5844	0.5091	0.4382	0.3714	0.3083	0.2484	0.1912	0.1356	0.0789	0.0
0.4000	0.6640	0.5840	0.5084	0.4372	0.3702	0.3070	0.2472	0.1901	0.1347	0.0784	0.0
0.3500	0.6640	0.5836	0.5077	0.4363	0.3691	0.3059	0.2461	0.1892	0.1339	0.0778	0.0
0.3000	0.6640	0.5830	0.5068	0.4352	0.3679	0.3047	0.2450	0.1882	0.1332	0.0773	0.0
0.2500	0.6640	0.5826	0.5059	0.4340	0.3666	0.3033	0.2437	0.1870	0.1323	0.0767	0.0
0.2000	0.6640	0.5823	0.5055	0.4334	0.3658	0.3024	0.2428	0.1861	0.1314	0.0761	0.0
0.1500	0.6640	0.5822	0.5051	0.4329	0.3652	0.3017	0.2420	0.1852	0.1306	0.0754	0.0
0.1000	0.6640	0.5821	0.5050	0.4327	0.3649	0.3013	0.2415	0.1848	0.1301	0.0750	0.0
0.0500	0.6640	0.5819	0.5046	0.4322	0.3642	0.3005	0.2407	0.1839	0.1293	0.0743	0.0
0.0000	0.6640	0.5819	0.5046	0.4322	0.3642	0.3005	0.2407	0.1839	0.1293	0.0743	0.0

Table 10. Enthalpy, H, as a function of α and β for M_s = 5.75

▼ I S U COMPUTATION CENTER; AMES, IOWA

A/(A-1)	PR	-HW	KE	DVR	IMAX	KMAX	I1	I3	KI	KF
6.0000	0.7200	0.8650	1.2720	1.9593	11	21	1	15	2	20

BETA=	0.0	0.1000	0.2000	0.3000	0.4000	0.5000	0.6000	0.7000	0.8000	0.9000	1.0
ALPHA	H FIELD (NEGATIVE VALUES)										
1.0000	0.8650	0.7518	0.6467	0.5494	0.4593	0.3760	0.2986	0.2264	0.1580	0.0900	0.0
0.9500	0.8650	0.7518	0.6467	0.5494	0.4593	0.3760	0.2986	0.2264	0.1580	0.0900	0.0
0.9000	0.8650	0.7517	0.6465	0.5491	0.4589	0.3755	0.2982	0.2260	0.1576	0.0898	0.0
0.8500	0.8650	0.7517	0.6464	0.5490	0.4588	0.3754	0.2980	0.2258	0.1575	0.0897	0.0
0.8000	0.8650	0.7517	0.6463	0.5488	0.4586	0.3751	0.2977	0.2256	0.1573	0.0896	0.0
0.7500	0.8650	0.7517	0.6462	0.5486	0.4583	0.3748	0.2975	0.2254	0.1572	0.0895	0.0
0.7000	0.8650	0.7516	0.6460	0.5483	0.4580	0.3745	0.2971	0.2251	0.1569	0.0894	0.0
0.6500	0.8650	0.7514	0.6456	0.5478	0.4574	0.3738	0.2965	0.2245	0.1565	0.0893	0.0
0.6000	0.8650	0.7511	0.6451	0.5470	0.4564	0.3727	0.2953	0.2233	0.1555	0.0887	0.0
0.5500	0.8650	0.7508	0.6444	0.5460	0.4552	0.3714	0.2939	0.2219	0.1543	0.0879	0.0
0.5000	0.8650	0.7503	0.6435	0.5447	0.4536	0.3695	0.2920	0.2201	0.1528	0.0870	0.0
0.4500	0.8650	0.7497	0.6425	0.5434	0.4519	0.3677	0.2901	0.2183	0.1514	0.0862	0.0
0.4000	0.8650	0.7491	0.6414	0.5419	0.4501	0.3657	0.2882	0.2167	0.1501	0.0854	0.0
0.3500	0.8650	0.7485	0.6403	0.5404	0.4484	0.3639	0.2864	0.2152	0.1489	0.0845	0.0
0.3000	0.8650	0.7479	0.6392	0.5389	0.4468	0.3623	0.2849	0.2138	0.1478	0.0838	0.0
0.2500	0.8650	0.7471	0.6378	0.5372	0.4449	0.3604	0.2831	0.2123	0.1466	0.0831	0.0
0.2000	0.8650	0.7465	0.6368	0.5359	0.4434	0.3588	0.2815	0.2107	0.1453	0.0822	0.0
0.1500	0.8650	0.7463	0.6363	0.5352	0.4424	0.3576	0.2802	0.2094	0.1441	0.0812	0.0
0.1000	0.8650	0.7461	0.6360	0.5348	0.4419	0.3570	0.2795	0.2087	0.1434	0.0806	0.0
0.0500	0.8650	0.7459	0.6356	0.5341	0.4410	0.3560	0.2784	0.2075	0.1422	0.0797	0.0
0.0000	0.8650	0.7459	0.6356	0.5341	0.4410	0.3560	0.2784	0.2075	0.1422	0.0797	0.0

Table 11. Enthalpy, H, as a function of α and β for M_s = 7.65

▼ I S U COMPUTATION CENTER; AMES, IOWA

A/(A-1)	PR	-HW	KE	DVR	IMAX	KMAX	I1	I3	KI	KF
7.5000	0.7200	0.9190	1.4120	2.3777	11	21	1	15	2	20

BETA= 0.0	0.1000	0.2000	0.3000	0.4000	0.5000	0.6000	0.7000	0.8000	0.9000	1.0
ALPHA	H FIELD (NEGATIVE VALUES)									
1.0000	0.9190	0.7971	0.6840	0.5796	0.4832	0.3943	0.3122	0.2359	0.1640	0.0931	0.0
0.9500	0.9190	0.7971	0.6840	0.5796	0.4832	0.3943	0.3122	0.2359	0.1640	0.0931	0.0
0.9000	0.9190	0.7970	0.6838	0.5793	0.4828	0.3939	0.3117	0.2355	0.1636	0.0929	0.0
0.8500	0.9190	0.7970	0.6837	0.5791	0.4826	0.3936	0.3115	0.2352	0.1635	0.0928	0.0
0.8000	0.9190	0.7970	0.6836	0.5789	0.4824	0.3934	0.3112	0.2350	0.1633	0.0927	0.0
0.7500	0.9190	0.7969	0.6835	0.5787	0.4821	0.3931	0.3109	0.2348	0.1631	0.0926	0.0
0.7000	0.9190	0.7969	0.6833	0.5784	0.4818	0.3927	0.3106	0.2345	0.1629	0.0925	0.0
0.6500	0.9190	0.7967	0.6829	0.5779	0.4812	0.3921	0.3100	0.2339	0.1625	0.0924	0.0
0.6000	0.9190	0.7964	0.6823	0.5771	0.4801	0.3909	0.3087	0.2327	0.1614	0.0918	0.0
0.5500	0.9190	0.7960	0.6816	0.5761	0.4789	0.3895	0.3072	0.2312	0.1602	0.0910	0.0
0.5000	0.9190	0.7955	0.6806	0.5747	0.4772	0.3876	0.3052	0.2293	0.1586	0.0900	0.0
0.4500	0.9190	0.7949	0.6795	0.5732	0.4754	0.3856	0.3031	0.2273	0.1570	0.0890	0.0
0.4000	0.9190	0.7942	0.6783	0.5716	0.4734	0.3834	0.3010	0.2254	0.1556	0.0881	0.0
0.3500	0.9190	0.7935	0.6771	0.5699	0.4714	0.3813	0.2990	0.2237	0.1542	0.0872	0.0
0.3000	0.9190	0.7928	0.6759	0.5683	0.4696	0.3795	0.2973	0.2222	0.1530	0.0864	0.0
0.2500	0.9190	0.7919	0.6744	0.5665	0.4677	0.3775	0.2955	0.2206	0.1517	0.0856	0.0
0.2000	0.9190	0.7912	0.6732	0.5648	0.4658	0.3755	0.2935	0.2188	0.1502	0.0846	0.0
0.1500	0.9190	0.7909	0.6725	0.5639	0.4646	0.3742	0.2920	0.2173	0.1488	0.0835	0.0
0.1000	0.9190	0.7907	0.6722	0.5634	0.4640	0.3735	0.2912	0.2165	0.1480	0.0828	0.0
0.0500	0.9190	0.7905	0.6717	0.5627	0.4631	0.3724	0.2900	0.2152	0.1468	0.0819	0.0
0.0000	0.9190	0.7905	0.6717	0.5627	0.4631	0.3724	0.2900	0.2152	0.1468	0.0819	0.0

Table 12. Enthalpy, H, as a function of α and β for M_s = 9.35

▼ I S U COMPUTATION CENTER; AMES, IOWA

A/(A-1)	PR	-HW	KE	CVR	IMAX	KMAX	I1	I3	KI	KF
9.0000	0.7200	0.9450	1.5090	2.7466	11	21	1	15	2	20

BETA= 0.0	0.1000	0.2000	0.3000	0.4000	0.5000	0.6000	0.7000	0.8000	0.9000	1.0
ALPHA	H FIELD (NEGATIVE VALUES)									
1.0000	0.9450	0.8180	0.7003	0.5919	0.4922	0.4004	0.3160	0.2379	0.1648	0.0932	0.0
0.9500	0.9450	0.8180	0.7003	0.5919	0.4922	0.4004	0.3160	0.2379	0.1648	0.0932	0.0
0.9000	0.9450	0.8179	0.7001	0.5916	0.4917	0.3999	0.3155	0.2375	0.1644	0.0930	0.0
0.8500	0.9450	0.8179	0.7000	0.5914	0.4915	0.3997	0.3152	0.2372	0.1643	0.0929	0.0
0.8000	0.9450	0.8179	0.6999	0.5912	0.4913	0.3994	0.3149	0.2370	0.1641	0.0928	0.0
0.7500	0.9450	0.8178	0.6998	0.5910	0.4910	0.3991	0.3147	0.2367	0.1639	0.0927	0.0
0.7000	0.9450	0.8177	0.6996	0.5907	0.4907	0.3988	0.3143	0.2364	0.1636	0.0926	0.0
0.6500	0.9450	0.8176	0.6992	0.5903	0.4901	0.3981	0.3137	0.2359	0.1633	0.0925	0.0
0.6000	0.9450	0.8172	0.6986	0.5894	0.4890	0.3969	0.3124	0.2347	0.1622	0.0919	0.0
0.5500	0.9450	0.8169	0.6979	0.5884	0.4877	0.3955	0.3109	0.2332	0.1609	0.0911	0.0
0.5000	0.9450	0.8163	0.6969	0.5869	0.4860	0.3935	0.3089	0.2312	0.1593	0.0901	0.0
0.4500	0.9450	0.8157	0.6957	0.5854	0.4841	0.3914	0.3067	0.2291	0.1576	0.0891	0.0
0.4000	0.9450	0.8150	0.6945	0.5836	0.4820	0.3891	0.3044	0.2271	0.1561	0.0881	0.0
0.3500	0.9450	0.8143	0.6931	0.5818	0.4799	0.3869	0.3023	0.2253	0.1547	0.0872	0.0
0.3000	0.9450	0.8135	0.6919	0.5802	0.4780	0.3850	0.3005	0.2237	0.1533	0.0862	0.0
0.2500	0.9450	0.8126	0.6903	0.5783	0.4760	0.3830	0.2986	0.2221	0.1521	0.0855	0.0
0.2000	0.9450	0.8118	0.6889	0.5764	0.4739	0.3807	0.2965	0.2201	0.1505	0.0844	0.0
0.1500	0.9450	0.8114	0.6881	0.5753	0.4725	0.3792	0.2948	0.2185	0.1490	0.0832	0.0
0.1000	0.9450	0.8112	0.6878	0.5748	0.4719	0.3784	0.2940	0.2175	0.1481	0.0825	0.0
0.0500	0.9450	0.8110	0.6873	0.5741	0.4709	0.3773	0.2927	0.2162	0.1468	0.0815	0.0
0.0000	0.9450	0.8110	0.6873	0.5741	0.4709	0.3773	0.2927	0.2162	0.1468	0.0815	0.0

Table 13. Enthalpy, H, as a function of α and β for M_s = 11.3

▼ I S U COMPUTATION CENTER; AMES, IOWA

A/(A-1)	PR	-HW	KE	DVR	IMAX	KMAX	I1	I3	KI	KP
10.0000	0.7200	0.9620	1.5980	3.1741	11	21	1	15	2	20

BETA= 0.0	0.1000	0.2000	0.3000	0.4000	0.5000	0.6000	0.7000	0.8000	0.9000	1.0
ALPHA	H FIELD (NEGATIVE VALUES)									
1.0000	0.9620	0.8308	0.7095	0.5980	0.4956	0.4019	0.3159	0.2369	0.1634	0.0920	0.0
0.9500	0.9620	0.8308	0.7095	0.5980	0.4956	0.4019	0.3159	0.2369	0.1634	0.0920	0.0
0.9000	0.9620	0.8307	0.7093	0.5977	0.4952	0.4014	0.3154	0.2365	0.1630	0.0918	0.0
0.8500	0.9620	0.8307	0.7092	0.5975	0.4950	0.4011	0.3152	0.2362	0.1629	0.0917	0.0
0.8000	0.9620	0.8307	0.7091	0.5973	0.4947	0.4008	0.3149	0.2360	0.1626	0.0916	0.0
0.7500	0.9620	0.8306	0.7089	0.5971	0.4945	0.4005	0.3146	0.2357	0.1625	0.0915	0.0
0.7000	0.9620	0.8306	0.7087	0.5968	0.4941	0.4002	0.3143	0.2354	0.1622	0.0914	0.0
0.6500	0.9620	0.8304	0.7084	0.5963	0.4936	0.3996	0.3137	0.2349	0.1619	0.0913	0.0
0.6000	0.9620	0.8301	0.7078	0.5955	0.4925	0.3984	0.3125	0.2337	0.1609	0.0907	0.0
0.5500	0.9620	0.8297	0.7071	0.5944	0.4913	0.3970	0.3109	0.2322	0.1596	0.0899	0.0
0.5000	0.9620	0.8292	0.7060	0.5930	0.4895	0.3950	0.3089	0.2303	0.1580	0.0890	0.0
0.4500	0.9620	0.8285	0.7049	0.5914	0.4875	0.3928	0.3066	0.2281	0.1562	0.0879	0.0
0.4000	0.9620	0.8278	0.7036	0.5896	0.4854	0.3905	0.3043	0.2260	0.1547	0.0869	0.0
0.3500	0.9620	0.8270	0.7022	0.5877	0.4832	0.3881	0.3020	0.2241	0.1532	0.0859	0.0
0.3000	0.9620	0.8263	0.7008	0.5860	0.4812	0.3861	0.3001	0.2224	0.1517	0.0849	0.0
0.2500	0.9620	0.8253	0.6993	0.5840	0.4791	0.3841	0.2982	0.2208	0.1505	0.0842	0.0
0.2000	0.9620	0.8244	0.6977	0.5820	0.4769	0.3817	0.2960	0.2187	0.1488	0.0831	0.0
0.1500	0.9620	0.8239	0.6968	0.5808	0.4754	0.3800	0.2942	0.2170	0.1472	0.0818	0.0
0.1000	0.9620	0.8237	0.6964	0.5802	0.4746	0.3792	0.2932	0.2160	0.1462	0.0810	0.0
0.0500	0.9620	0.8235	0.6959	0.5795	0.4737	0.3780	0.2920	0.2146	0.1450	0.0800	0.0
0.0000	0.9620	0.8235	0.6959	0.5795	0.4737	0.3780	0.2920	0.2146	0.1450	0.0800	0.0

Table 14. Enthalpy, H, as a function of α and β for $M_s = 14$

▼ I S U COMPUTATION CENTER; AMES, IOWA

A/(A-1)	PR	-HW	KE	DVR	IMAX	KMAX	I1	I3	KI	KF
10.6500	0.7200	0.9750	1.6200	3.9531	11	21	1	15	2	20

BETA= 0.0	0.1000	0.2000	0.3000	0.4000	0.5000	0.6000	0.7000	0.8000	0.9000	1.0
ALPHA	H FIELD (NEGATIVE VALUES)									
1.0000	0.9750	0.8423	0.7195	0.6065	0.5029	0.4078	0.3207	0.2406	0.1660	0.0935	0.0
0.9500	0.9750	0.8423	0.7195	0.6065	0.5029	0.4078	0.3207	0.2406	0.1660	0.0935	0.0
0.9000	0.9750	0.8422	0.7193	0.6062	0.5024	0.4074	0.3202	0.2402	0.1657	0.0933	0.0
0.8500	0.9750	0.8422	0.7192	0.6060	0.5022	0.4071	0.3200	0.2399	0.1654	0.0932	0.0
0.8000	0.9750	0.8421	0.7190	0.6058	0.5019	0.4068	0.3197	0.2396	0.1652	0.0930	0.0
0.7500	0.9750	0.8421	0.7189	0.6056	0.5017	0.4065	0.3194	0.2394	0.1650	0.0929	0.0
0.7000	0.9750	0.8421	0.7187	0.6054	0.5014	0.4062	0.3191	0.2391	0.1649	0.0928	0.0
0.6500	0.9750	0.8419	0.7185	0.6050	0.5009	0.4057	0.3186	0.2387	0.1646	0.0927	0.0
0.6000	0.9750	0.8417	0.7180	0.6043	0.5001	0.4048	0.3177	0.2378	0.1639	0.0925	0.0
0.5500	0.9750	0.8413	0.7172	0.6032	0.4988	0.4033	0.3161	0.2363	0.1626	0.0917	0.0
0.5000	0.9750	0.8408	0.7163	0.6019	0.4972	0.4015	0.3143	0.2345	0.1611	0.0908	0.0
0.4500	0.9750	0.8401	0.7150	0.6002	0.4951	0.3992	0.3119	0.2322	0.1592	0.0896	0.0
0.4000	0.9750	0.8394	0.7137	0.5984	0.4929	0.3968	0.3094	0.2300	0.1575	0.0885	0.0
0.3500	0.9750	0.8386	0.7122	0.5964	0.4906	0.3943	0.3070	0.2279	0.1558	0.0875	0.0
0.3000	0.9750	0.8377	0.7108	0.5945	0.4883	0.3919	0.3048	0.2260	0.1543	0.0864	0.0
0.2500	0.9750	0.8368	0.7093	0.5925	0.4862	0.3899	0.3029	0.2243	0.1529	0.0855	0.0
0.2000	0.9750	0.8358	0.7076	0.5904	0.4839	0.3875	0.3006	0.2223	0.1513	0.0845	0.0
0.1500	0.9750	0.8352	0.7065	0.5889	0.4821	0.3855	0.2986	0.2203	0.1495	0.0831	0.0
0.1000	0.9750	0.8350	0.7060	0.5883	0.4813	0.3846	0.2975	0.2192	0.1485	0.0823	0.0
0.0500	0.9750	0.8347	0.7055	0.5875	0.4803	0.3834	0.2962	0.2178	0.1472	0.0812	0.0
0.0000	0.9750	0.8347	0.7055	0.5875	0.4803	0.3834	0.2962	0.2178	0.1472	0.0812	0.0

Table 15. Heat transfer parameter, $\bar{Q}$, as a function of α and M_s

	Shock Mach Number, M_s						
	1.60	3.15	5.75	7.65	9.35	11.30	14.00
Alpha	Heat Transfer Parameter, $\bar{Q}$						
1.00	0.2247	0.8489	1.6093	1.9938	2.3151	2.5733	2.8300
0.95	0.2137	0.7722	1.4068	1.6969	1.9222	2.1036	2.2912
0.90	0.2033	0.7074	1.2514	1.4820	1.6519	1.7904	1.9386
0.85	0.1931	0.6507	1.1253	1.3150	1.4496	1.5609	1.6836
0.80	0.1835	0.6010	1.0204	1.1806	1.2910	1.3838	1.4886
0.75	0.1743	0.5565	0.9309	1.0687	1.1618	1.2412	1.3326
0.70	0.1653	0.5163	0.8533	0.9737	1.0536	1.1229	1.2036
0.65	0.1567	0.4801	0.7846	0.8909	0.9606	1.0218	1.0939
0.60	0.1485	0.4472	0.7247	0.8195	0.8809	0.9352	0.9992
0.55	0.1408	0.4174	0.6705	0.7554	0.8101	0.8588	0.9168
0.50	0.1337	0.3906	0.6226	0.6993	0.7482	0.7921	0.8438
0.45	0.1261	0.3659	0.5801	0.6493	0.6930	0.7325	0.7794
0.40	0.1203	0.3428	0.5401	0.6040	0.6443	0.6807	0.7230
0.35	0.1150	0.3258	0.5068	0.5630	0.5980	0.6302	0.6699
0.30	0.1095	0.3090	0.4806	0.5327	0.5645	0.5932	0.6263
0.25	0.1069	0.2974	0.4571	0.5050	0.5342	0.5612	0.5928
0.20	0.1064	0.2946	0.4477	0.4909	0.5162	0.5392	0.5671
0.15	0.1066	0.2949	0.4470	0.4894	0.5139	0.5356	0.5607
0.10	0.1067	0.2955	0.4478	0.4900	0.5142	0.5357	0.5606
0.05	0.1069	0.2960	0.4489	0.4914	0.5159	0.5376	0.5623
0.00	0.1069	0.2960	0.4489	0.4914	0.5159	0.5376	0.5623

described calculations account for the variation of C with temperature according to the following equation given by Mirels (23).

$$C = \frac{\rho_w \mu_w}{\rho_o \mu_o} \left[\frac{1.5481}{\sqrt{\frac{H+1}{H_w+1}}} - \frac{0.5481}{\frac{H+1}{H_w+1}} + 0.0028 \left(\frac{H-H_w}{H_w+1}\right) - 5.74 \times 10^{-5} \left(\frac{H-H_w}{H_w+1}\right)^2 \right] \qquad (52)$$

This equation is accurate within 3 per cent over the range considered here. Selected results from Tables 1 thru 15 are plotted in Figure 6 thru 11. In Figure 6 the heat transfer parameter, $\bar{Q} = (\phi H_\beta)_w$, evaluated at the wall is plotted as a function of M_s with α as a parameter. In Figure 7 $\bar{Q}$ is plotted as a function of α with M_s as a parameter. The shear stress at the wall, ϕ_w, is plotted against M_s with α as a parameter in Figure 8. In Figure 9 it is plotted against α with M_s as a parameter.

Figures 10 and 11 show steady state values of α as a function of M_s taken from the heat transfer and shear stress calculations respectively. For values of α less than the given indicated steady state value the heat transfer or shear stress will be within the given percentage of the final steady state value. Curves are shown for 1, 5, and 10 per cent. The scatter in the points may be attributed to reading error since the steady values are approached asymptotically.

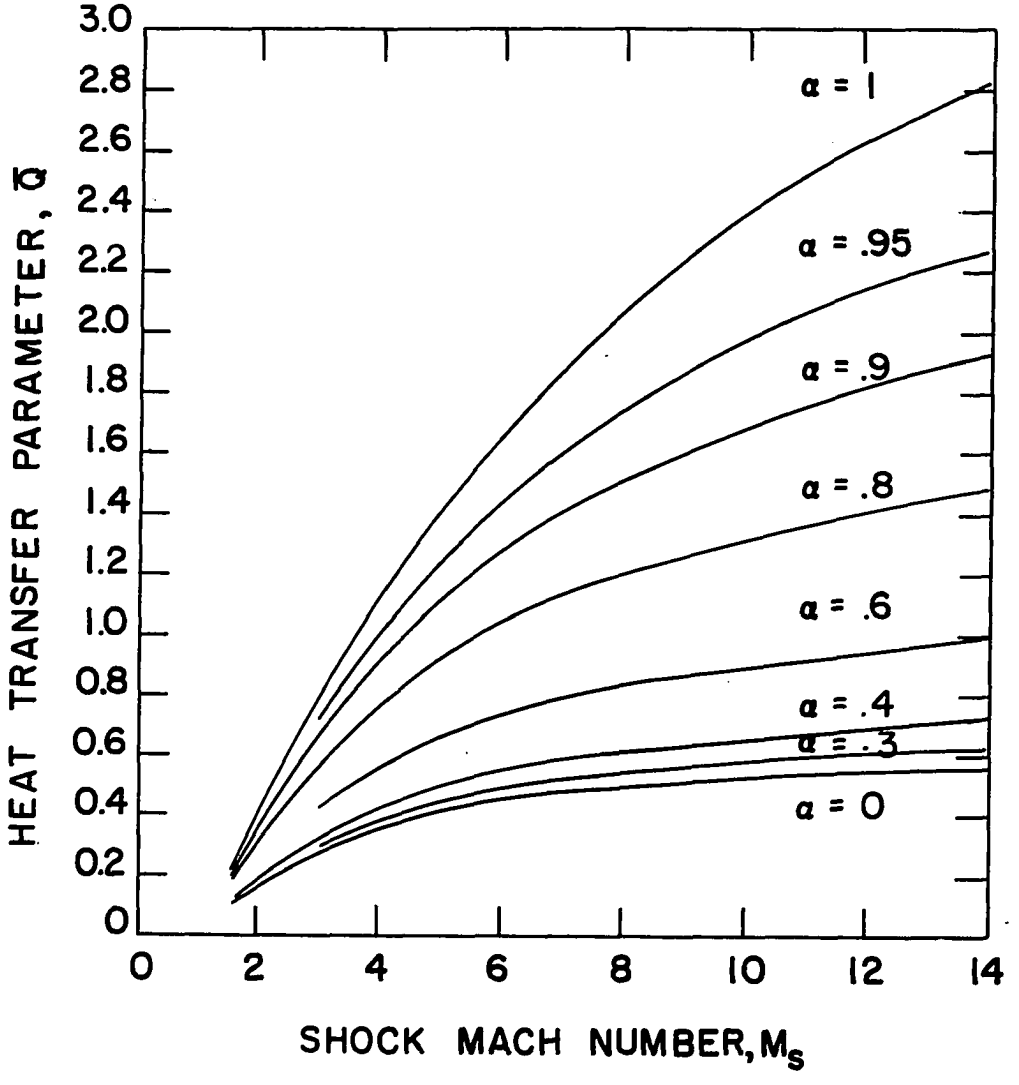

Figure 6. Heat transfer parameter, $\bar{Q}$, as a function of shock Mach number with α as a parameter

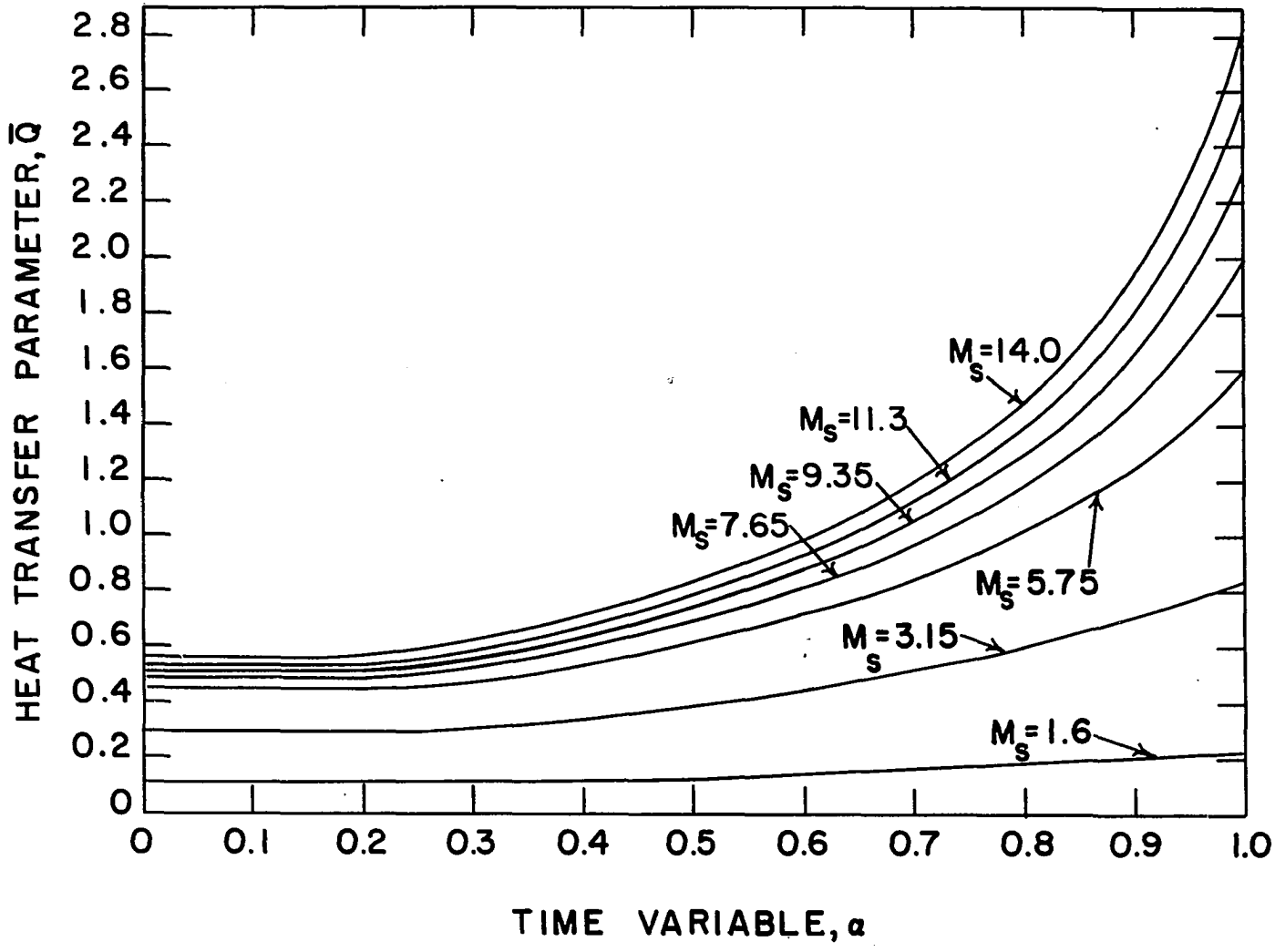

Figure 7. Heat transfer parameter, $\bar{Q}$, as a function of α with shock Mach number as a parameter

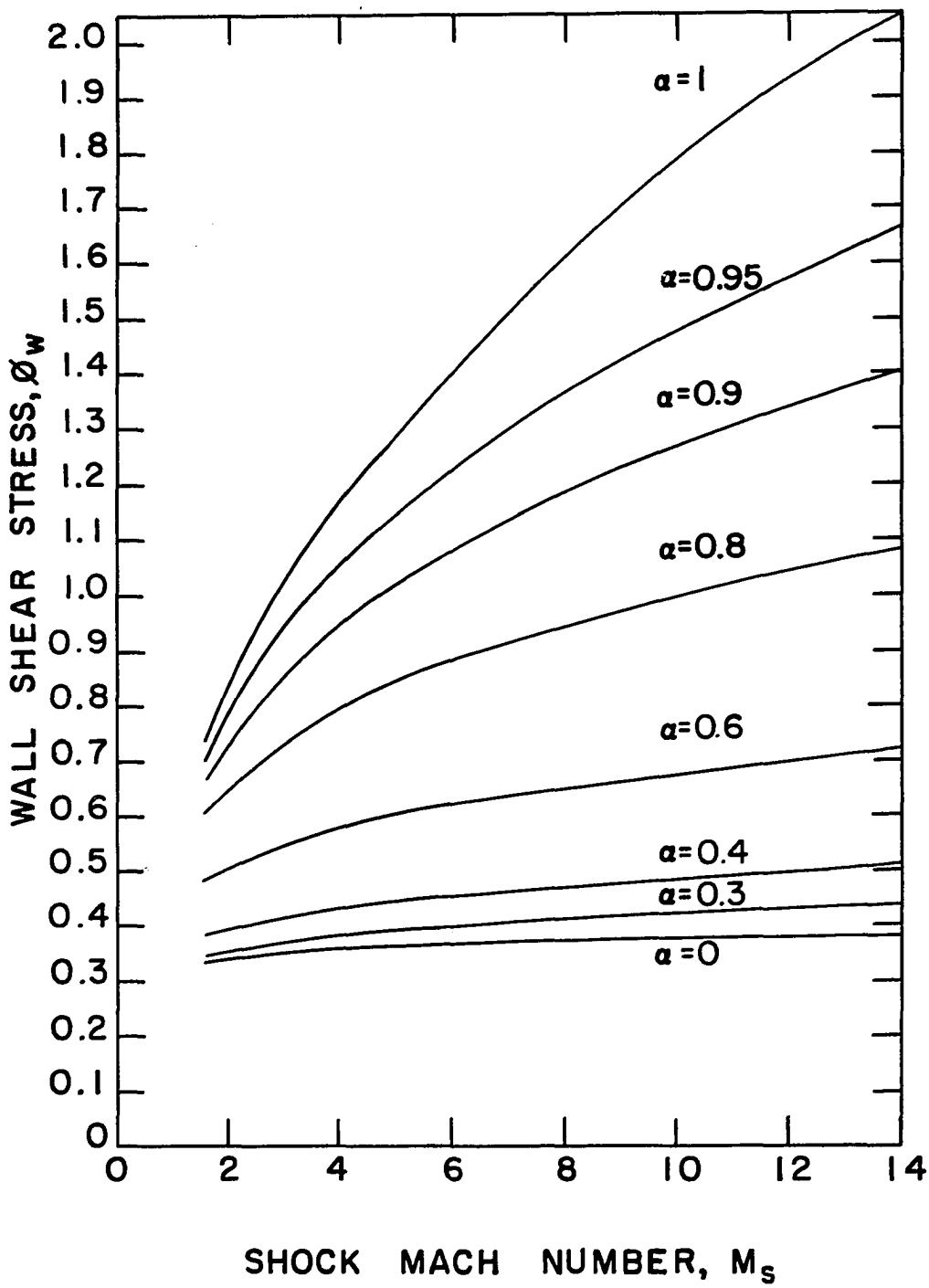

Figure 8. Wall shear stress, ϕ_w, as a function of shock Mach number with α as a parameter

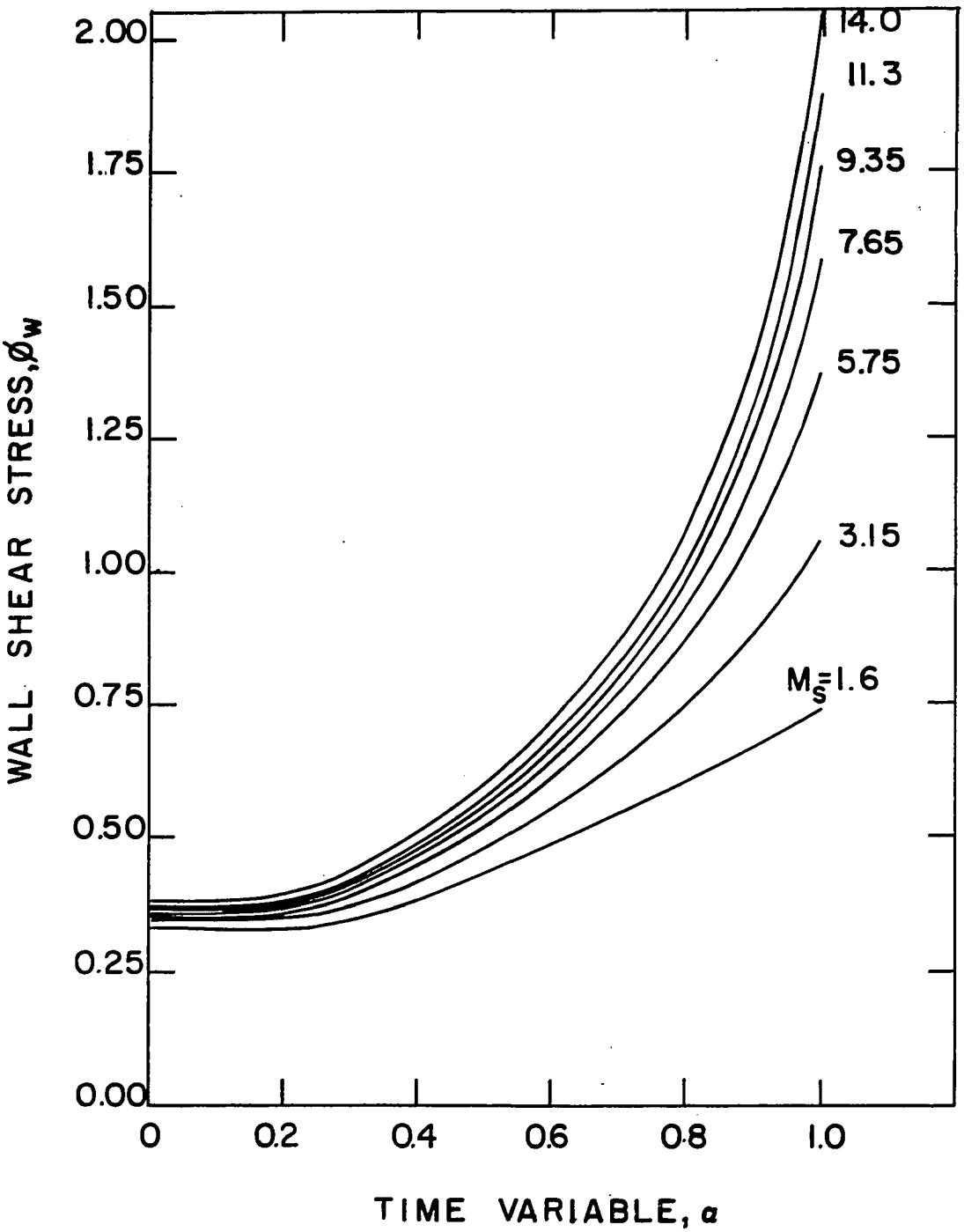

Figure 9. Wall shear stress, ϕ_w, as a function of α with shock Mach number as a parameter

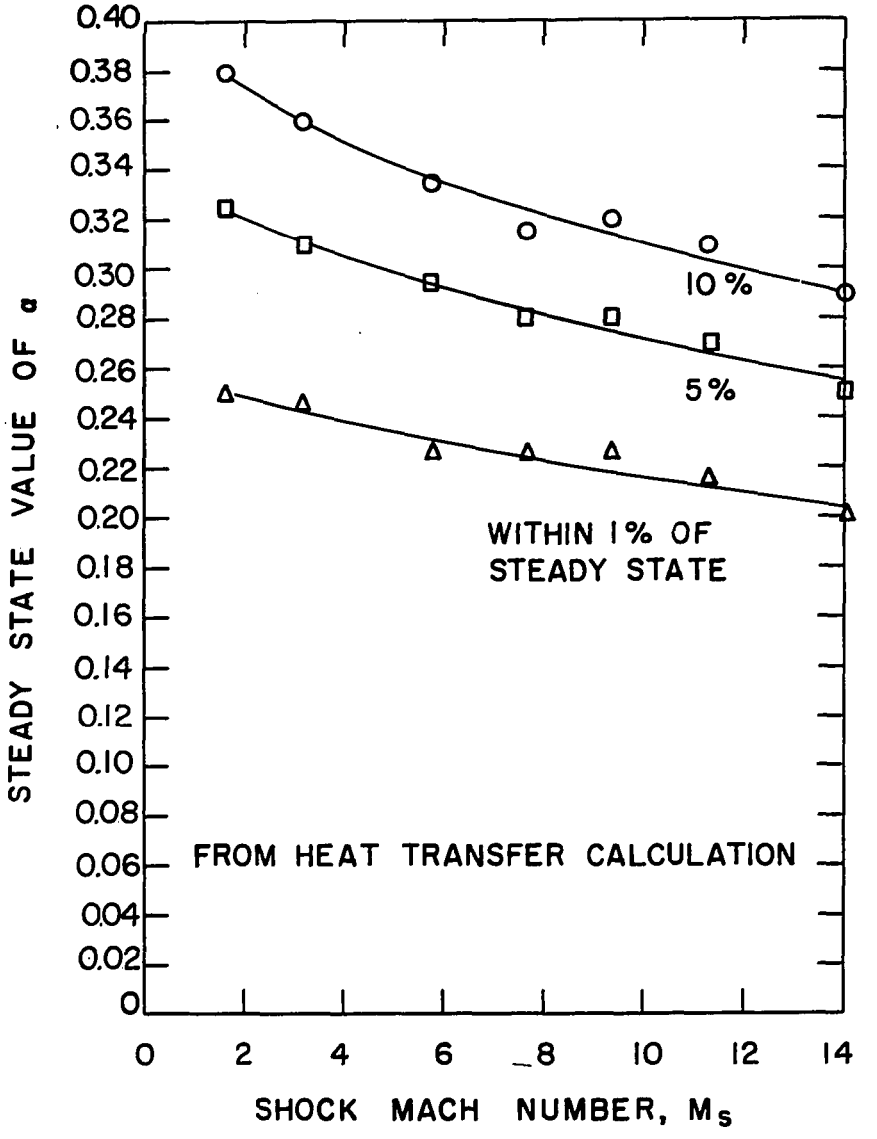

Figure 10. Steady state values of α as a function of shock Mach number taken from the heat transfer calculations

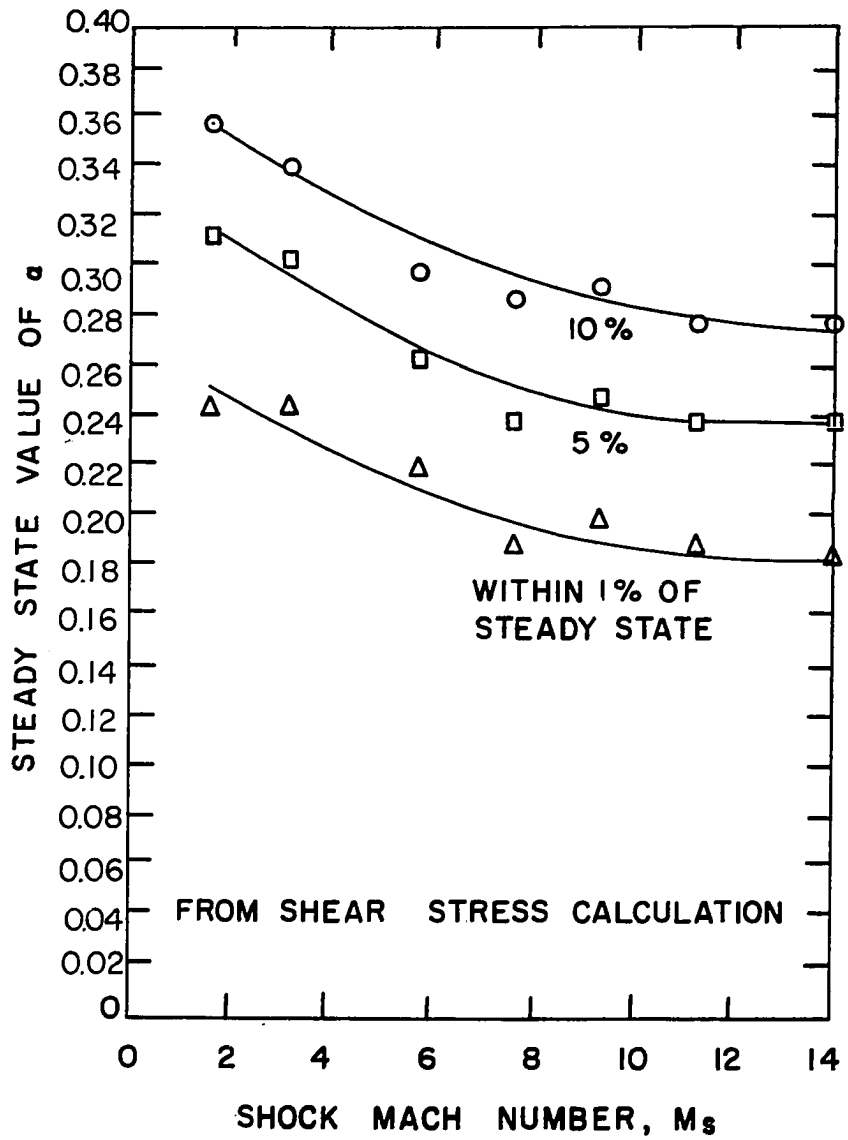

Figure 11. Steady state values of α as a function of shock Mach number taken from the shear stress calculations

Calculations were carried out at M_s values of 1.6, 3.15, and 5.75 for the case of C = 1. Comparisons with the C ≠ 1 results are shown in Figures 12 and 13 for heat transfer and shear stress at the wall respectively. It is noted that for the case of M_s = 5.75 the results are from 15 - 20 per cent low when C is assumed equal to one. From the results of Mirels (23) valid at α = 1 it can be seen that this variation becomes much greater at higher shock Mach numbers.

Numerical solutions for a projectile penetrating a barrier

An attempt was made to obtain numerical results for the boundary layer development on a flat plate penetrating a barrier. It was noted before that for this case A = 1. Hence the point α = 1 is at the barrier. The shear stress becomes infinite at the barrier, in this case at α = 1. One cannot apply an infinite boundary condition in a numerical solution, however, one can apply several very large values in lieu of the infinite boundary condition and study the behavior of the resulting solutions. In view of the highly approximate nature of this analysis solutions were carried out only for C = 1. As A approaches one, A/A-1 approaches infinity. Solutions to the momentum equation were carried out for A/A-1 = 200, 300, and 400. The results of these calculations in the form of shear stress at the wall are plotted against α in Figure 14. For values of α near one some difference is noted between the solutions. However, for α = 0.8 and smaller

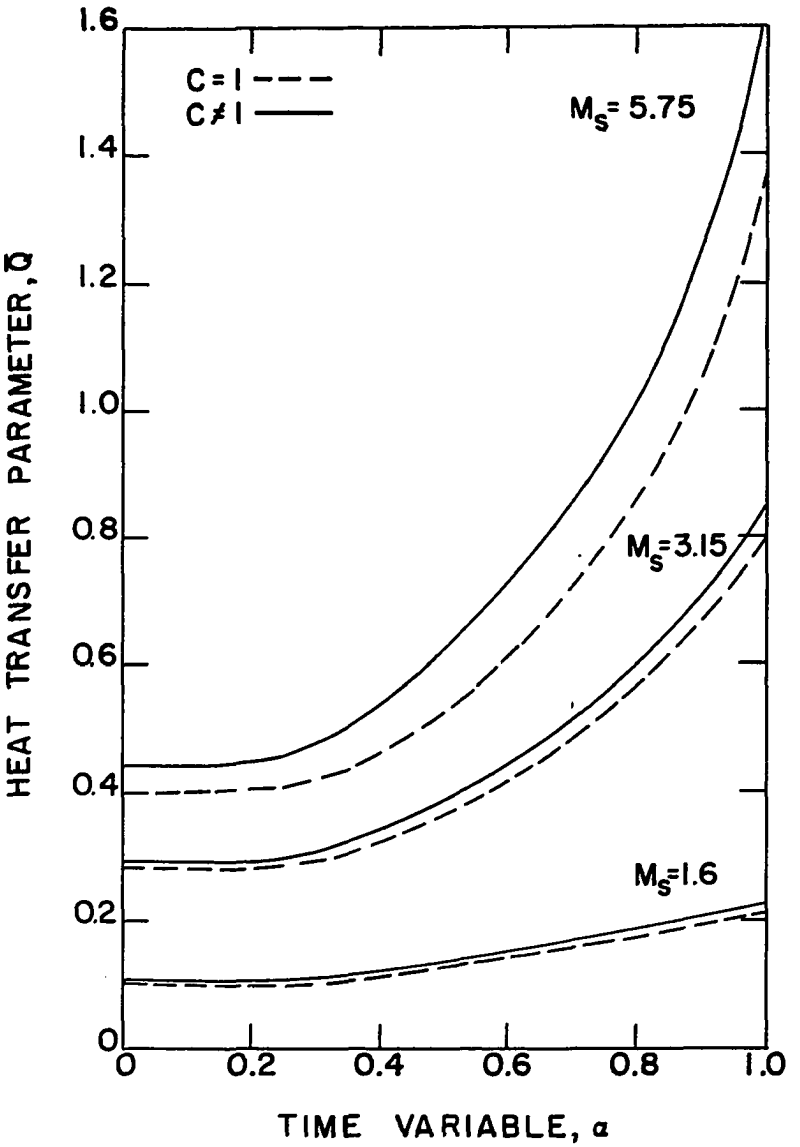

Figure 12. Comparison of heat transfer results accounting for variable properties with results obtained by assuming viscosity proportional to temperature

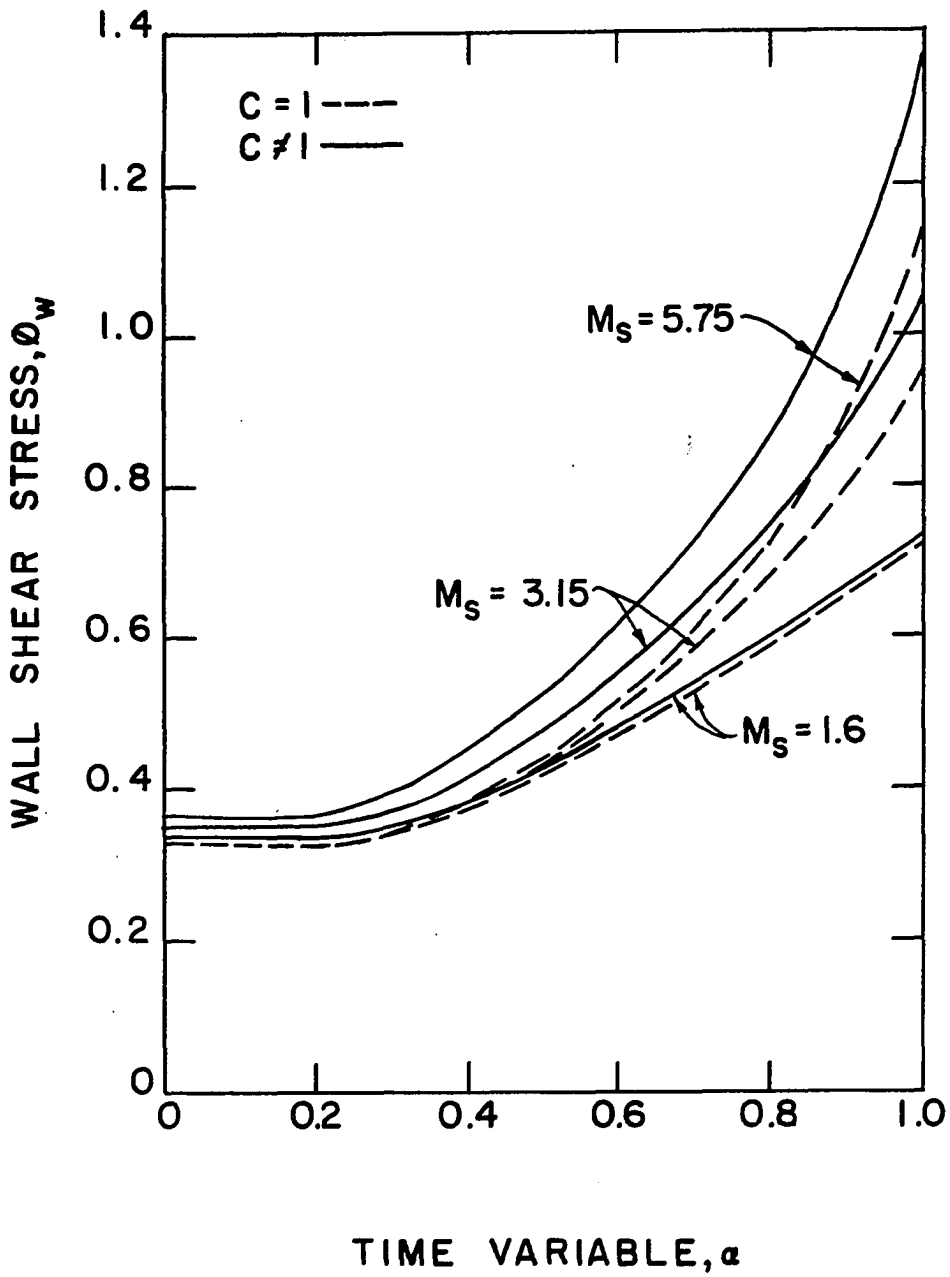

Figure 13. Comparison of shear stress results accounting for variable properties with results obtained by assuming viscosity proportional to temperature

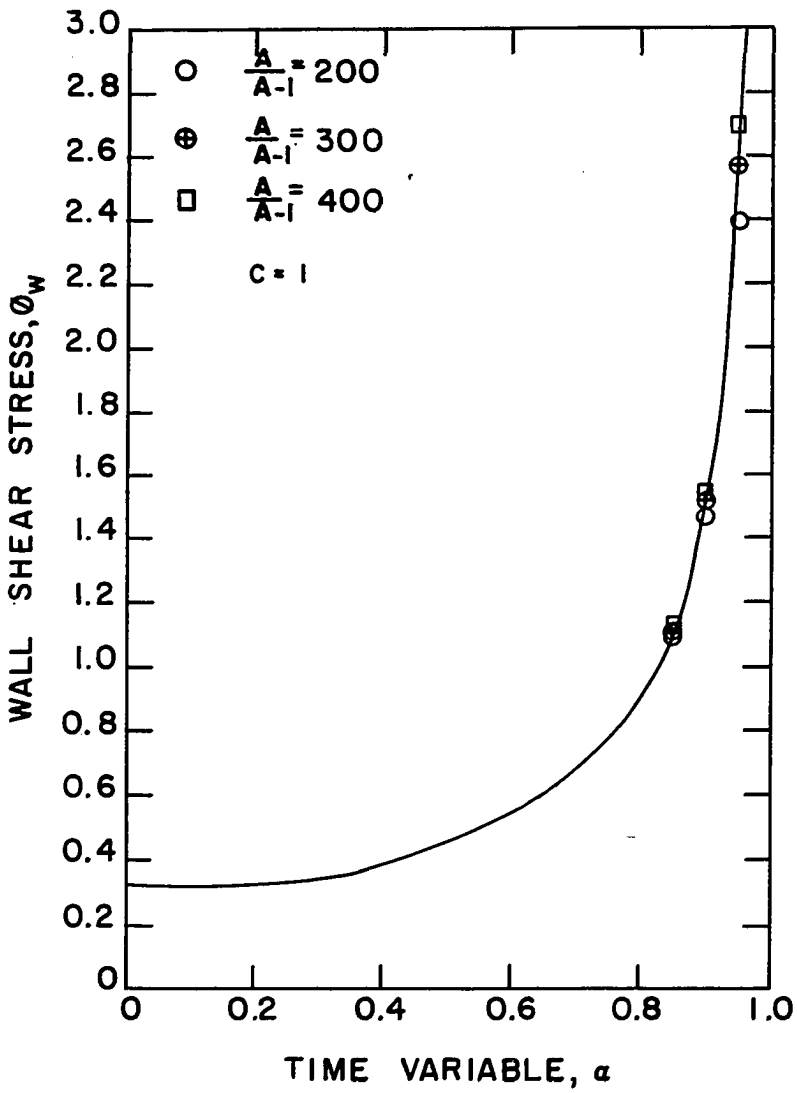

Figure 14. Wall shear stress, ϕ_w, as a function of α for the case of A approaching one

the solutions are indistinguishable. This would lead one to believe that one might use the results plotted in Figure 14 as an approximate solution for the case of A = 1, at least for smaller values of α.

Using the solution for ϕ corresponding to $\bar{A}/\bar{A}-1 = 400$ a series of solutions were carried out for the energy equation. For this case the values of $\frac{u_o^2}{h_o}$ and H_w are not determined by the value of A but may vary independently of each other and of A. Figures 15 and 16 show the heat transfer parameter, $\bar{Q}$, as a function of α for several values of $\frac{u_o^2}{h_o}$ and H_w. In Figure 15 H_w is held constant at -0.5 and $\frac{u_o^2}{h_o}$ is allowed to take on the values 0.25, 1 and 3. In Figure 16 $\frac{u_o^2}{h_o}$ is held constant at a value of one and H_w takes the values -0.1, -0.5, and -0.9. The heat transfer results exhibit the logical characteristics of tending to very large values near $\alpha = 1$ where the boundary layer is very thin and tending to a steady value at small values of α.

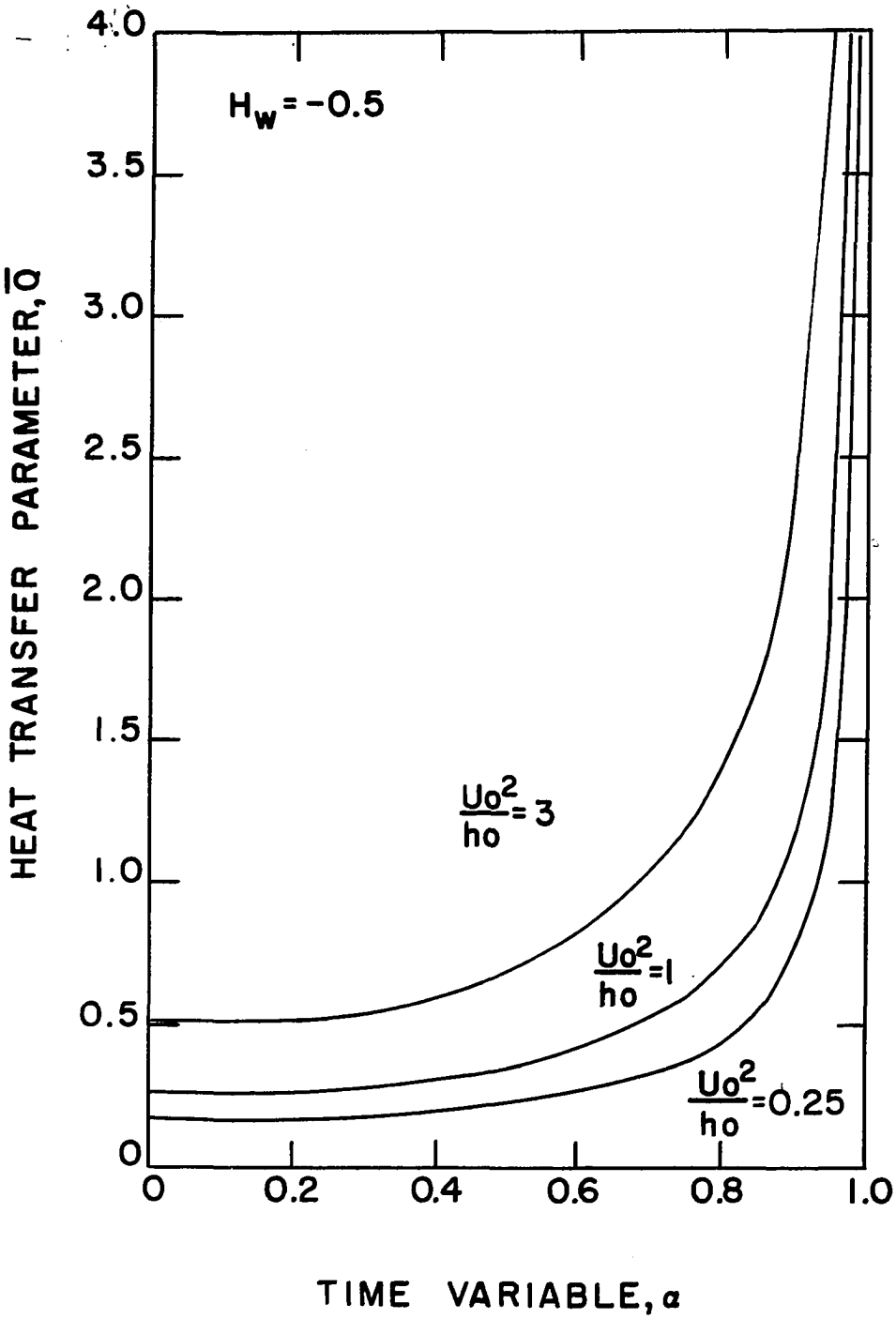

Figure 15. Heat transfer parameter, $\bar{Q}$, as a function of α for the case of A approaching one, showing the effect of variation in the kinetic energy parameter, u_o^2/h_o

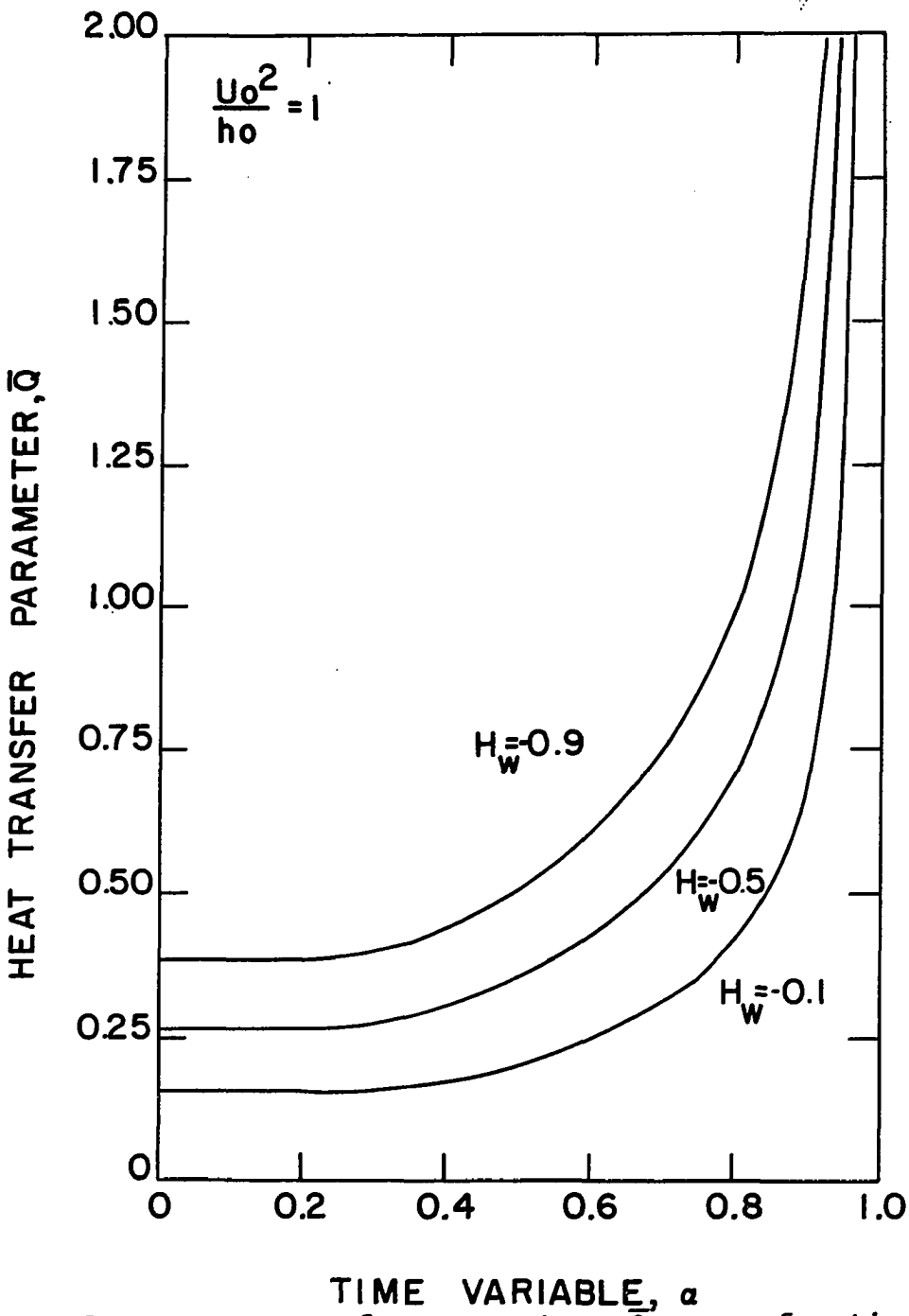

Figure 16. Heat transfer parameter, $\bar{Q}$, as a function of α, for the case of A approaching one, showing the effect of variation in wall enthalpy, H_w

EXPERIMENTAL VERIFICATION

Experimental Equipment

Shock tube

The shock tube as a device for generating flows of high velocity and enthalpy has been amply described in the literature (10,11). A shock tube consists basically of a high pressure section and a low pressure section separated by a diaphragm. When the diaphragm is ruptured pressure pulses soon steepen to form a shock wave which propagates into the low pressure section or channel. The shock Mach number, which characterizes the strength of the wave, is defined as the speed of the shock wave divided by the speed of sound in the gas initially at rest in the channel. This shock wave heats and accelerates the gas in the channel. By applying the conservation equations across the shock wave the properties behind the shock wave can be determined. Glass and Patterson (11) give the necessary relations for the case of a perfect gas. Feldman (8) presents the properties behind the shock wave in chart form for equilibrium air.

The Iowa State University Shock Tube has been described in some detail by Hall (12). It has a three inch by six inch internal cross section and is thirty-eight feet long. The test gas used was air while the driver gas was air, helium, or mixtures of air and helium.

Two experimental measurements are necessary to determine

the conditions in the shock tube. It is necessary to measure the pressure of the gas initially in the channel section. This was done with a Dubrovin vacuum gage for the higher pressures and with a Vecco Thermocouple vacuum gage for the lower pressures. A McCloud vacuum gage was used as a calibration standard. Since the gas is assumed to be initially at room temperature this is sufficient to fix the initial state of the gas.

It is also necessary to measure the speed of the initial shock wave. This was accomplished with two platinum thin film resistance thermometers, similar to the heat transfer gages to be described later, mounted two feet apart on the side wall of the shock tube. The outputs of these two sensing devices were fed to a Beckman/Berkeley Model 7361U Eput and Counter which recorded the amount of time required for the shock wave to pass between the two stations.

Model design

The model used was a simple flat plate as shown in Figure 17. The basic plate was machined from mild steel plate. Slots were machined in the top of the plate to accept pyrex inserts on which the thin platinum film heat transfer gages were mounted. Heat transfer gages were mounted at 2.58, 4.62, and 6.55 inches back from the leading edge of the plate. Three gages were mounted at each position. Provisions were made for passing lead wires from the heat transfer gages out

Figure 17. Photograph of the flat plate showing the heat transfer gages

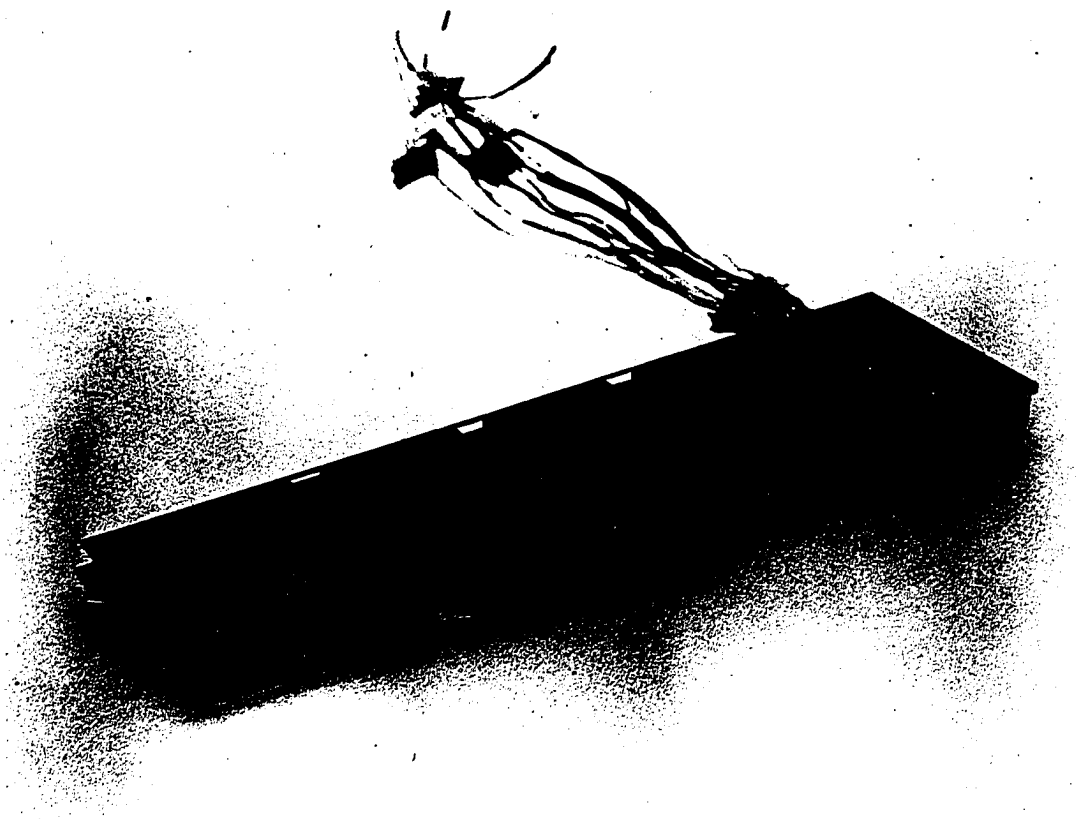

through the center of the plate. The leading edge was formed by a 7 degree included angle. This allowed operation with an attached shock on the underside of the plate, with the plate mounted at zero angle of attack, for a shock Mach number of greater than 2.8. A drawing of the plate with pertinent dimensions is shown in Figure 18.

The plate was mounted spanning the tube horizontally near the vertical center of the tube as shown in Figure 19. The plate was supported by a rod and cam system internal to the model. This method was used in order to avoid any choking effects due to external model supports.

Heat transfer gages

The thin platinum film heat transfer measuring technique has been described by several authors (3,5,27,36). The technique used here is essentially that previously developed in the Iowa State University Shock Tube Laboratory (5,6,7,12). A summary is included here along with any changes in the procedure made for this investigation.

Construction The platinum films were mounted on pyrex plates. The plates were constructed with a series of four countersunk holes along the centerline as shown in Figure 18. Three gages were constructed on each plate. The countersunk faces of the holes were polished before mounting the gages. The surface of the plate was finally cleaned with acetone. Liquid-Bright Platinum #05-X, a suspension of platinum in an

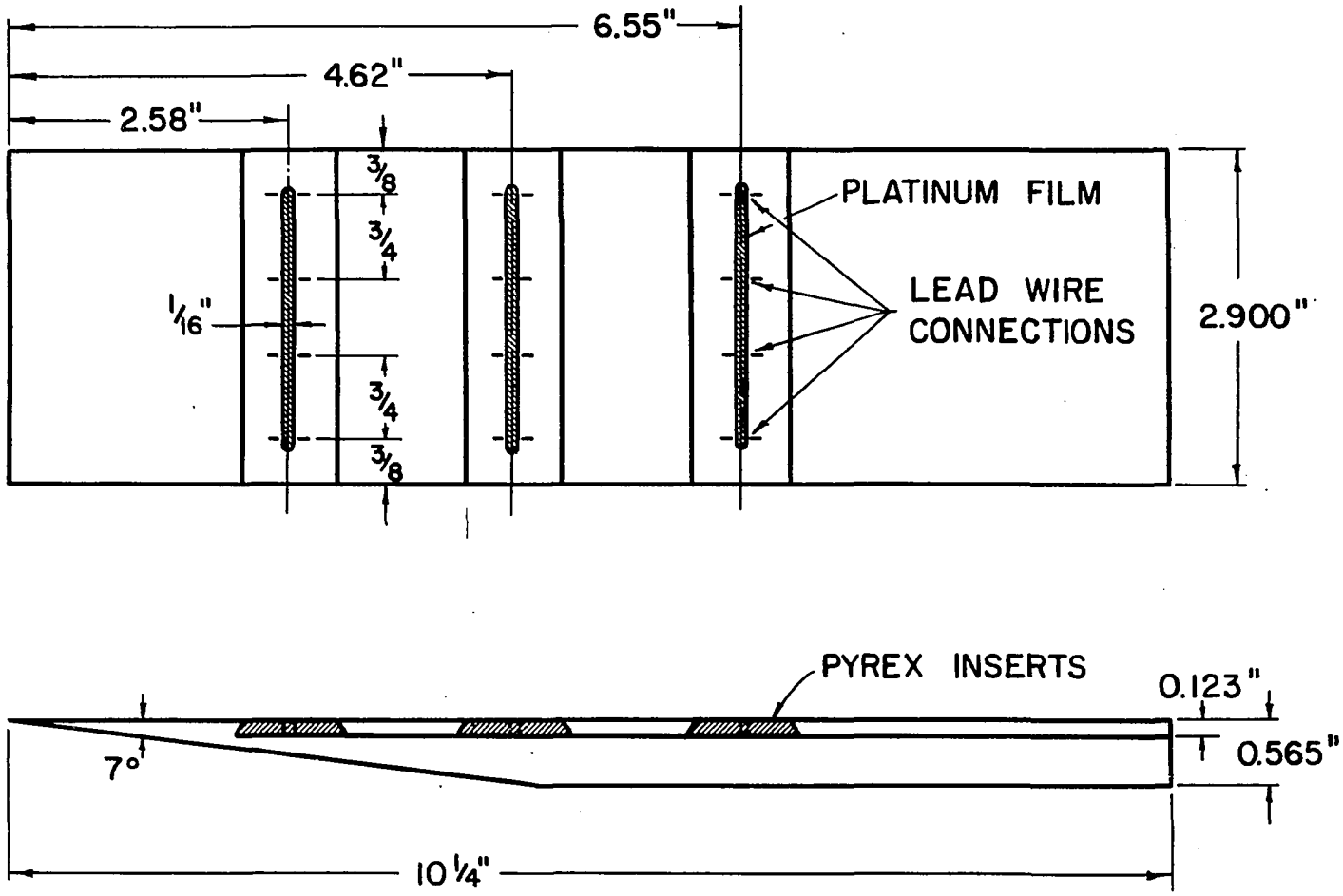

Figure 18. Drawing of the flat plate

Figure 19. Photograph of the flat plate mounted in the shock tube

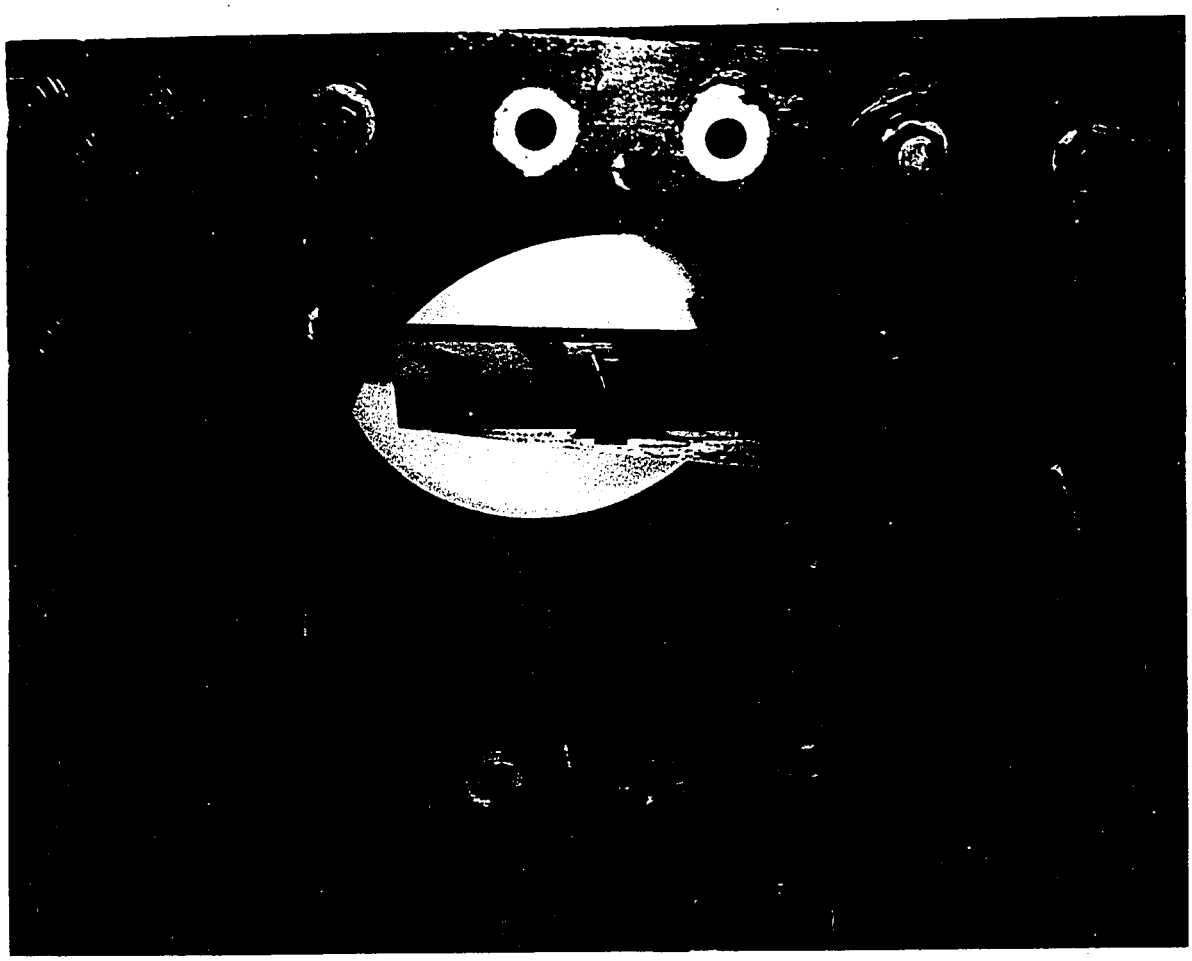

organic solvent manufactured by Engelhard Industries, Inc., East Newark, New Jersey, was used for the gages. A thin coating of this material was applied to the pyrex with a fine sable hair paint brush. The pyrex was then heated to 900 degrees Fahrenheit in an open furnace at which time the organic carrier had burned off and the platinum had been deposited on the pyrex. The pyrex was then heated to 1280-1320 degrees Fahrenheit in order to soften the pyrex and allow the platinum to bond well to the pyrex. Aging for three or four hours at somewhat lower temperatures was found to increase the durability of the film.

Lead wires were tinned and inserted in the holes in the pyrex in a position suitable for soldering. The assembly was preheated to about 520 degrees Fahrenheit in a furnace. A flux of 42 parts of zinc chloride, 18 parts of ammonium chloride, and 100 parts of water by weight was applied to the film in the region to be soldered. Bits of 50-50 lead-tin solder were dropped into the countersunk holes and the solder connection was completed in a furnace. Excess solder was carefully ground off and any unfilled portions of the countersunk holes were filled with circuit paint.

Calibration In order to obtain heat transfer rates it is necessary to determine the temperature coefficient of resistance, δ, of the platinum film and the quantity Γ of the pyrex backing. The temperature coefficient of resistance was

obtained by immersing the gage in a Hallikainen Model 1124c constant temperature oil bath. Resistance measurements were made with an Electro-Scientific Industries Model 250 DA impedance bridge.

A method developed by Skinner (30) was used to determine the quantity Γ. This method involves subjecting the gage to a pulse of electrical energy that is repeatable and observing the response. The gage is pulsed in air and also while immersed in some fluid. When pulsed in air heat is dissipated only into the pyrex since that lost to the air is negligible. When immersed, heat is dissipated into both the fluid and the pyrex. The properties of the pyrex and the fluid are related, in terms of the ratio of amplitude of the responses when pulsed in air and in the fluid, by the following equation.

$$\Gamma_b = \Gamma_1 (B/B^* - 1)^{-1} \qquad (53)$$

Since the properties of the fluid are known the properties of the pyrex can now be determined. With this method any repeatable energy input may be used. However, it has been observed that the voltage zero is very hard to locate precisely although the time zero can be easily determined. If a step input of energy is used the response will vary parabolically with time as shown by Hall (12). The parabola may then be extrapolated to the time zero thus fixing the voltage zero. The bridge circuit used for calibration is shown in Figure 20. Six

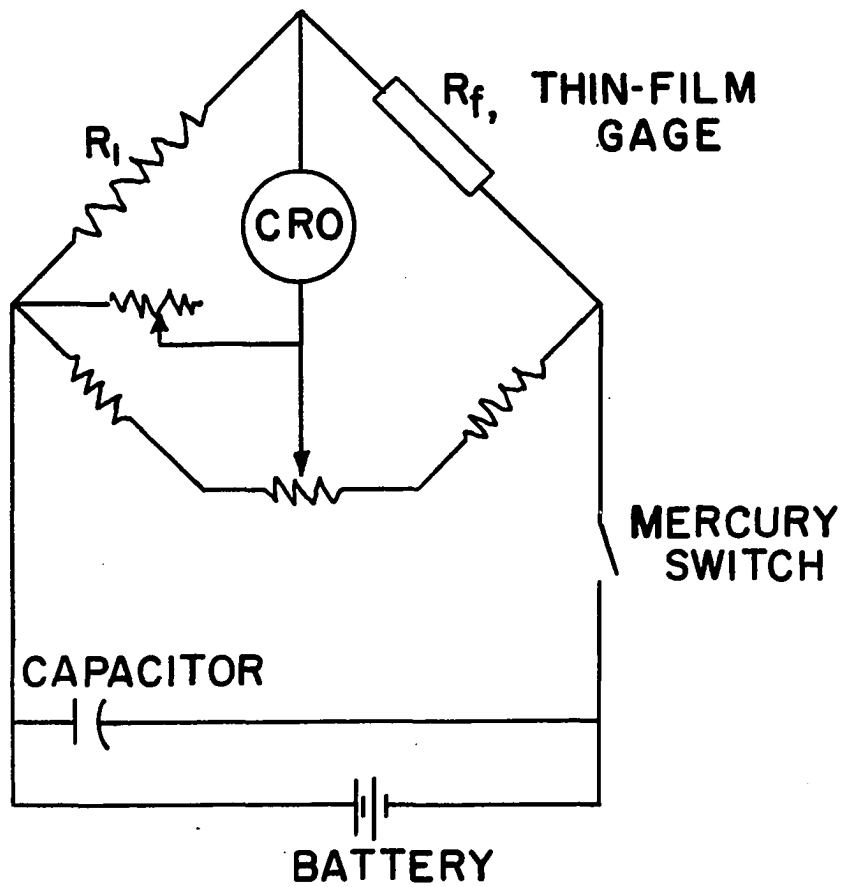

Figure 20. Gage calibrator circuit

forty-five volt batteries in parallel and a mercury switch were used to obtain a clean step input of power.

Two fluids were tried in the calibrations. Water had been used in most work reported previously. However, when the gage is left in water for extended periods, in some cases only a few minutes, a resistance change and a change in the character of response of the gage is noted. It is necessary to complete the calibration before this change in response which causes deviation from a parabola takes place. It was suggested by Hall[1] that Freon 113 could be used as a calibration fluid without this undesirable effect on gage resistance. However, as is shown in the error analysis in Appendix A, the effects of errors are much greater with Freon 113 than with water. Since the techniques are the same in both cases with the exception of the fluid one would expect the errors in measuring the voltage amplitudes to be about the same. With this assumption the uncertainty in Γ is found to be three times as great with Freon 113 as with water. Hence it was decided to use water as the calibration fluid. Care was taken to finish the calibration before the resistance effects had rendered the results unusable.

Data collection method The thin platinum film heat transfer gages are operated as a resistance thermometer. A constant current circuit such as shown in Figure 21 is used to

[1]Hall, Jerry L. Ames, Iowa. Use of Freon 113 as a calibration fluid. Private communication. 1966.

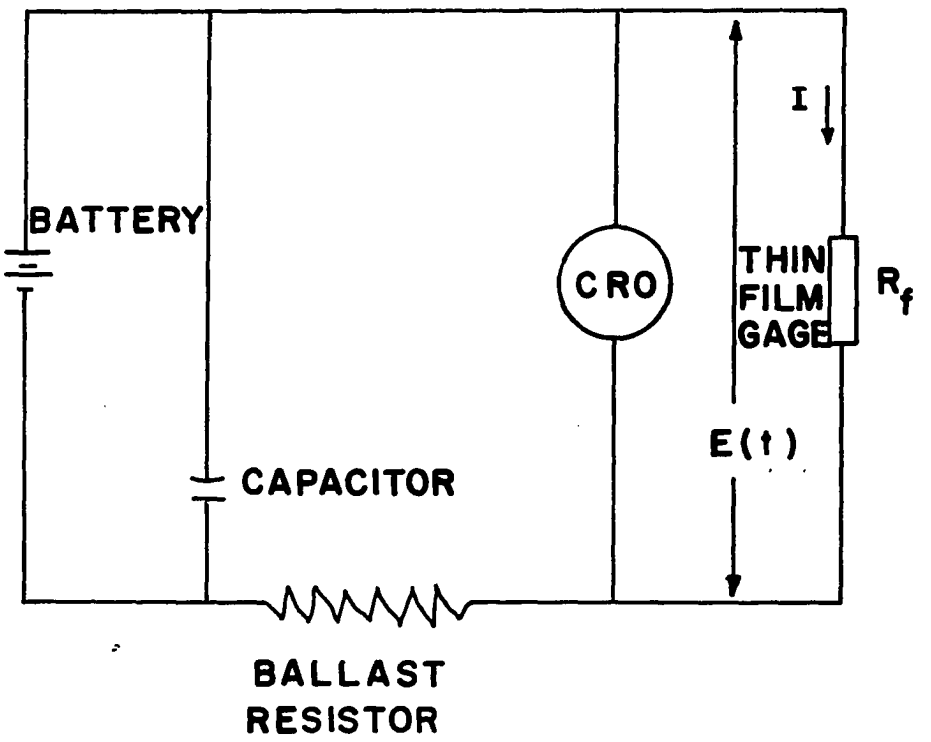

Figure 21. Operating gage circuit

measure resistance and hence temperature changes. If the ballast resistor R_b is made large enough the error due to current changes can be reduced to a negligible level. By measuring the voltage change across the platinum film with an oscilloscope it is then possible to obtain the resistance change. The thin platinum films are sufficiently thin so that they have negligible heat capacity, hence it may be assumed that the thin film resistance thermometers measure the surface temperature of the backing material.

If one dimensional heat flow is assumed and the backing is treated as a semi-infinite medium it is found that the surface temperature record as a function of time is sufficient to determine the heat transfer rate into the body. The mathematical analysis of this problem is given in considerable detail by Hall (12). If the voltage-time record from the resistance thermometer is approximated by a piecewise linear function it has been shown by Cook and Felderman (5) that the final expression for heat transfer rate can be written as:

$$q_n(t) = \frac{\Gamma}{\pi^{1/2}\delta\, E_f}\left[\frac{E(t_n)}{t_n^{1/2}} + \sum_{i=1}^{n-1}\left\{\frac{E(t_n)-E(t_i)}{(t_n-t_i)^{1/2}} - \right.\right.$$

$$\left.\left. - \frac{E(t_n)-E(t_{i-1})}{(t_n-t_{i-1})^{1/2}} + 2\,\frac{E(t_i)-E(t_{i-1})}{(t_n-t_i)^{1/2}+(t_n-t_{i-1})^{1/2}}\right\}\right.$$

$$+ \frac{E(t_n)-E(t_{n-1})}{(\Delta t)^{1/2}} \Bigg] \qquad (54)$$

This expression can be further reduced to:

$$q_n(t) = \frac{2\Gamma}{\Pi^{1/2}\delta\, E_f} \left[\frac{E(t_n)-E(t_{n-1})}{(t_n-t_{n-1})^{1/2}} \right.$$

$$\left. + \sum_{i=1}^{n-1} \frac{E(t_i)-E(t_{i-1})}{(t_n-t_i)^{1/2}+(t_n-t_{i-1})^{1/2}} \right] \qquad (55)$$

Where i = 0, 1, 2, --- n are the points, not necessarily equally spaced, at which voltage values are evaluated. Time zero corresponds to i = 0.

Voltage-time curves from the heat transfer gages were recorded using two Tektronix 502 dual-beam oscilloscopes fitted with oscilloscope cameras. The results from a typical run is shown in Figure 22. Transparancies of the photographs were made and enlarged records were projected on graph paper. Voltage and time values were read from these graphs and punched on IBM data cards. A program for the IBM 360/50 computer was written to evaluate heat transfer rates from the voltage-time data using Equation 55. A copy of the program is included in Appendix B.

Figure 22. Typical photograph of output from the four heat transfer gages. From top to bottom, the outputs are from gages mounted 2.58, 6.55, 6.55, and 4.62 inches back from the leading edge.

Shock Mach number = 5.61
Initial channel pressure = 1.25 mm Hg
Horizontal sensitivity = 50 microseconds/cm
Vertical sensitivity = 2 millivolts/cm

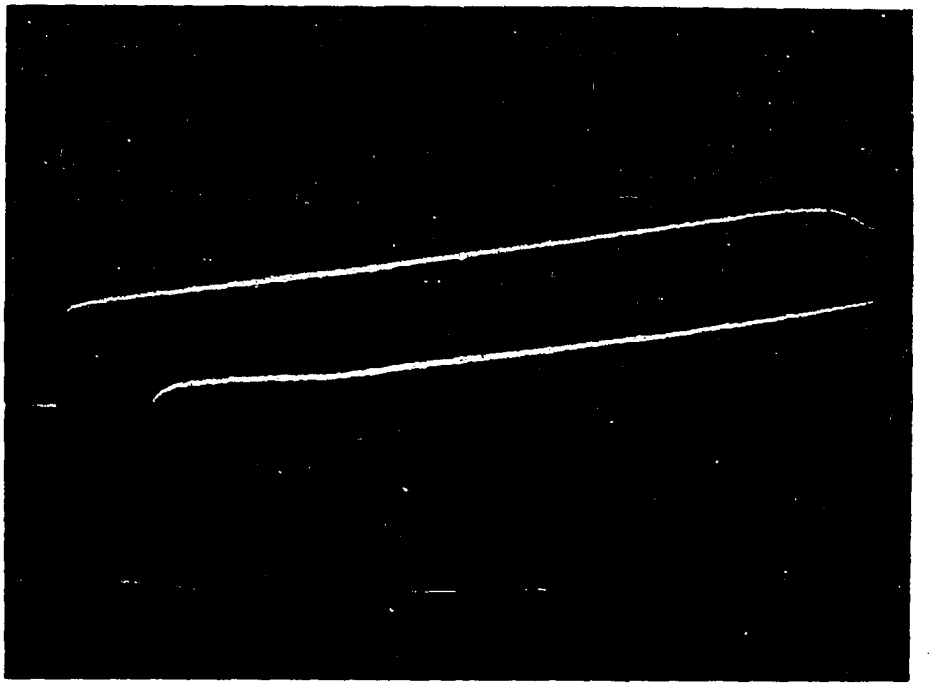

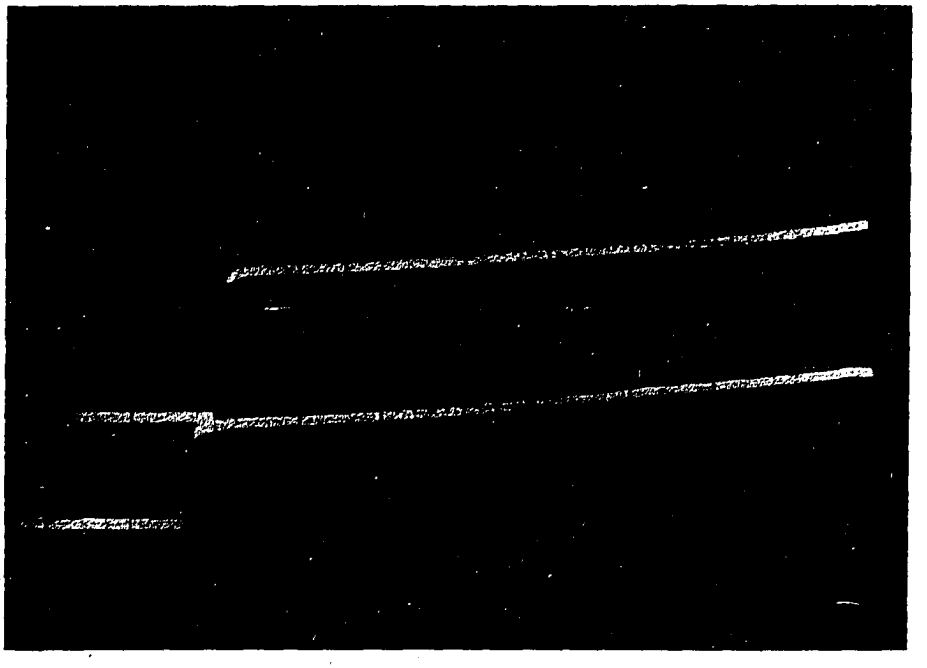

Presentation of Experimental Data

The three variables of concern in this problem are the shock Mach number, the initial channel pressure, and the position on the plate. As noted before, the first of these is the only parameter entering into the numerical solutions previously discussed. It was not possible to obtain experimental data over the complete range of shock Mach number for which numerical solutions were obtained due to limitations of the shock tube facilities. In order to maintain an attached shock wave on the underside of the leading edge of the flat plate it was necessary to have a shock Mach number of three or greater. By evacuating the channel to as low a pressure as possible and pressurizing the high pressure section to as high a pressure as allowable a shock Mach number of 6.74 was attained. Within these limits data were obtained at shock Mach numbers of 3.0, 4.0, 5.0, 5.7, and 6.74. The range of initial channel pressure, P_1, that could be achieved at these shock strengths was somewhat limited especially at the higher shock strengths. The maximum variation at any shock strength was by a factor of six. Data were taken at three positions on the plate; 2.58, 4.62, and 6.55 inches back from the leading edge. Three gages were available at each station. The availability of two dual-beam oscilloscopes allowed the output of four gages to be recorded. One gage was selected from each of the two forward stations and two from the rear station.

The outputs of all gages at a station were compared before the gages to be used were selected. The two gages used at the rear station yielded results that were almost identical in most cases. In order to reduce congestion on the data plots frequently the results of only one of these two gages was plotted.

The data were plotted in the form of the dimensionless heat transfer parameter $\bar{Q} = \frac{q_w Pr \sqrt{x}}{\sqrt{\rho_o \mu_o u_o h_o}}$ as a function of α, the primary time variable. The data for shock Mach numbers of 3.0, 4.0, 5.0, 5.7, and 6.74 are plotted in Figures 23 thru 27 respectively. The initial channel pressure, P_1, and the plate position, x, are noted for each data symbol appearing on a figure. The theory line which appears in each figure is taken from the numerical results presented in Figure 6. At the large values of α, corresponding to very early times in the testing period, the errors in data reduction would be expected to be significant. Considerable scatter is noted especially at the weaker shock strengths. Maximum deviation from the theory line for α less than one is 30 per cent in Figure 23, 35 per cent in Figure 24, 25 per cent in Figure 25, 25 per cent in Figure 26, and 10 per cent in Figure 27. Although the scatter is considerable the data are generally seen to center about the theory line.

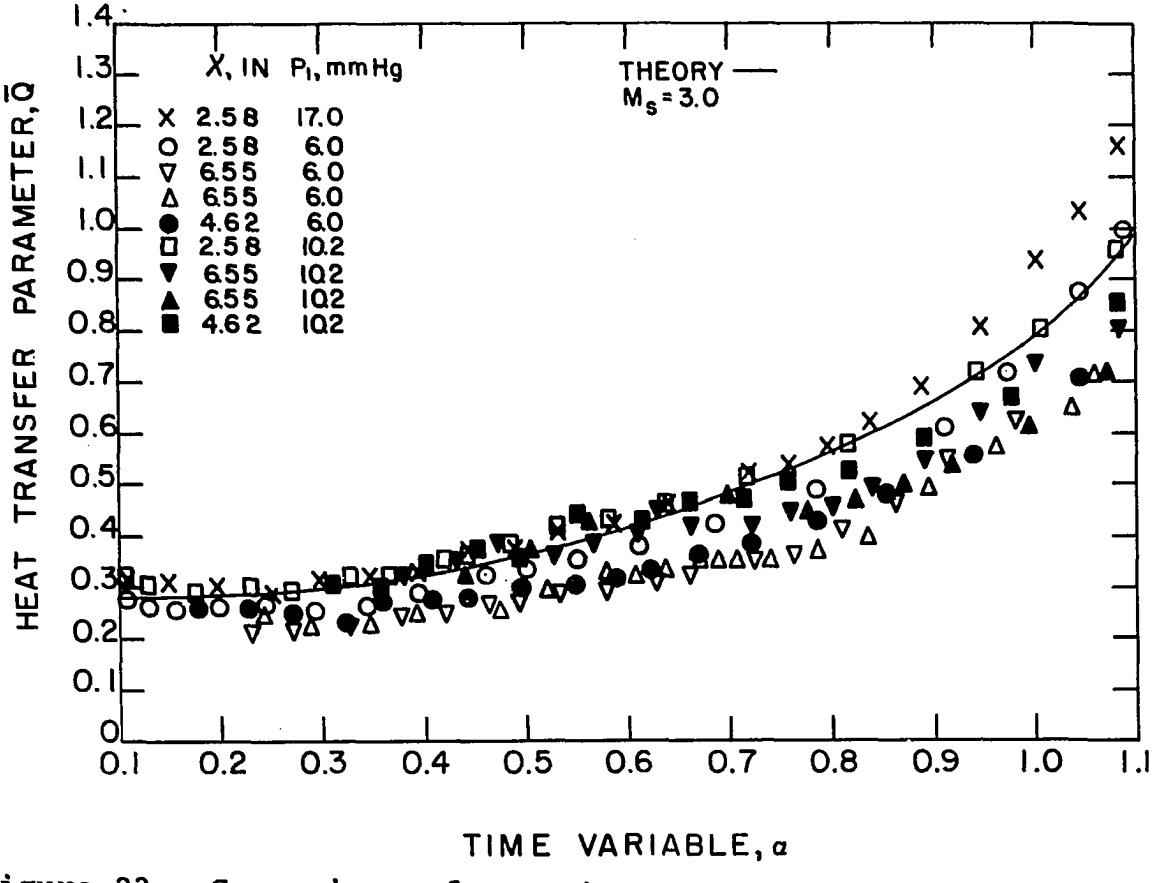

Figure 23. Comparison of experimental heat transfer data with theory for a shock Mach number of 3.0

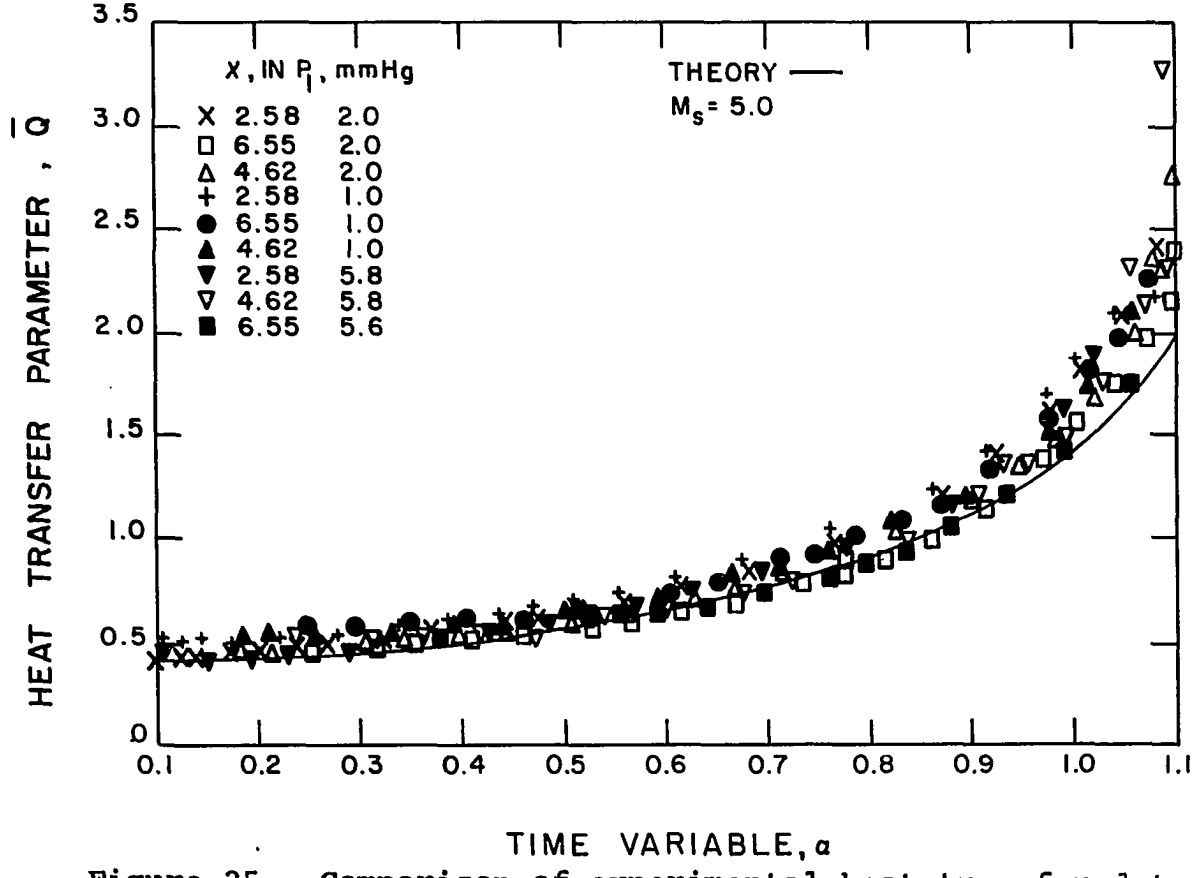

Figure 25. Comparison of experimental heat transfer data with theory for a shock Mach number of 5.0

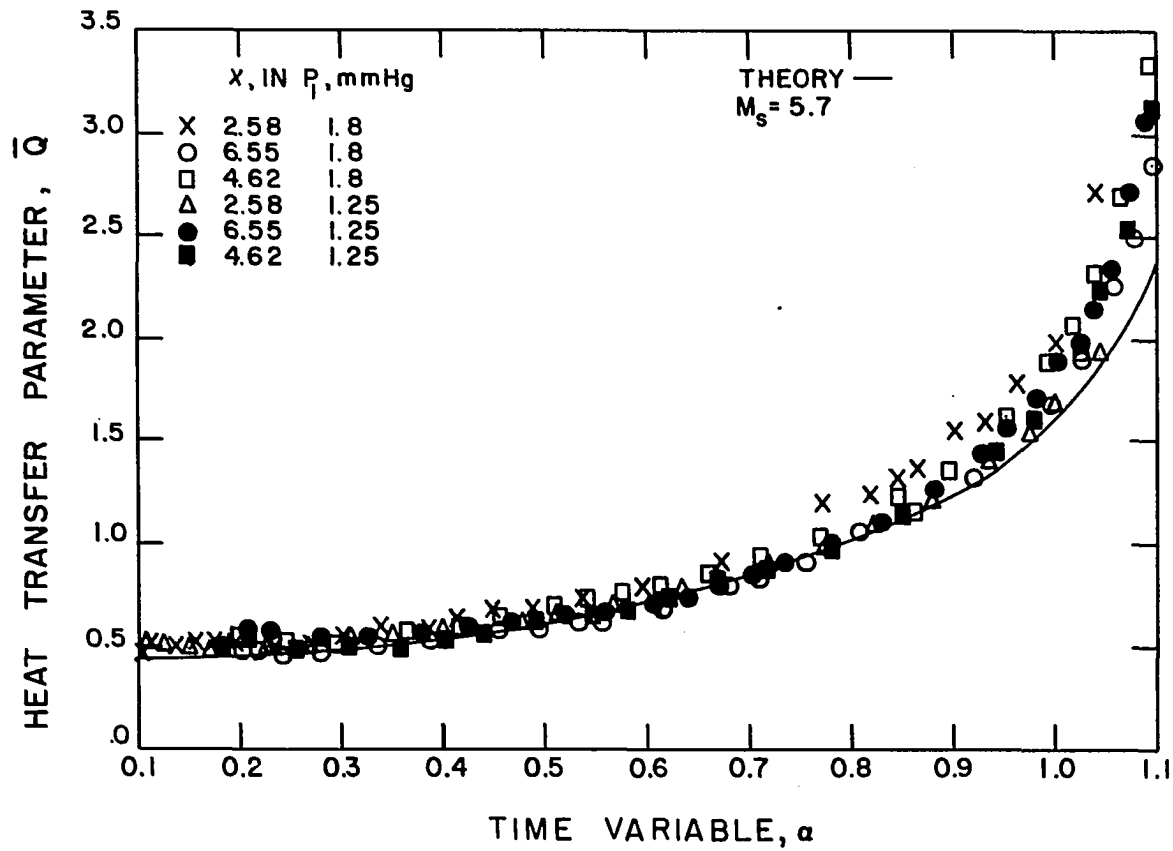

Figure 26. Comparison of experimental heat transfer data with theory for a shock Mach number of 5.7

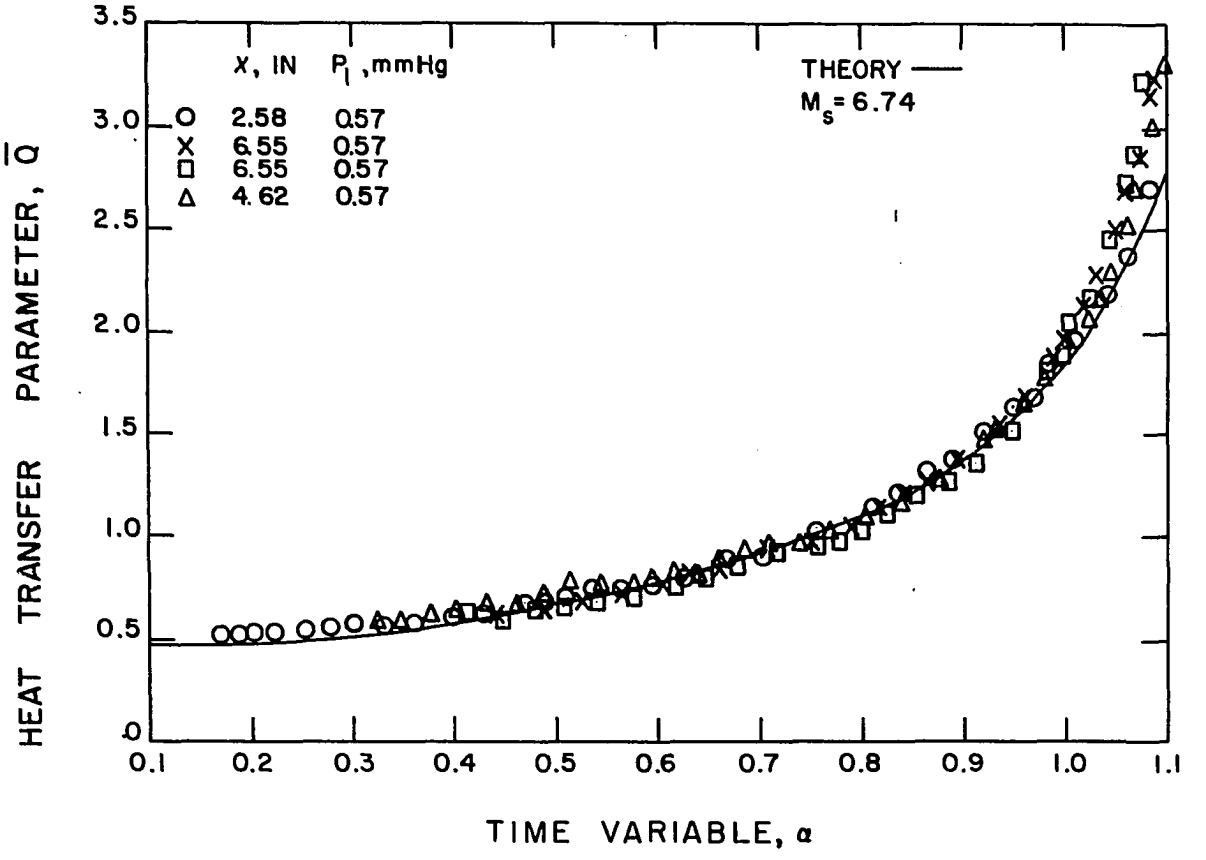

Figure 27. Comparison of experimental heat transfer data with theory for a shock Mach number of 6.74

CONCLUSIONS

It can be seen from Figures 23 thru 27 that the experimental data verifies the theoretical predictions. One of the crucial assumptions in obtaining the theoretical predictions was that of neglecting derivatives of ϕ and H with respect to γ in the momentum and energy equations. The agreement between the data and theory would seem to substantiate this assumption. The definition of ϕ made use of the steady state solution dependence on distance from the leading edge. Hence it depends on the boundary condition requiring shear stress to be infinite at the leading edge. It would seem that this approach would be valid whenever a sharp leading edge is involved. It would definitely seem to be valid for other cases of unsteady semi-infinite flat plate flow.

Figures 10 and 11 show that there are definite limits on the design of models for use in shock tubes and limited duration flow devices in general. The limitations are noted to become somewhat more stringent with increasing shock Mach number. The available testing time for a particular flow device is fixed. Hence, to obtain a value of α less than or equal to that required for steady state it is necessary to restrict the model to less than a certain length. One can, however, relax these restrictions somewhat by accepting values within a certain percentage of the steady state values. This is shown by the three curves shown both in Figures 10 and 11.

The variation between results obtained by assuming viscosity proportional to temperature and by accounting for the correct temperature variation is shown in Figures 12 and 13. Assuming viscosity proportional to temperature results in considerable simplification of the problem. However, at higher values of shock Mach number it results in a significant amount of error.

The case when A = 1 is of considerable practical interest since it has been shown to apply to the case of a missile launched from under water. The results presented in Figures 14, 15, and 16 are obtained for the case of A approaching one and should be viewed as only an approximate solution for the case of A = 1. The results are also limited by the assumption of viscosity proportional to temperature. In spite of these approximations the results are expected to give a realistic indication of the general behavior of the boundary layer.

RECOMMENDATIONS FOR FURTHER STUDY

During the courses of this investigation certain related problems and extensions of the present problem became apparent. Some of these will be itemized below.

1. As mentioned earlier the experimental verification of the present analysis was limited to shock Mach numbers of up to 6.74. Experimental verification should be obtained for higher shock Mach numbers.

2. Experimental verification for heat transfer rates to the side wall of a shock tube is available only up to a shock Mach number of 7.5. This work should be extended to higher shock Mach numbers.

3. The present analysis should be extended to include the effects of attenuation of the initial shock wave. Non-uniformities in the region behind the initial shock wave such as those due to relaxation effects might also be included.

4. The effects of dissociating and reacting flows might be included in the present boundary layer analysis.

5. The effect of a pressure gradient in the flow might be included in the present analysis.

6. Additional work should be done for the case of $A = 1$ in order to eliminate some of the assumptions and inaccuracies of the present analysis.

7. An attempt should be made to solve the case of $A = 1$ allowing for acceleration of the flat plate. A missile

launched from under water would likely be accelerating as it left the water.

8. The feasibility of applying the unsteady boundary layer equations to other flows in the form presented here with partial derivatives with respect to γ assumed negligible should be further investigated. A first step would be to apply the method to other unsteady semi-infinite flat plate flows. Both theoretical and experimental work is necessary. The method might be applied to the problem of a flat plate in a free stream with oscillating properties. The results could then be compared with available small pertubation solutions. Another case that might be considered is that of a flat plate in an initially steady free stream with an abrupt change in conditions imposed upon it.

BIBLIOGRAPHY

1. Becker, Ernst. Instationäre grenzschichten hinter verdichtungsstössen und expansionswellen. Zeitschrift für Flugwissenschaften 7: 61-73. 1959.

2. Bershader, D. and Allport, J. On the laminar boundary layer induced by a travelling shock wave. Princeton University Department of Physics Technical Report 2-22. 1956.

3. Bromberg, Robert. Use of the shock tube wall boundary layer in heat transfer studies. Jet Propulsion 26: 737-740. 1956.

4. Chen, Che Jen and Emrich, Raymond J. Investigation of the shock-tube boundary layer by a tracer method. Physics of Fluids 6: 1-9. 1963.

5. Cook, W. J. and Felderman, E. J. Reduction of data from thin-film heat transfer gages: a concise numerical technique. American Institute of Aeronautics and Astronautics Journal 4: 561-562. 1966.

6. Cook, William John. Heat transfer in the region of interaction of an oblique shock wave and a laminar boundary layer. Unpublished Ph.D. thesis. Ames, Iowa, Library, Iowa State University of Science and Technology. 1964.

7. Felderman, Elmer John. Shock tube investigation of stagnation point heat transfer on ellipsoids of revolution. Unpublished M.S. thesis. Ames, Iowa, Library, Iowa State University of Science and Technology. 1964.

8. Feldman, Saul. Hypersonic gas dynamic charts for equilibrium air. Everett, Massachusetts, Avco Research Laboratory. 1957.

9. Gion, E. J. Measured velocity profiles in the laminar boundary layer behind a shock. Physics of Fluids 8: 546-547. 1965.

10. Glass, I. I. and Hall, J. Gordon. Shock tubes. U.S. Navy Bureau of Ordinance Report 1488, Vol. 6, Section 18. 1959.

11. Glass, I. I. and Patterson, C. N. A theoretical and experimental study of shock tube flows. Journal of the Aeronautical Sciences 22: 73-100. 1955.

12. Hall, Jerry L. Shock tube investigation of heat transfer in two-dimensional laminar separated flow behind a backward-facing step. Unpublished M.S. thesis. Ames, Iowa, Library, Iowa State University of Science and Technology. 1963.

13. Harlow, F. H. and Meixner, B. D. Motion of a viscous compressible gas adjacent to a sliding plate. Physics of Fluids 4: 1202-1206. 1961.

14. Hartunian, R. A., Russo, A. L. and Marrone, P. V. Boundary-layer transition and heat transfer in shock tubes. Journal of the Aerospace Sciences 27: 587-594. 1960.

15. Howarth, L. Some aspects of Rayleigh's problem for a compressible fluid. Quarterly Journal of Mechanics and Applied Mathematics 4: 157-169. 1951.

16. Illingworth, C. R. Unsteady laminar flow of a gas near an infinite flat plate. Cambridge Philosophical Society Proceedings 46: 603-613. 1950.

17. Keenan, Joseph H. and Kaye, Joseph. Gas tables. New York, New York, John Wiley and Sons, Inc. 1961.

18. Kline, S. J. and McClintock, F. Describing uncertainties in single sample experiments. Mechanical Engineering 75: 3-8. 1953.

19. Lam, S. H. and Crocco, L. Note on the shock-induced unsteady laminar boundary layer on a semi-infinite flat plate. Journal of the AeroSpace Sciences 26: 54-56. 1959.

20. Lam, Sau-Hai. Shock induced unsteady laminar compressible boundary layers on a semi-infinite flat plate. Unpublished Ph.D. thesis. Princeton, New Jersey, Library, Princeton University. 1958.

21. Martin, W. A. An experimental study of the boundary layer behind a moving plane shock wave. University of Toronto Institute of Aerophysics Report No. 47. 1957.

22. Mirels, Harold. Boundary layer behind shock or thin expansion wave moving into stationary fluid. U.S. National Advisory Committee for Aeronautics Technical Note 3712. 1956.

23. Mirels, Harold. Laminar boundary layer behind a strong shock moving into air. U.S. National Aeronautics and Space Administration Technical Note D-291. 1961.

24. Mirels, Harold. Laminar boundary layer behind shock advancing into stationary fluid. U.S. National Advisory Committee for Aeronautics Technical Note 3401. 1955.

25. Mirels, Harold. The wall boundary layer behind a moving shock wave. In Gortler, H., ed. Boundary layer research. pp. 283-293. Berlin, Germany, Springer Verlag. 1958.

26. Mirels, Harold and Hamman, Jesse. Laminar boundary layer behind strong shock moving with nonuniform velocity. Physics of Fluids 5: 91-96. 1962.

27. Rose, P. H. and Stark, W. I. Stagnation point heat transfer measurements in air at high temperature. Avco Research Laboratory Research Note 24. 1956.

28. Sarma, G. N. Unified theory for the solutions of the unsteady thermal boundary layer equations. Cambridge Philosophical Society Proceedings 61: 809-825. 1965.

29. Schlichting, Hermann. Boundary layer theory. New York, New York, McGraw-Hill. 1960.

30. Skinner, G. T. A new method of calibrating thin film gauge backing materials. Cornell Aeronautical Laboratory Report No. CAL-105. 1962.

31. Stewartson, K. On the impulsive motion of a flat plate in a viscous fluid. Quarterly Journal of Mechanics and Applied Mathematics 4: 182-198. 1951.

32. Stewartson, K. The theory of laminar boundary layers in compressible fluids. New York, New York, Oxford University Press. 1964.

33. Stewartson, K. The theory of unsteady laminar boundary layers. In Dryden, H. L. and von Kármán, Th., eds. Advances in applied mechanics. Volume G. pp. 1-37. New York, New York, Academic Press. 1960.

34. Traugott, S. C. Impulsive motion of an infinite plate in a compressible fluid with non-uniform external flow. Journal of Fluid Mechanics 13: 400-416. 1962.

35. Trimpi, Robert L. and Cohen, Nathaniel B. An integral solution to the flat-plate laminar boundary-layer flow existing inside and after expansion waves and after shock waves moving into quiescent fluid with particular application to the complete shock tube flow. U.S. National Advisory Committee for Aeronautics Technical Note 3944. 1957.

36. Vidal, R. Model instrumentation techniques for heat transfer and force measurements in a hypersonic shock tunnel. Cornell Aeronautical Laboratory Report AD-917-A-1. 1956.

ACKNOWLEDGMENTS

The author wishes to express his thanks to the members of his graduate study committee. Especially to Professor H. M. Black who served as chairman and Dr. C. T. Hsu who served as co-chairman.

The financial assistance, necessary to carry out the experimental phase of this project, which was provided by the Engineering Research Institute is gratefully acknowledged.

APPENDIX A

Uncertainty of the Experimental Results

The method used to estimate the uncertainty of the experimental results was essentially that given by Kline and McClintock (18) for single sample experiments. The uncertainty, W_R, of some quantity, $R = R(v_1, v_2, -- v_n)$, which is a function of the independent variables, $v_1, v_2, --v_n$, can be written as:

$$(W_R)^2 = \left(\frac{\partial R}{\partial v_1} W_{v_1}\right)^2 + \left(\frac{\partial R}{\partial v_2} W_{v_2}\right)^2 + --+ \left(\frac{\partial R}{\partial v_n} W_{v_n}\right)^2 \qquad (56)$$

The uncertainty intervals W_{v_n} must be estimated by the observer in accordance with specified odds that an observation will fall within the interval. Uncertainty intervals were estimated so that the odds were approximately 20 to 1.

Calibration uncertainties

In Equation 53 the calibration factor Γ_b is expressed in terms of the voltage amplitudes B and B^*. It will be assumed that the properties of the calibration fluid are known with negligible uncertainty. The uncertainty for Γ_b may be written as:

$$(W_{\Gamma_b})^2 = \left(\frac{\partial \Gamma_b}{\partial B} W_B\right)^2 + \left(\frac{\partial \Gamma_b}{\partial B^*}\right)^2 (W_{B^*})^2$$

Using Equation 53 one obtains:

$$\left(\frac{W_{\Gamma_b}}{\Gamma_b}\right)^2 = \left[\frac{B/B^*}{B/B^* - 1}\right] \left[\left(\frac{-W_B}{B}\right)^2 + \left(\frac{W_{B^*}}{B^*}\right)^2\right] \qquad (57)$$

From this equation it can be seen that the uncertainty in Γ_b is significantly affected by the value of B/B^*. For distilled water it is found that $B/B^* = 2$ while for Freon 113 the approximate results are $B/B^* = 1.2$. If the same uncertainties for B and B* are assumed to hold in both cases, it is noted that the uncertainty in Γ_b is 3 times as large when Freon 113 is used as when water is used.

On the basis of past experience an uncertainty of ± 3 per cent was assumed for both B and B^*. Since distilled water was used in the calibrations this yielded an uncertainty of ± 8.5 per cent for Γ_b.

Heat transfer measurement uncertainty

The heat transfer reduction equation, Equation 55, states that the experimental heat transfer rate is a function of Γ_b, δ, E_f, and the voltage-time summation term which we will call D. In addition the flow condition depends on the initial channel pressure, P_1, and the shock Mach number, M_s. It will be assumed that the uncertainty in the measurement of M_s is negligible. Equation 45 shows that the heat transfer rate is proportional to the square root of P_1. Hence one can write for q:

$$q = q(\Gamma_b, \delta, E_f, D, P_1, --) \qquad (58)$$

The uncertainty interval for q is:

$$(W_q)^2 = \left(\frac{\partial q}{\partial \Gamma_b} W_{\Gamma_b}\right)^2 + \left(\frac{\partial q}{\partial \delta} W_\delta\right)^2 + \left(\frac{\partial q}{\partial E_f} W_{E_f}\right)^2$$

$$+ \left(\frac{\partial q}{\partial D} W_D\right)^2 + \left(\frac{\partial q}{\partial P_1} W_{P_1}\right)^2$$

Using Equations 45 and 55 this becomes:

$$\left(\frac{W_q}{q}\right)^2 = \left(\frac{W_{\Gamma_b}}{\Gamma_b}\right)^2 + \left(\frac{-W_\delta}{\delta}\right)^2 + \left(\frac{-W_{E_f}}{E_f}\right)^2 + \left(\frac{W_D}{D}\right)^2 + \left(\frac{W_{P_1}}{2P_1}\right)^2 \quad (59)$$

The uncertainty for Γ_b has been shown to be ± 8.5 per cent. The uncertainty for δ, E_f, D, and P_1 were estimated to be ± 5, ± 3, ± 5, and ± 10 per cent respectively. Using these values in Equation 59 yields an uncertainty of 13.5 per cent for the heat transfer rate q.

APPENDIX B

Computer Programs and Flow Diagrams

Three computer programs were used in this investigation. In Figure 29 the program to solve the boundary layer momentum equation, Equation 34, is reproduced. The program to solve the boundary layer energy equation, Equation 44, is reproduced in Figure 31. The program to reduce the experimental heat transfer data using Equation 55 is found in Figure 33.

Flow diagrams for the three programs are found in Figures 28, 30, and 32 respectively. The sections of the programs listed in the flow diagrams are similarly labeled by comment cards inserted in the programs.

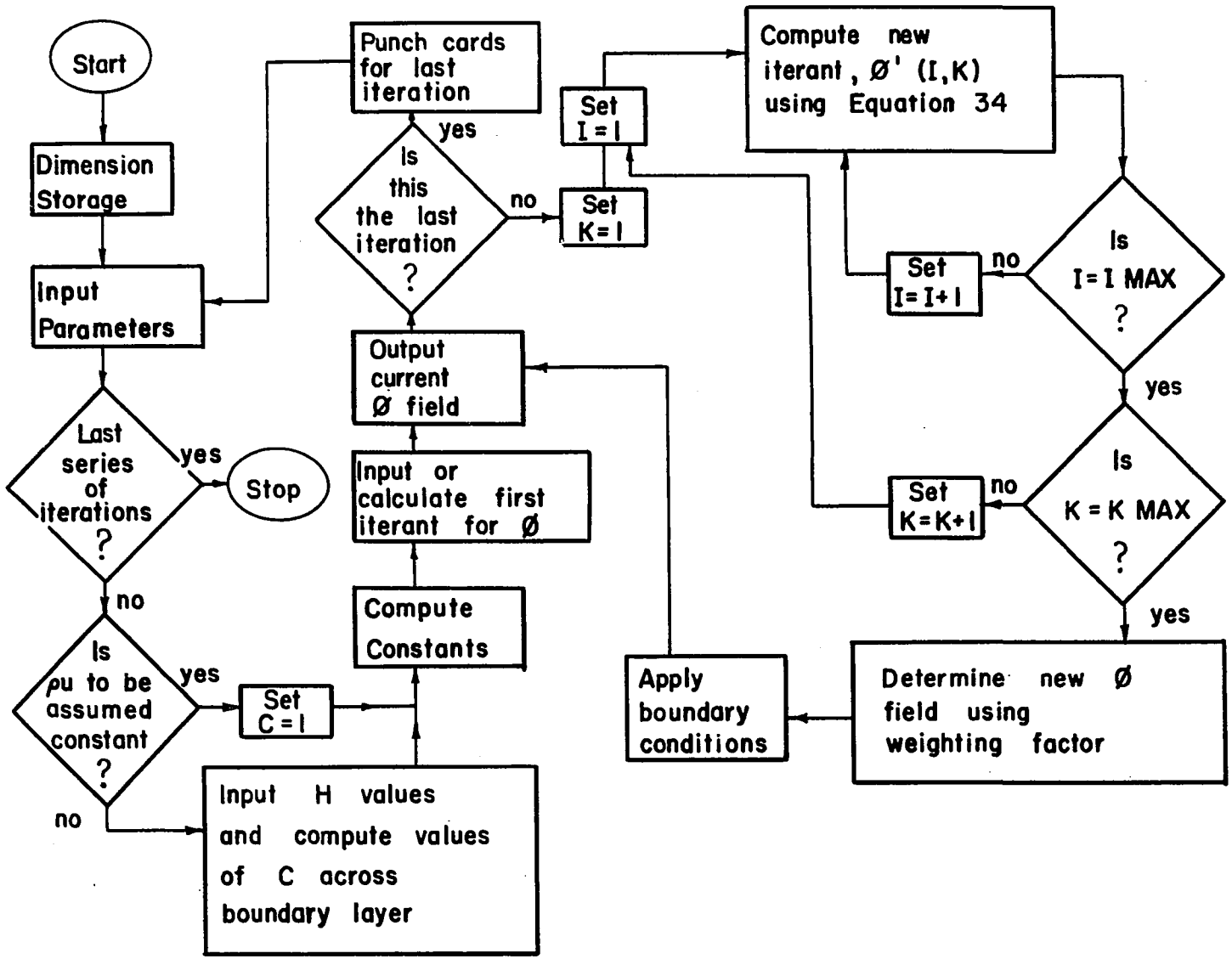

Figure 28. Flow diagram for computer program to solve boundary layer momentum equation

```
! ISU COMPUTATION CENTER; AMES, IOWA

 ISU DISK RES SPOOLED BPS FORTRAN
/JOB                    I0267 FELDERMAN 1 MINUTES                    U38
/FTC     SIZE=62K,NOMAP
BEGIN COMPILATION
      C      INTEGRAL ITERATION OF MOMENTUM EQN OF LAMINAR B L
      C      DIMENSION STORAGE
S.0001        REAL AM,PR,HW,KE,M(42),MA(12),MO(12)
S.0002        DOUBLE PRECISION PHI(12,42),C1(12,42),C2(12,42),R(12),P(12),
     1C5(12),C6(12),C7(12),C8(12),DPHI,DC,CS,C3,C4,C12,RR,PS,PSM,PSSM,
     1PSS,RRR,RRRR,RL,P1(12),PP(12,42)
S.0003        DIMENSION A(42),B(11),C(11),RO(11),SO(11)
      C      INPUT PARAMETERS
S.0004      1 READ (1,2) AM,PR,HW,KE,DVR,IMAX,KMAX,I1,I2,KI,KF
S.0005      2 FORMAT (F5.2,F4.2,3F6.4/6I2)
      C      TEST FOR FINAL DATA SET
S.0006        IF (I2) 3,3,4
S.0007      3 STOP
      C      VARIABLE PROPERTIES DECISION
S.0008      4 IF (DVR-1.01) 55,55,53
S.0009     53 HI = 1./(-HW+1.)
S.0010        HJ = HW*HI
S.0011        DVR = 1./(1.5481/SQRT(HI)-0.5481/HI+0.0028*HJ-HJ*HJ*5.74E-5)
S.0012        READ (1,54) (RO(I),I=1,IMAX)
S.0013     54 FORMAT (10F6.4,F3.1)
S.0014        DO 56 I=1,IMAX
S.0015        HO = -RO(I)
S.0016        HI = (HO+1.)/(-HW+1.)
S.0017        HJ = (HO+HW)/(-HW+1.)
```

Figure 29. Computer program to solve boundary layer momentum equation

```
S.0018        56 C(I) = DVR*(1.5481/SQRT(HI)-0.5481/HI+0.0028*HJ-HJ*HJ*5.74E-5)
S.0019           GO TO 58
S.0020        55 DO 57 I=1,IMAX
S.0021        57 C(I) = 1.
S.0022        58 CONTINUE
              C     COMPUTE CONSTANTS
S.0023           F = 1./(IMAX-1.)
S.0024           D = 1./(KMAX-1.)
S.0025           DO 6 K=1,KMAX
S.0026           A(K) = 1.-(K-1)*D
S.0027         6 M(K) = 1.+7.*A(K)
S.0028           DO 11 I=1,IMAX
S.0029        11 B(I) = (I-1)*F
              C     INPUT OR CALCULATE FIRST ITERANT FOR PHI
S.0030           IF (II-1) 20,20,19
S.0031        19 READ (1,17) ((PHI(I,K),I=1,IMAX),K=1,KMAX)
S.0032        18 FORMAT (10F6.4,F3.1)
S.0033           GO TO 26
S.0034        20 READ (1,18) (MA(I),I=1,IMAX)
S.0035           READ (1,18) (MO(I),I=1,IMAX)
S.0036           DO 23 K=1,KMAX
S.0037           AP = A(K)/(AM-A(K)*(AM-1.))
S.0038           AS = SQRT(AP)
S.0039           DO 23 I=1,IMAX
S.0040           FOE = AS*MA(I)-MO(I)
S.0041           IF (FOE) 21,21,22
S.0042        21 PHI(I,K) = MO(I)
S.0043           GO TO 23
S.0044        22 PHI(I,K) = AS*MA(I)
S.0045        23 CONTINUE
```

Figure 29 (Continued)

```
                C     COMPUTE NEW ITERANT FOR PHI OVER COMPLETE FIELD
S.0046             26 I3 = I1
S.0047                IMIN = IMAX-1
S.0048                GO TO 46
S.0049             24 DO 35 L=1,KMAX
S.0050                DO 35 J=2,IMAX
S.0051                DPHI = PHI(J,L)-PHI(J-1,L)
S.0052                C1(J,L) = F/DPHI
S.0053             35 C2(J,L) = B(J-1)-F*PHI(J-1,L)/DPHI
S.0054                E = -D
S.0055                DO 40 K=KI,KF
S.0056                DO 34 I=2,IMAX
S.0057                DC = C1(I,K-1)-C1(I,K+1)
S.0058                CS = C1(I,K+1)*C1(I,K-1)
S.0059                C3 = DC*C1(I,K)/CS
S.0060                C4 =(DC*C2(I,K)+C1(I,K+1)*C2(I,K-1)-C1(I,K-1)*C2(I,K+1))/CS
S.0061                A2 = A(K)*A(K)
S.0062                C12 = C1(I,K)*C1(I,K)
S.0063                C5(I) = C1(I,K)*C2(I,K)-(A(K)/E)*C1(I,K)*(C2(I,K)*C3+C1(I,K)*C4)
                     1+A2*C1(I,K)*C3/E
S.0064                C6(I) = C12-A(K)*C12*C3/E
S.0065                C7(I) = (A(K)*C1(I,K)*C2(I,K)*C4-A2*C1(I,K)*C4)/E
S.0066                CAV = (C(I)+C(I-1))/2.
S.0067                C5(I) = CAV*C5(I)
S.0068                C6(I) = CAV*C6(I)
S.0069             34 C7(I) = CAV*C7(I)
S.0070                P(1) = 0
S.0071                DO 36 I=2,IMIN
S.0072                RR = DLOG(PHI(I,K)/PHI(I-1,K))
S.0073             36 P(I) = P(I-1)+C5(I)*RR+C6(I)*(PHI(I,K)-PHI(I-1,K))+C7(I)*
                     1(1./PHI(I,K)-1./PHI(I-1,K))
S.0074                C8(1) = 0
```

Figure 29 (Continued)

```
S.0075          DO 38 J=2,IMAX
S.0076       38 C8(J) = P(J-1)-(C5(J)*DLOG(PHI(J-1,K))+C6(J)*PHI(J-1,K)+C7(J)/
                1PHI(J-1,K))
S.0077          DO 37 J=2,IMIN
S.0078          PS = PHI(J,K)*PHI(J,K)
S.0079          PSS = PS*PHI(J,K)
S.0080          PSM = PHI(J-1,K)*PHI(J-1,K)
S.0081          PSSM = PSM*PHI(J-1,K)
S.0082          RRR = PS*(0.5*DLOG(PHI(J,K))-0.25)
S.0083          RRRR = PSM*(0.5*DLOG(PHI(J-1,K))-0.25)
S.0084       37 R(J)=C1(J,K)*(C5(J)*(RRR-RRRR)+(C6(J)/3.)*(PSS-PSSM)+C7(J)*
                1(PHI(J,K)-PHI(J-1,K))+C8(J)*(PS-PSM)/2.)
S.0085          PSM = PHI(10,K)*PHI(10,K)
S.0086          PSSM = PHI(10,K)*PSM
S.0087          RL = C5(11)*PSM*(0.25-0.5*DLOG(PHI(10,K)))
S.0088          R(11)=C1(11,K)*(RL-C6(11)*PSSM/3.-C7(11)*PHI(10,K)-C8(11)*PSM/2.)
S.0089          P1(IMAX) = 0
S.0090          DO 39 J=1,IMIN
S.0091          L = IMAX-J
S.0092          P1(L) = R(L+1)+P1(L+1)
S.0093          IF (P1(L)) 50,41,41
S.0094       50 PP(L,K) = PHI(L,K)
S.0095          WRITE (3,119) A(K),B(L)
S.0096          GO TO 39
S.0097       41 PP(L,K) =DSQRT(P1(L))
S.0098       39 CONTINUE
S.0099       40 PP(IMAX,K) = 0
             C  DETERMINE NEW PHI FIELD USING WEIGHTING FACTOR
S.0100          DO 45 K=KI,KP
S.0101          DO 45 I=1,IMAX
S.0102       45 PHI(I,K) = (M(K)*PHI(I,K)+PP(I,K))/(1.+M(K))
```

Figure 29 (Continued)

```
      C     APPLY BOUNDARY CONDITIONS
S.0103        DO 48 I=1,IMAX
S.0104     48 PHI(I,21) = PHI(I,20)
S.0105        WRITE (3,200)
S.0106        WRITE (3,131) (A(K),(PP(I,K),I=1,IMAX),K=1,KMAX)
S.0107        I3 = I3+1
      C     OUTPUT CURRENT PHI FIELD
S.0108     46 WRITE (3,127)
S.0109        WRITE (3,128) AM,PR,HW,KE,DVR,IMAX,KMAX,I1,I3,KI,KF
S.0110        WRITE (3,129) (B(I),I=1,IMAX)
S.0111        WRITE (3,130)
S.0112        WRITE (3,131) (A(K),(PHI(I,K),I=1,IMAX),K=1,KMAX)
      C     TEST FOR LAST ITERATION
S.0113        IF (I3-I2) 24,140,140
S.0114    140 WRITE (2,17) ((PHI(I,K),I=1,IMAX),K=1,KMAX)
S.0115        GO TO 1
S.0116    127 FORMAT ('1  A/(A-1)    PR        HW        KE        DVR       IMAX
             1 KMAX  I1   I3   KI   KF')
S.0117    128 FORMAT (' ',5F10.4,6I5)
S.0118    129 FORMAT ('0BETA= ',10F7.4,F4.1)
S.0119    130 FORMAT (' ALPHA      PHI FIELD')
S.0120    131 FORMAT (12F7.4)
S.0121    119 FORMAT ('  SQ RT OF NEG NO   ALPHA =',F10.4,'  BETA =',F10.4)
S.0122     17 FORMAT (5F15.13/5F15.13,F3.1)
S.0123    200 FORMAT ('1 THE NEXT ITERANT IS')
S.0124        END
                 SIZE OF COMMON  00000    PROGRAM  22612
END OF COMPILATION  MAIN
        COMPILATION TIME WAS    0003.56  SECONDS
```

Figure 29 (Continued)

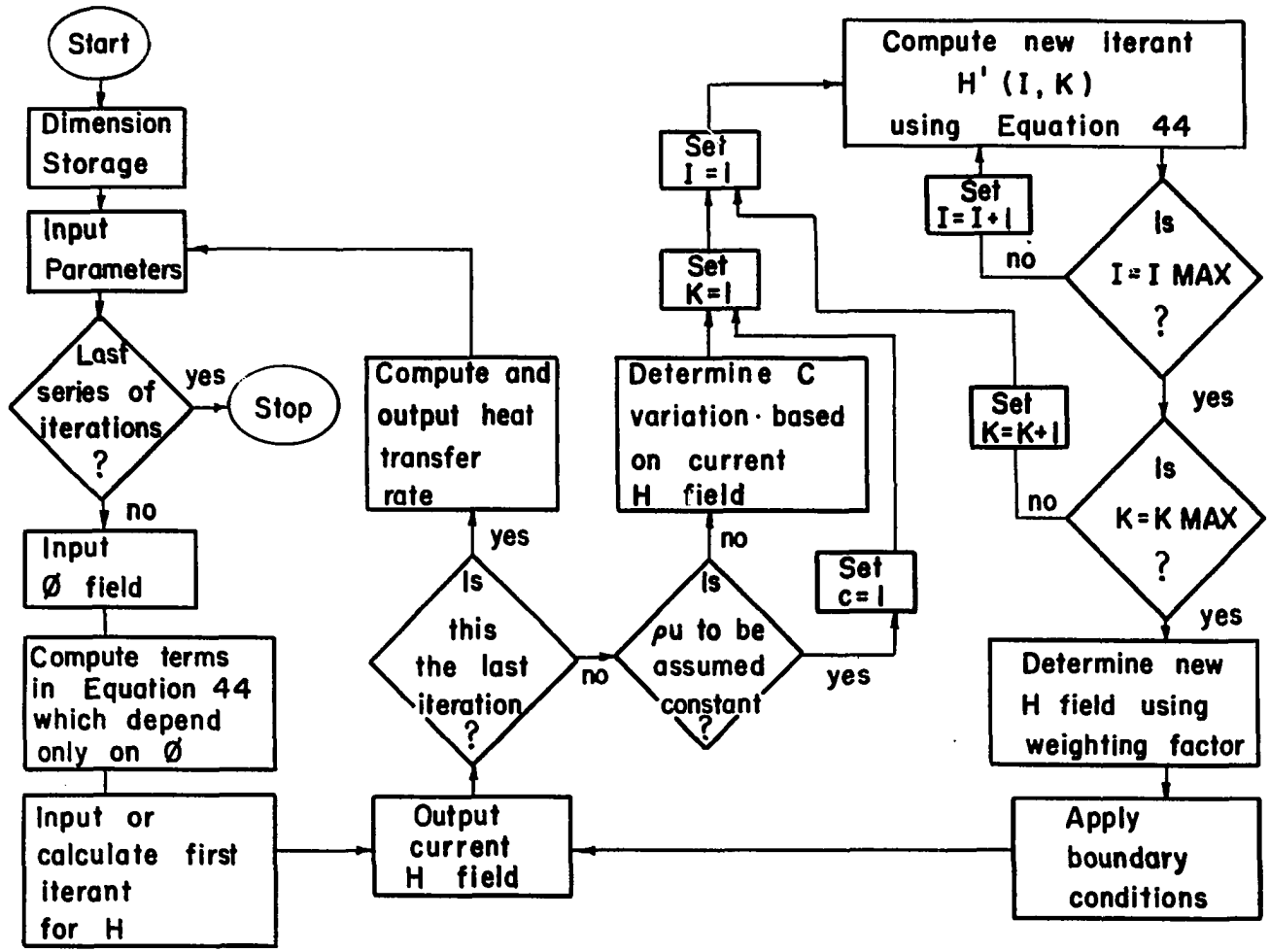

Figure 30. Flow diagram for computer program to solve boundary layer energy equation

```
 ISU COMPUTATION CENTER; AMES, IOWA

 ISU DISK RES SPOOLED BPS FORTRAN

/JOB                    I0267 FELDERMAN 1 MINUTES                    U48
/FTC     SIZE=62K,NOMAP
BEGIN COMPILATION
         C      INTEGRAL ITERATION OF ENERGY EQN OF LAMINAR B L
         C      DIMENSION STORAGE
S.0001           REAL AM,PR,HW,KE,DVR,M(21)
S.0002           DOUBLE PRECISION PHI(11,21),PPR(11,21),POMPR(11,21),PTMPR(11,21),
                1DP(11,21),DPPR(11,21),DPOMPR(11,21),DPTMPR(11,21),DPMPR(11,21),
                1DPS(11,21),C1(11,21),C2(11,21),TERMA(11,21),TERMB(11,21),
                1H(11,21),HH(11,21),C3(11,21),C4(11,21),ELN(11,21),PS(11),C21(11),
                1C7(11),C8(11),C9(11),C10(11),FLN(11),TERMC(11),C11(11),C77(11),
                1C5(11),C6(11),CINT,CINTA,HBB
S.0003           DIMENSION A(21),B(11),RA(11),SA(11),RO(11),SO(11),HB(21),C(11,21)
         C      INPUT PARAMETERS
S.0004       1   READ (1,2) AM,PR,HW,KE,DVR,IMAX,KMAX,I1,I2,KI,KF
S.0005       2   FORMAT (F5.2,F4.2,3F6.4,6I2)
         C      TEST FOR FINAL DATA SET
S.0006           IF (I2) 3,3,4
S.0007       3   STOP
         C      COMPUTE CONSTANTS
S.0008       4   F = 1./(IMAX-1.)
S.0009           D = 1./(KMAX-1.)
S.0010           IF (DVR-1.01) 8,8,9
S.0011       9   HI = 1./(-HW+1.)
S.0012           HJ = HW*HI
S.0013           DVR = 1./(1.5481/SQRT(HI)-0.5481/HI+0.0028*HJ-HJ*HJ*5.74E-5)
```

Figure 31. Computer program to solve boundary layer energy equation

```
S.0014        8 DO 6 K=1,KMAX
S.0015          A(K) = 1.-(K-1)*D
S.0016        6 M(K) = 12.
S.0017          DO 7 I=1,IMAX
S.0018        7 B(I) = (I-1)*F
              C     INPUT PHI FIELD
S.0019          READ (1,17) ((PHI(I,K),I=1,IMAX),K=1,KMAX)
S.0020       17 FORMAT (5F15.13/5F15.13,F3.1)
S.0021          WRITE (3,127)
S.0022          WRITE (3,128) AM,PR,HW,KE,DVR,IMAX,KMAX,II,I3,KI,KF
S.0023          WRITE (3,129) (B(I),I=1,IMAX)
S.0024          WRITE (3,140)
S.0025          WRITE (3,131) (A(K),(PHI(I,K),I=1,IMAX),K=1,KMAX)
S.0026      140 FORMAT (' ALPHA  THE PHI FIELD USED WAS')
S.0027          IMIN = IMAX-1
              C     COMPUTE TERMS DEPENDING ONLY ON PHI
S.0028       10 DO 19 K=KI,KF
S.0029          DO 11 I=1,IMAX
S.0030          PS(I) = PHI(I,K)*PHI(I,K)
S.0031          PPR(I,K) = PHI(I,K)**PR
S.0032          POMPR(I,K) = PHI(I,K)**(1.-PR)
S.0033       11 PTMPR(I,K) = PHI(I,K)**(2.-PR)
S.0034          C2I(I) = 0
S.0035          DO 18 I=2,IMIN
S.0036       18 DPMPR(I,K) = 1./PPR(I,K)-1./PPR(I-1,K)
S.0037          DO 12 I=2,IMAX
S.0038          DP(I,K) = PHI(I,K)-PHI(I-1,K)
S.0039          DPPR(I,K) = PPR(I,K)-PPR(I-1,K)
S.0040          DPOMPR(I,K) = POMPR(I,K)-POMPR(I-1,K)
S.0041          DPTMPR(I,K) = PTMPR(I,K)-PTMPR(I-1,K)
S.0042          DPS(I,K) = PS(I)-PS(I-1)
```

Figure 31 (Continued)

```
S.0043          C1(I,K) = F/DP(I,K)
S.0044          C2(I,K) = B(I-1)-C1(I,K)*PHI(I-1,K)
S.0045          C21(I) = C1(I,K)*DPTMPR(I,K)/(2.-PR)+C21(I-1)
S.0046       12 C11(I) = C21(I-1)-C1(I,K)*PTMPR(I-1,K)/(2.-PR)
S.0047          TERMA(IMAX,K) = 0
S.0048          TERMB(IMAX,K) = 0
S.0049          DO 13 J=1,IMIN
S.0050          L = IMAX-J
S.0051          TERMA(L,K) = POMPR(1,K)/PR*C1(L+1,K)*DPPR(L+1,K)+TERMA(L+1,K)
S.0052       13 TERMB(L,K) = PR*KE*(C1(L+1,K)*C11(L+1)*DPPR(L+1,K)/PR+C1(L+1,K)*
                1C1(L+1,K)*DPS(L+1,K)/(2.*(2.-PR)))+TERMB(L+1,K)
S.0053          ELN(IMAX,K) = 0
S.0054          DO 19 I=2,IMIN
S.0055       19 ELN(I,K) = C1(I,K)*DLOG(PHI(I,K)/PHI(I-1,K))
             C     INPUT OR CALCULATE FIRST ITERANT FOR H
S.0056          IF (I1-1) 50,50,51
S.0057       51 READ (1,17) ((H(I,K),I=1,IMAX),K=1,KMAX)
S.0058          GO TO 53
S.0059       50 READ (1,54) (RA(I),I=1,IMAX)
S.0060          READ (1,54) (SA(I),I=1,IMAX)
S.0061          READ (1,54) (RO(I),I=1,IMAX)
S.0062          READ (1,54) (SO(I),I=1,IMAX)
S.0063       54 FORMAT (10F6.4,F3.1)
S.0064          DO 55 K=1,KMAX
S.0065          DO 55 I=1,IMAX
S.0066          HA = (KE/2.)*RA(I)+(-HW-KE/2.*RA(1))*SA(I)
S.0067          HO = (KE/2.)*RO(I)+(-HW-KE/2.*RO(1))*SO(I)
S.0068       55 H(I,K) = HO+A(K)*(HA-HO)
S.0069       53 I3 = I1
S.0070          GO TO 56
```

Figure 31 (Continued)

```
      C     OUTPUT CURRENT H FIELD
S.0071     57 I3 = I3+1
S.0072     56 WRITE (3,127)
S.0073        WRITE (3,128) AM,PR,HW,KE,DVR,IMAX,KMAX,I1,I3,KI,KF
S.0074        WRITE (3,129) (B(I),I=1,IMAX)
S.0075        WRITE (3,130)
S.0076        DO 85 K=1,KMAX
S.0077        C(IMAX,K) = 0
S.0078        DO 85 I=1,IMIN
S.0079     85 C(I,K) = -H(I,K)
S.0080        WRITE (3,131) (A(K),(C(I,K),I=1,IMAX),K=1,KMAX)
      C     TEST FOR LAST ITERATION
S.0081        IF (I3-I2) 80,81,81
      C     COMPUTE HEAT TRANSFER RATE
S.0082     81 DO 82 K=1,KMAX
S.0083        HB(K) = (3.*HW+4.*H(2,K)-H(3,K))/(2.*F)
S.0084     82 C(1,K) = HB(K)*PHI(1,K)
S.0085        WRITE (3,127)
S.0086        WRITE (3,128) AM,PR,HW,KE,DVR,IMAX,KMAX,I1,I3,KI,KF
S.0087        WRITE (3,135)
S.0088    135 FORMAT ('0ALPHA          HB          QP')
S.0089        WRITE (3,136) (A(K),HB(K),C(1,K),K=1,KMAX)
S.0090    136 FORMAT (3F10.4)
S.0091        GO TO 1
      C     VARIABLE PROPERTIES DECISION
S.0092     80 IF (DVR-1.01) 86,86,87
S.0093     86 DO 89 K=KI,KF
S.0094        DO 89 I=1,IMAX
S.0095     89 C(I,K) = 1.0
```

Figure 31 (Continued)

```
S.0096          GO TO 88
S.0097       87 DO 83 K=KI,KF
S.0098          DO 83 I=1,IMAX
S.0099          HI = (H(I,K)+1.)/(-HW+1.)
S.0100          HJ = (H(I,K)+HW)/(-HW+1.)
S.0101       83 C(I,K) = DVR*(1.5481/SQRT(HI)-0.5481/HI+0.0028*HJ-HJ*HJ*5.74E-5)
             C     COMPUTE NEW ITERANT FOR H OVER COMPLETE FIELD
S.0102       88 DO 21 K=1,KMAX
S.0103          DO 21 I=2,IMAX
S.0104          C4(I,K) = (H(I,K)-H(I-1,K))/F
S.0105       21 C3(I,K) = H(I-1,K)-C4(I,K)*B(I-1)
S.0106          DO 25 K=KI,KF
S.0107          C77(1) = 0
S.0108          DO 23 I=2,IMAX
S.0109          CINT = C4(I,K+1)-C4(I,K-1)
S.0110          C5(I) = C3(I,K+1)-C3(I,K-1)+C2(I,K)*CINT
S.0111          C6(I) = C1(I,K)*CINT
S.0112          CINTA = C1(I,K)*(C(I,K)+C(I-1,K))/(4.*D)
S.0113          C8(I) = CINTA*C5(I)*(A(K)-C2(I,K))/PR
S.0114          C9(I) = (C1(I,K)*C5(I)-C6(I)*(A(K)-C2(I,K)))*CINTA/(1.-PR)
S.0115          C10(I) = CINTA*C1(I,K)*C6(I)/(2.-PR)
S.0116          C77(I) = C8(I)*DPMPR(I,K)+C9(I)*DPOMPR(I,K)+C10(I)*DPTMPR(I,K)+
               1C77(I-1)
S.0117          C7(I) = C77(I-1)-C8(I)/PPR(I-1,K)-C9(I)*POMPR(I-1,K)-C10(I)*
               1PTMPR(I-1,K)
S.0118       23 FLN(I) = C8(I)*ELN(I,K)
S.0119          TERMC(IMAX) = 0
S.0120          DO 25 J=1,IMIN
S.0121          L = IMAX-J
S.0122          TERMC(L) = C1(L+1,K)*(C7(L+1)*DPPR(L+1,K)/PR+C9(L+1)*DP(L+1,K)+
               1C10(L+1)*DPS(L+1,K)/2.)+FLN(L+1)+TERMC(L+1)
S.0123          HBB = -(3.*HW+4.*H(2,K)-H(3,K))/(2.*F)
S.0124       25 HH(L,K) =HBB*TERMA(L,K)+TERMB(L,K)-A(K)*PR*TERMC(L)
```

Figure 31 (Continued)

```
                C       DETERMINE NEW H FIELD USING WEIGHTING FACTOR
S.0125                  DO 90 K=KI,KF
S.0126                  DO 90 I=2,IMIN
S.0127             90   H(I,K) = (M(K)*H(I,K)+HH(I,K))/(1.+M(K))
                C       APPLY BOUNDARY CONDITIONS
S.0128                  DO 91 I=2,IMIN
S.0129                  H(I,1) = H(I,2)
S.0130             91   H(I,21) = H(I,20)
S.0131                  GO TO 57
S.0132            127   FORMAT ('1  A/(A-I)    PR        -HW        KE        DVR       IMAX
                   1 KMAX  I1   I3   KI   KF')
S.0133            128   FORMAT (' ',5F10.4,6I5)
S.0134            129   FORMAT ('0BETA= ',10F7.4,F4.1)
S.0135            130   FORMAT (' ALPHA     H FIELD (NEGATIVE VALUES)')
S.0136            131   FORMAT (12F7.4)
S.0137                  END
                        SIZE OF COMMON  00000    PROGRAM  44150
END OF COMPILATION  MAIN
          COMPILATION TIME WAS    0004.05  SECONDS
```

Figure 31 (Continued)

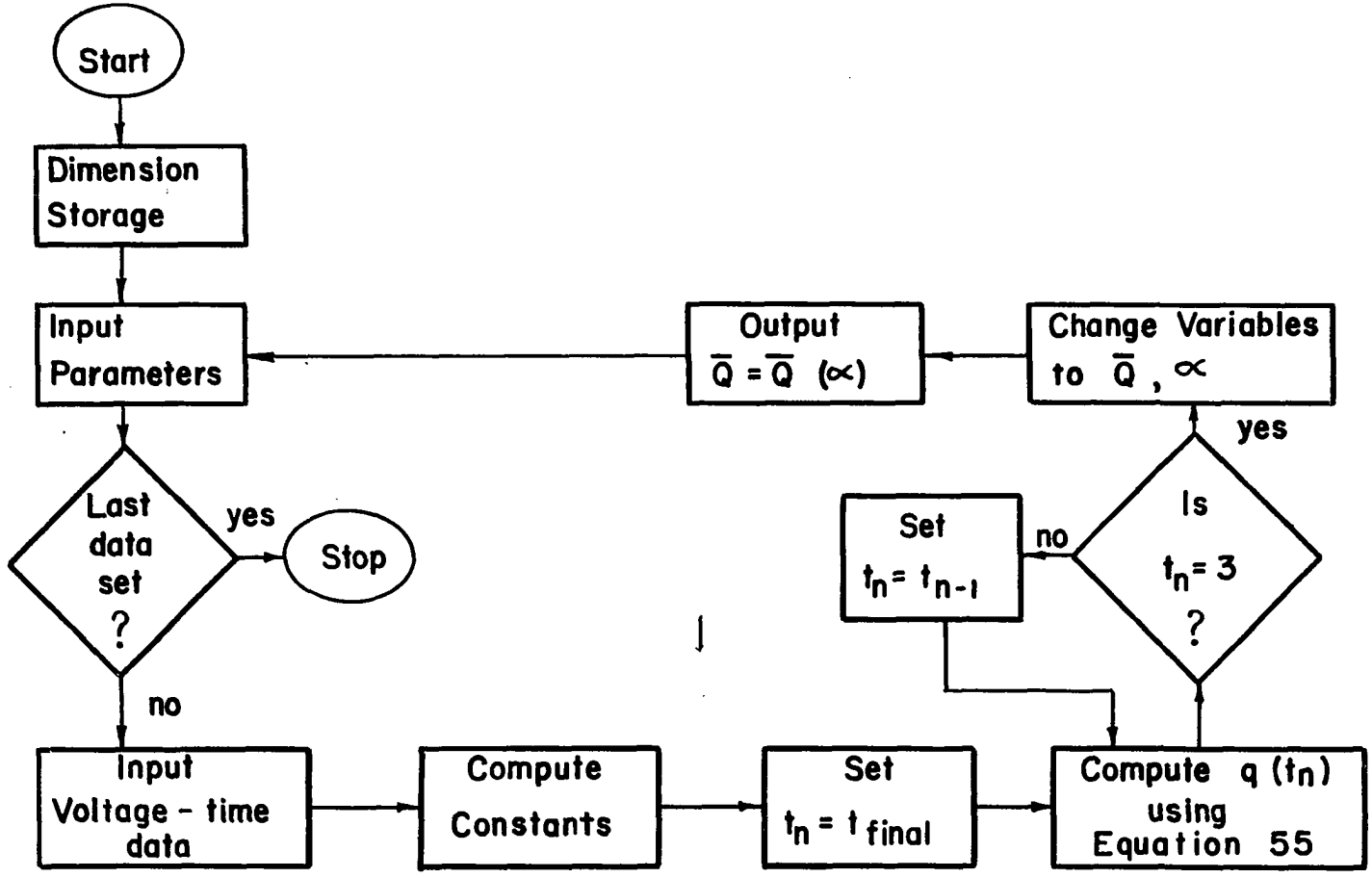

Figure 32. Flow diagram for computer program to reduce experimental heat transfer data

```
ISU COMPUTATION CENTER; AMES, IOWA

ISU DISK RES SPOOLED BPS FORTRAN
/JOB                    IO267 FELDERMAN 1 MINUTES                    U41
/FTC    NOMAP
BEGIN COMPILATION
              C     HEAT TRANSFER RATE DATA REDUCTION
              C     DIMENSION STORAGE
S.0001                DIMENSION TA(99),VA(99),T(99),V(99),RT(99),CN(5),
                     1RTV(99),QC(99),QCSQ(99),QW(99),QB(99),AXTEMP(99),
                     1ALPHA(99),QP(99),RALP(99),
                     2XLAB(5),YLAB(5),GLAB(5),DATLAB(5)
              C     INPUT PARAMETERS
S.0002                READ(1,105) XLAB,YLAB,GLAB,DATLAB,KS
S.0003           105  FORMAT(19A4,A3,A1)
S.0004            11  READ(1,100)(CN(J),J=1,5),80A,REF,VS,VSF,HSF,TN
S.0005           100  FORMAT(5A4,6F10.4)
S.0006                WRITE (3,300)
S.0007           300  FORMAT (1H1)
              C     TEST FOR FINAL DATA SET
S.0008                IF(TN)13,13,1
S.0009             1  READ (1,500) X,P1,SM,CMS
S.0010           500  FORMAT (4F10.4)
S.0011                WRITE(3,301)(CN(J),J=1,5),80A,REF,VS,VSF,HSF,TN,X,P1,SM,CMS
S.0012           301  FORMAT(3X,'RUNCODE',2X,'TRACE',4X,'BETA/ALPHA',3X,'RECIPEF',2X,
                     1'VERTSENS',1X,'V SCALE F',2X,'H SCALE F',2X,'POINTS',5X,'X',9X,
                     2'P1',9X,'MS',8X,'CMS'/5A4,10F10.4/15X,'CAL/SQCM SQRTSEC',3X,
                     3'VOLTS',4X,'MV/CM',4X,'UNITS/CM',3X,'UNITS/USEC',13X,'IN',6X,
                     4'MM HG'//)
S.0013                N=TN
```

Figure 33. Computer program to reduce experimental heat transfer data

```
      C     INPUT VOLTAGE AND TIME VALUES
S.0014      READ(1,102)(TA(I),VA(I),I=1,N)
S.0015  102 FORMAT (10F8.4)
S.0016      DO 2 I=1,N
S.0017      T(I)=TA(I)/HSF
S.0018      V(I)=VA(I)*VS/VSF
S.0019    2 AXTEMP(I)=V(I)*REF
S.0020      WRITE(3,303)
S.0021  303 FORMAT(4X,'V(MV)',4X,'T(USEC)',3X,'SQRT T',7X,'QC',8X,'QB',7X,
     1'QW',8X,'QCSQ',11X,'VA',9X,'TA',6X,'1/ALPHA',4X,'ALPHA',5X,'QP',/
     330X,'CAL/SQCM SEC',2X,'BTU/SQFT SEC',2X,'WATTS/SQCM'/)
S.0022      TC = X/(SM*0.00112*12.0)
S.0023      UO = 1100.0*SM-850.0
S.0024      CSQ = 0.72*SQRT(X/(P1*UO))/(CMS*0.01508)
      C     COMPUTE HEAT TRANSFER RATES
S.0025   10 TT=T(N)
S.0026      RTZ=SQRT(TT)
S.0027      RTY(N)=RTZ
S.0028      DO 3 I=2,N
S.0029      IF(TT-T(I-1)) 11,11,3
S.0030    3 RT(I-1)=SQRT(TT-T(I-1))
S.0031      S=0
S.0032      M=N-1
S.0033      DO 4 I=2,M
S.0034    4 S=(V(I)-V(I-1))/(RT(I)+RT(I-1))+S
S.0035      BRCKT=S+(V(1)/(RT(1)+RTZ))+((V(N)-V(N-1))/RT(N-1))
S.0036      QC(N)=1.12838*REF*BOA*BRCKT
S.0037      QCSQ(N)=QC(N)*QC(N)
S.0038      QW(N)=4.18600*QC(N)
S.0039      QB(N)=0.88056*QW(N)
```

Figure 33 (Continued)

```
      C     CHANGE VARIABLES
S.0040      TT = T(N)+TO
S.0041      ALPHA(N) = X/(UO*TT*12.0)*1.0E+6
S.0042      RALP(N) = 1.0/ALPHA(N)
S.0043      QP(N) = QB(N)*CSQ
      C     OUTPUT RESULTS
S.0044      WRITE(3,304)V(N),T(N),RTY(N),QC(N),QB(N),QW(N),QCSQ(N),VA(N),
           1TA(N),RALP(N),ALPHA(N),QP(N)
S.0045    304 FORMAT(3F10.4,3F10.4,E15.7,5F10.4)
S.0046      N=N-1
S.0047      IF (N-2) 11,11,10
S.0048     13 STOP
S.0049      END
            SIZE OF COMMON  00000     PROGRAM  07754
END OF COMPILATION  MAIN
      COMPILATION TIME WAS    0001.81  SECONDS
```

Figure 33 (Continued)